Synthesis and Release of Docosahexaenoic Acid by the RPE Cells of *prcd*-Affected Dogs

Huiming Chen,[1,2,3] *Jharna Ray,*[4] *Virginia Scarpino,*[4] *Gregory M. Acland,*[4] *Gustavo D. Aguirre,*[4] *and Robert E. Anderson*[1,2,3,5,6]

Purpose. Dogs affected with progressive rod-cone degeneration (*prcd*) have reduced levels of docosahexaenoic acid (DHA, 22:6n-3) in their plasma and rod photoreceptor outer segments (ROS). Dietary supplementation of DHA has failed to increase the ROS DHA levels to that of unaffected control dogs. The present study was undertaken to test the hypothesis that *prcd*-affected dogs have a reduced capacity for the synthesis and/or release of DHA in retinal pigment epithelial (RPE) cells.

Methods. RPE cells (first passage cultures) from *prcd*-affected and normal dogs were incubated with [^{3}H]eicosapentaenoic acid (EPA, 20:5n-3) for 24 and 72 hours. After incubation, the radiolabeled fatty acids in the cells and media were analyzed.

Results. DHA and all its metabolic intermediates were detected in RPE cells from *prcd*-affected and normal dogs. No significant difference was found in the amount of products (including DHA) synthesized between normal and affected RPE cells at either time point. In the culture media, RPE cells from *prcd*-affected dogs released significantly more DHA than cells from normal dogs after 72-hour incubation, but not after 24-hour incubation.

Conclusions. RPE cells from *prcd*-affected dogs can synthesize and release DHA at least as efficiently as cells from normal dogs. Therefore, synthesis of DHA from its precursor and its release from RPE cells does not appear to contribute to the reduction in ROS DHA levels found in *prcd*-affected animals. (*Invest Ophthalmol Vis Sci.* 1999;40:2418–2422)

From the Departments of [1]Ophthalmology, [5]Cell Biology, and [6]Biochemistry and Molecular Biology, and [2]Oklahoma Center for Neuroscience, University of Oklahoma Health Sciences Center, Oklahoma City; and [3]Dean A. McGee Eye Institute, Oklahoma City, Oklahoma; and [4]James A. Baker Institute for Animal Health, College of Veterinary Medicine, Cornell University, Ithaca, New York.

Supported by the National Institutes of Health (Grants EY06855, EY00871, and EY04149); Research to Prevent Blindness, Inc.; The Foundation Fighting Blindness; Samuel Roberts Noble Foundation; and Presbyterian Health Foundation. REA is a Senior Scientific Investigator for Research to Prevent Blindness, Inc.

Submitted for publication December 10, 1998; revised April 7, 1999; accepted May 5, 1999.

Proprietary interest category: N.

Corresponding author: Robert E. Anderson, Dean A. McGee Eye Institute, 608 Stanton L. Young Boulevard, Room 409, Oklahoma City, OK 73104.
E-mail: robert-anderson@ouhsc.edu

Although gene mutations for photoreceptor-specific proteins are generally considered the primary causative factor for retinitis pigmentosa, abnormalities in systemic levels of essential long-chain polyunsaturated fatty acids, particularly docosahexaenoic acid (DHA, 22:6n-3), frequently have been reported to be associated with various forms of retinitis pigmentosa in humans. Dogs with progressive rod-cone degeneration (*prcd*) have reduced DHA levels in the plasma,[1] similar to the findings in humans with retinitis pigmentosa, and also have lower DHA levels (approximately 20%) in their rod photoreceptor outer segments (ROS).[2] Although ROS DHA levels in humans with retinitis pigmentosa have not yet been examined, pronounced reduction in DHA levels has been observed in the sperm (the only other body fluid or tissue in the body, besides retina and brain, that is enriched in DHA) of male patients affected with retinitis pigmentosa.[3] Thus, the *prcd*-affected dogs are an excellent animal model for the human disease to study the mechanisms underlying the lower DHA phenotype and its cause-and-effect relationship with the disease process.

In an effort to correct or slow down the progressive loss of photoreceptor cells, we previously gave daily DHA supplements to *prcd*-affected dogs for 5 months and assessed subsequently the *prcd* disease phenotype.[2] We found that, although DHA supplementation produced a sustained elevation in plasma and liver DHA levels, the ROS DHA levels in the affected animals remained lower than those in control dogs, and the *prcd* disease phenotype was not changed by this dietary manipulation. These results suggest that the synthesis of DHA-containing phospholipid molecular species in the retinas or the delivery of DHA from circulation to the retina could be downregulated in the affected animals.

In the present study, we examined the possible contribution by retinal pigment epithelial (RPE) cells to the lower ROS DHA phenotype. Our study indicates that RPE cells from affected animals have a similar capability for synthesis of DHA from eicosapentaenoic acid (20:5n-3) and for release of DHA to the surrounding media, compared to those cells from normal animals.

Materials and Methods

Animals

The dogs used in this study were derived from miniature poodles and were homozygous normal or affected with the *prcd* mutation; the dogs were bred and raised as part of a colony supported by an NEI/NIH grant (EY06855, "Models of Hereditary Retinal Degeneration"). All dogs were maintained in the same animal care facility (Retinal Disease Studies Facility, Kennett Square, PA) with controlled cyclic illumination (12-hour light–dark). Four *prcd*-affected animals (2–3 months old) and three age-matched normal dogs were used for the studies. The *prcd*-affected animals at this age show no morphologic evidence of retinal disease. All studies described were performed in compliance with ARVO Resolution on the Use of Animals in Ophthalmic and Vision Research and followed protocols approved by the animal protocol review committees of Cornell University and University of Oklahoma Health Sciences

Investigative Ophthalmology & Visual Science, September 1999, Vol. 40, No. 10

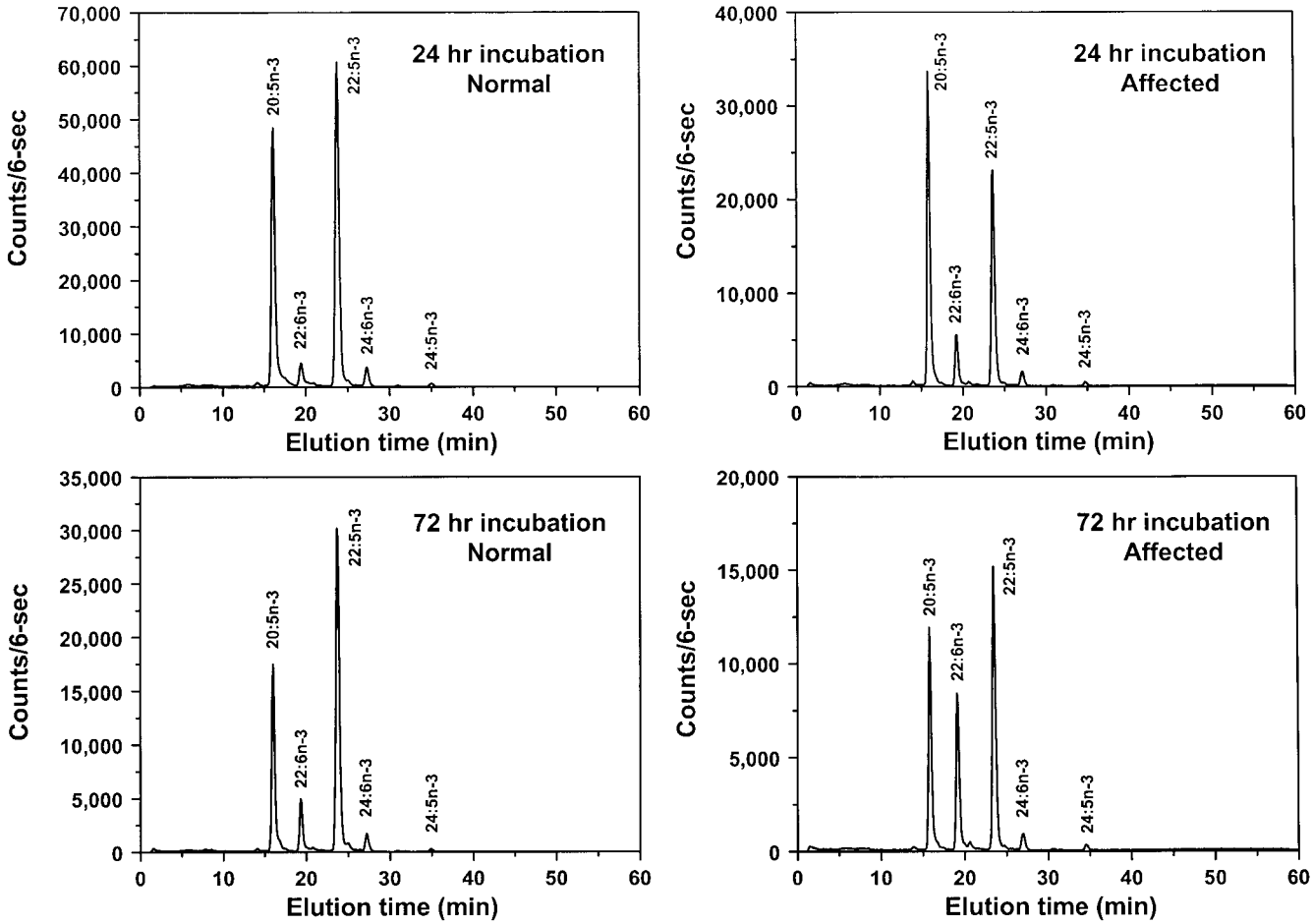

Figure 1. HPLC elution profiles of radiolabeled 20:5n-3 and its metabolic products from normal and *prcd*-affected dog RPE cells after incubation for 24 and 72 hours. Confluent dog RPE cells (3 normal and 4 affected) were incubated in duplicate at 37°C for 24 and 72 hours with 2 ml of HL-1 medium containing 10% fetal bovine serum and 15 μCi [^{3}H]20:5n-3. Total lipids from the cells were saponified, and the released free fatty acids were converted to phenacyl esters and analyzed by HPLC and flow-through scintillation counting.

Center. The dogs were euthanatized with a barbiturate overdose, and the eyes were enucleated and transported to the laboratory in a chilled Puck F saline with calcium and antibiotics.

RPE Cultures

RPE cells from normal and *prcd*-affected animals were isolated as previously described.[4] Briefly, after lens, vitreous, and retinas were removed aseptically, the RPE cells were released by repeated trypsinization. Dissociated cells were placed in DMEM medium containing 15% fetal bovine serum (FBS) and plated in 35-mm dishes at a density of 2×10^5 cells/dish. The cells were allowed to attach to the plate and grow. At confluence, RPE cells were subcultured (1:3 ratio) by trypsinization. The confluent first passage (P1) cultures from both normal and affected RPE cells were used for the following isotope incubations.

Incubation Conditions

Elongation and desaturation of [^{3}H]20:5n-3 (American Radiolabeled Chemicals, St. Louis, MO) were studied in confluent P1 RPE cultures grown in HL-1 medium (Hycor Biomedical, Irvine, CA) containing 10% FBS on 35-mm dishes. Incubations were carried out for 24 and 72 hours in duplicate with 2 ml culture medium containing 15 μCi (0.75 nmol) of [^{3}H]20:5n-3 (conjugated with delipidated bovine serum albumin [BSA] at a molar ratio of 2:1). The cells were maintained at 37°C in an incubator containing 5% CO_2. At the end of the incubation period, the media were removed from the cells and centrifuged to remove cellular debris; the cells were rinsed twice with ice-cold HL-1 medium containing 10 μM fatty acid–free BSA and harvested by trypsinization. Both cells and clarified media were stored at −80°C until analysis.

Lipid Extraction and Saponification

Before lipid extraction, the culture media were centrifuged at 100,000*g* for 1 hour to remove subcellular membrane contaminants. Total lipids from the cells and media were extracted twice with chloroform/methanol. Lipid extracts were dried under nitrogen and suspended in a known volume of ethanol. Aliquots were taken for total radioactivity determination; the remaining lipid extracts were suspended in 1 ml of 2% KOH (wt/vol) in ethanol and saponified at 100°C for 30 minutes. After cooling to room temperature, 1 ml water and 75 μl concentrated HCl were added, and the released free fatty acids were extracted three times with 2 ml hexane.

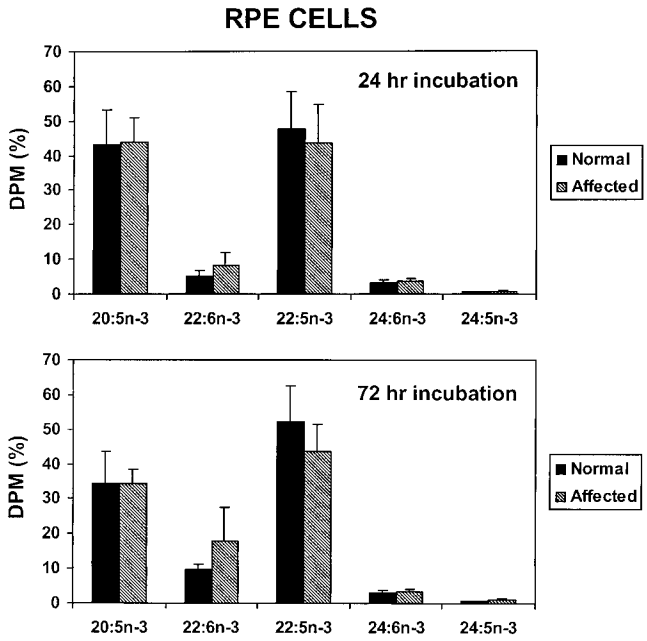

FIGURE 2. Relative distribution of radioactivity in 20:5n-3 and its metabolic products from normal and *prcd*-affected dog RPE cells after incubation for 24 and 72 hours. Confluent dog RPE cells (3 normal and 4 affected) were incubated in duplicate at 37°C for 24 and 72 hours with 2 ml of HL-1 medium containing 10% fetal bovine serum and 15 μCi [^{3}H]20:5n-3. Total lipids from the cells were saponified, and the released free fatty acids were converted to phenacyl esters and analyzed by HPLC and flow-through scintillation counting. Values are means ± SD.

HPLC Analysis of Fatty Acids

The extracted free fatty acids were converted to phenacyl esters and separated by high-performance liquid chromatography (HPLC) on a Sulpeco LC-18 column (25 cm × 4.6 mm).[5] The fatty acid phenacyl esters were eluted at a flow rate of 2 ml/min with a linear gradient of acetonitrile/water from 80/20 (vol/vol) to 92:8 (vol/vol) for 45 minutes, followed by holding at 92:8 (vol/vol) for 10 minutes and returning to 80:20 (vol/vol) for 5 minutes. The radioactivity profile was monitored by online scintillation counting (Flo-one A250; Radiomatic, Tampa, FL) using Ultima-Flo M (Packard Instrument, Downers Grove, IL) at 2.5:1 (vol/vol) ratio of cocktail to mobile phase. The phenacyl esters were monitored at an absorbance of 242 nm. Identities of individual fatty acids have been previously determined[5] and further confirmed by catalytic hydrogenation and HPLC analysis of hydrogenated products.

RESULTS

RPE cells from normal and *prcd*-affected dogs grew well in culture and maintained a nice, distinguishable epithelial cell morphology. The affected cells appeared the same as normal cells, except that they grew and reached confluency slightly faster than normal cells.

Labeling in the Cells

The labeling profiles from both normal and affected RPE cells after 24- and 72-hour incubation with [^{3}H]20:5n-3 are shown in Figure 1. Elongation and desaturation products of 20:5n-3, namely 22:5n-3, 24:5n-3, 24:6n-3, and 22:6n-3, were all detected. The identities of these labeled compounds were confirmed by HPLC analysis of their respective hydrogenation products (data not shown).

The relative percentages of radioactivity in precursor 20:5n-3 and its products are shown in Figure 2. No significant difference was found on the relative amounts of labeling in DHA and other metabolites between normal and affected cells at either time point, although affected cells tended to have more but variable labeling in DHA. With increasing incubation time, both RPE cells had more labeling in 22:6n-3 and proportionally less labeling in 20:5n-3.

Labeling in the Media

Distributions of radioactivity in 20:5n-3 and its metabolic products from culture media are shown in Figures 3 and 4. After 24-hour incubation, no significant difference was detected on the relative (Fig. 3) or total amount (Fig. 4) of labeling in any of the fatty acids from normal and affected RPE cells. However, after 72-hour incubation, there was significantly more labeling (both relative and total amount) in DHA from affected cells than from normal ones. With increasing incubation time from 24 to 72 hours, the total amount of radioactivity in DHA was increased 4 times from affected cells and only 2 times from normal ones, whereas changes for 22:5n-3 and other products were much smaller.

It is worth noting that the labeling in the media did not simply reflect that in the cells. Compared to the radioactivity

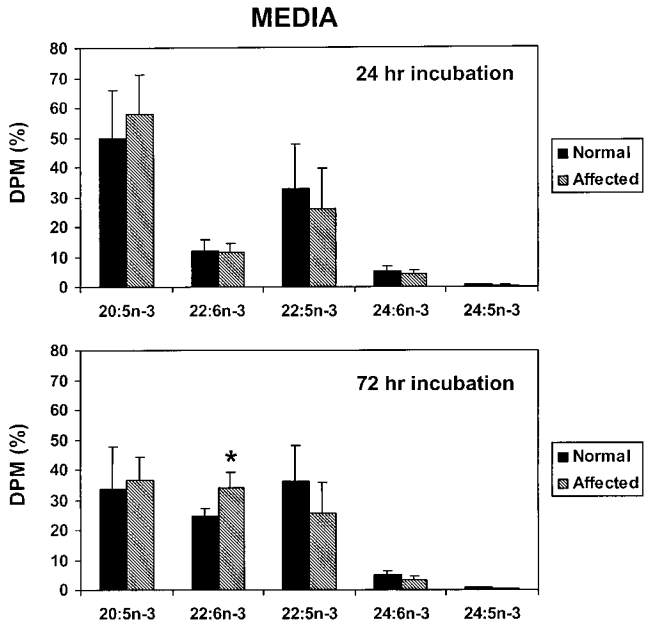

FIGURE 3. Relative distribution of radioactivity in 20:5n-3 and its metabolic products from culture media of 24- and 72-hour incubations with normal and *prcd*-affected dog RPE cells. Confluent dog RPE cells (3 normal and 4 affected) were incubated in duplicate at 37°C for 24 and 72 hours with 2 ml of HL-1 medium containing 10% fetal bovine serum and 15 μCi [^{3}H]20:5n-3. Total lipids were extracted from the media and saponified, and the released free fatty acids were converted to phenacyl esters and analyzed by HPLC and flow-through scintillation counting. Values are means ± SD. *Statistically significant difference ($P < 0.05$) as assessed by Student's two-tail *t*-test.

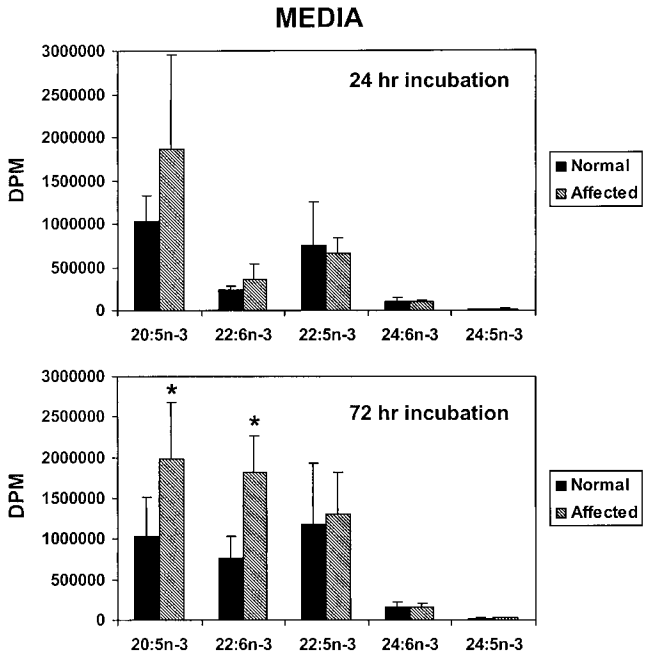

FIGURE 4. Total radioactivity in 20:5n-3 and its metabolic products from the culture media of 24- and 72-hour incubations with normal and *prcd*-affected dog RPE cells. Confluent dog RPE cells (3 normal and 4 affected) were incubated in duplicate at 37°C for 24 and 72 hours with 2 ml of HL-1 medium containing 10% fetal bovine serum and 15 μCi [^{3}H]20:5n-3. Total lipids were extracted from the media and saponified, and the released free fatty acids were converted to phenacyl esters and analyzed by HPLC and flow-through scintillation counting. Values are means ± SD. *Statistically significant difference ($P < 0.05$) as assessed by Student's two-tail *t*-test.

distribution in the cells (Fig. 2), relatively more DHA and less 22:5n-3 was found in the media at either incubation time (Fig. 3) for both types of cells. As a result, the ratio of DHA/22:5n-3 was 3 times higher in the media than in the cells, indicative of preferential release of DHA over 22:5n-3 in these cells.

DISCUSSION

Dogs with *prcd* have abnormalities in long-chain polyunsaturated fatty acid metabolism, with reduced DHA levels (approximately 20%–25%) in plasma and ROS and slightly elevated levels in the liver, compared to unaffected dogs.[1,2] The mechanism for the reduction in ROS DHA levels in *prcd*-affected animals is not clear. It was initially thought that synthesis of DHA in the liver and/or transport to the target tissues could be affected. We tested this hypothesis previously and tried to bypass the possible defect in DHA production in the liver by providing preformed DHA to affected and normal dogs for up to 5 months.[2] We found that supplementation caused a rapid and sustained elevation in plasma DHA levels in both groups, but had no effect on the progression of the disease in *prcd*-affected animals. The *prcd*-affected dogs fed a DHA-enriched diet still had significantly lower DHA levels in ROS compared to control dogs.[2] In dogs supplemented with DHA for up to 24 days, levels of DHA were lower in ROS and higher in the liver from *prcd*-affected dogs. These studies indicate that the lower content of ROS DHA in *prcd*-affected dogs is not the result of a dietary deficiency of DHA and its precursor fatty acids. Besides a possible problem in packaging DHA into lipoproteins in the liver,[6] these results suggest the possibility that the problem in *prcd*-affected animals could be in DHA trafficking between the blood and the retina, possibly involving passage through RPE cells.

In this study, we investigated a possible defect in RPE of *prcd*-affected dogs in the synthesis and release of DHA to the extracellular space, by comparing these two activities in the RPE of *prcd*-affected and normal animals. This is important because RPE cells could use 22:5n-3, which is slightly elevated in the plasma of affected animals,[1] to synthesize DHA to compensate for the reduced DHA levels in ROS of *prcd*-affected animals. RPE cells of frogs have been shown to readily synthesize DHA from its precursors.[7] Also, because RPE cells are the major nutrient supplier for the photoreceptors and play central roles in recycling of DHA from daily shed ROS tips back to photoreceptors,[8,9] it is conceivable that alterations in DHA metabolism in the RPE could affect photoreceptor DHA content. We found that RPE cells from both *prcd*-affected and normal dogs can elongate 20:5n-3 to 22:5n-3 and further convert 22:5n-3 to 22:6n-3 through Sprecher's Δ4-desaturase independent pathway[10] (22:5n-3 → 24:5n-3 → 24:6n-3 → 22:6n-3). Rates for DHA synthesis appeared only slightly higher for affected RPE compared to normal cells. Thus, in agreement with our previous in vivo studies,[11] there is no defect in DHA synthesis in the RPE of *prcd*-affected dogs. Furthermore, under our experimental conditions, RPE cells from *prcd*-affected animals showed no apparent defect in releasing DHA, inasmuch as the level of DHA in the culture media from affected cells was clearly not lower than that from normal cells.

It is noteworthy that the labeling pattern in the culture media did not simply reflect that of the cells. When the distribution of radioactivity was compared, clearly more DHA and less 22:5n-3 was found in the media than in the cells. Thus, dog RPE cells appeared to favor the release of DHA over 22:5n-3, although both are similar in structure, with 22:5n-3 having one less *cis* double bond. Evidently the types of fatty acids in the media are not the result of equilibration, but rather of cellular regulation, which also has been demonstrated in retinal and cerebral microvascular endothelial cells.[12,13]

In light of our earlier[2,11,14] and present studies on *prcd*-affected dogs, it is possible that lower ROS DHA levels could be due to cellular upregulation of DHA catabolism and/or downregulation of DHA incorporation into membranes to reduce disease-originated metabolic (perhaps oxidative) stress. DHA provides optimal lipid environment for rhodopsin and probably other membrane proteins in photoreceptors and thus is essential for optimal photoreceptor function. On the other hand, DHA is highly unsaturated (six double bonds) and easily peroxidized, especially in the photoreceptor cells, where high levels of oxygen and unsaturated fatty acid content and light exposure provide the ideal environment for lipid peroxidation. Toxic factors from lipid hydroperoxides derived from DHA could affect photoreceptor enzyme activities and damage photoreceptor membranes, as has been reported for light damage in albino rats.[15–17] Biological adaptation, such as shortened ROS length, reduced levels of rhodopsin and DHA-containing glycerolipids, and increased antioxidants vitamin E and vitamin C and glutathione-dependent enzyme activities, as well as neurotrophic factors, in response to light stress has been shown in the retinas of rats raised in bright cyclic light compared to

controls raised in dim cyclic light.[16–19] Similarly, oxidative stress achieved through the stimulation of endogenous oxidant generation in human spermatozoa can cause DNA fragmentation and loss in their capacities for movement and oocyte fusion.[20] Therefore, it is possible that reduction in DHA levels in retinas and plasma could be part of a biological adaptation to metabolic stress, possibly oxidative, caused by different mutations in retinitis pigmentosa. We currently are testing the hypothesis that mutations in a number of genes encoding retina-specific proteins can cause lower DHA phenotypes.

References

1. Anderson RE, Maude MB, Alvarez RA, Acland GM, Aguirre GD. Plasma lipid abnormalities in the miniature poodle with progressive rod-cone degeneration. *Exp Eye Res.* 1991;52:349–355.
2. Aguirre GD, Acland GM, Maude MB, Anderson RE. Diets enriched in docosahexaenoic acid fail to correct progress rod-cone degeneration (prcd) phenotype. *Invest Ophthalmol Vis Sci.* 1997;38:2387–2407.
3. Connor WE, Weleber RG, DeFrancesco C, Lin DS, Wolf DP. Sperm abnormalities in retinitis pigmentosa. *Invest Ophthalmol Vis Sci.* 1997;38:2619–2628.
4. Ray J, Wu Y, Aguirre GD. Characterization of β-glucuronidase in the retinal pigment epithelium. *Curr Eye Res.* 1997;16:131–143.
5. Chen H, Anderson RE. Quantitation of phenacyl esters of retinal fatty acids by high-performance liquid chromatography. *J Chromatogr.* 1992;578:124–129.
6. Bazan NG, Rodriguez de Turco EB. Alterations in plasma lipoproteins and DHA transport in progressive rod-cone degeneration (*prcd*). In: Kato S, Osborne NN, Tamai M, eds. *Retinal Degeneration and Regeneration.* Amsterdam: Kugler; 1996:89–97.
7. Wang N, Anderson RE. Synthesis of docosahexaenoic acid by retina and retinal pigment epithelium. *Biochemistry.* 1993;32:13703–13709.
8. Gordon WC, Rodriguez de Turco EB, Bazan NG. Retinal pigment epithelial cells play a central role in the conservation of docosahexaenoic acid by photoreceptor cells after shedding and phagocytosis. *Curr Eye Res.* 1992;11:78–83.
9. Chen H, Wiegand RD, Koutz CA, Anderson RE. Docosahexaenoic acid increases in frog retinal pigment epithelium following rod photoreceptor shedding. *Exp Eye Res.* 1992;55:93–100.
10. Voss A, Reinhart M, Sankarappa S, Sprecher H. The metabolism of 7,10,13,16,19-docosapentaenoic acid to 4,7,10,13,16,19-docosahexaenoic acid in rat liver is independent of a 4-desaturase. *J Biol Chem.* 1991;266:19995–20000.
11. Alvarez RA, Aguirre GD, Acland GM, Anderson RE. Docosapentaenoic acid is converted to docosahexaenoic acid in the retinas of normal and prcd-affected miniature poodle dogs. *Invest Ophthalmol Vis Sci.* 1994;35:402–408.
12. Delton-Vandenbroucke I, Grammas P, Anderson RE. Polyunsaturated fatty acid metabolism in retinal and cerebral microvascular endothelial cells. *J Lipid Res.* 1997;38:147–159.
13. Delton–Vandenbroucke I, Grammas P, Anderson RE. Regulation of n-3 and n-6 fatty acid metabolism in retinal and cerebral microvascular endothelial cells by high glucose. *J Neurochem.* 1998;70:841–849.
14. Anderson RE, Maude MB, Acland GM, Aguirre GD. Plasma lipid changes in prcd-affected and normal miniature poodles given oral supplements of linseed oil. Indications for the involvement of n-3 fatty acids in inherited retinal degenerations. *Exp Eye Res.* 1994;58:129–137.
15. Wiegand RD, Giusto NM, Rapp LM, Anderson RE. Evidence for rod outer segment lipid peroxidation following constant illumination of the rat retina. *Invest Ophthalmol Vis Sci.* 1983;24:1433–1435.
16. Organisciak DT, Wang H–M, Xie A, Reeves DS, Donoso LA. Intense-light mediated changes in rat rod outer segment lipids and proteins. In: Hollyfield JG, Anderson RE, LaVail MM, eds. *Degenerative Retinal Disorders: Clinic and Laboratory Investigations.* New York: Alan R Liss; 1989:4455–4468.
17. Organisciak DT, Darrow RM, Jiang YL, Blanks JC. Retinal light damage in rats with altered levels of rod outer segment docosahexaenoate. *Invest Ophthalmol Vis Sci.* 1996;37:2243–2257.
18. Penn JS, Anderson RE. Effects of light history on the rat retina. In: Osborne N, Chader G, eds. *Progress in Retinal Research.* New York: Pergamon Press; 1992:75–98.
19. Liu C, Peng M, Laties AM, Wen R. Preconditioning with bright light evokes a protective response against light damage in the rat retina. *J Neurosci.* 1998;18:1337–1344.
20. Aitken RJ, Gordon E, Harkiss D, et al. Relative impact of oxidative stress on the functional competence and genomic integrity of human spermatozoa. *Biol Reprod.* 1998;59:1037–1046.

Increase in Orthotopic Murine Corneal Transplantation Rejection Rate with Anterior Synechiae

Satoru Yamagami and Tadahiko Tsuru

Purpose. To evaluate the immunologic effect of anterior synechiae (AS) in a murine model of corneal transplantation.

Methods. Orthotopic penetrating keratoplasty with 12 interrupted sutures was performed on C57BL/6 donor mice and BALB/c recipient mice without AS (AS− group). In contrast to suturing in the AS− group, 3 of the 12 sutures were placed to create AS (AS+ group). The average graft opacity scores and rejection rates of both groups were compared. Cytotoxic T-lymphocyte (CTL) reactions and delayed hypersensitivity (DH) were evaluated 3 weeks after transplantation. Corneal cytokine expression was evaluated.

Results. The opacity scores of the AS+ group were consistently greater than those of the AS− group, and the rejection rate of the AS+ group was significantly greater than that of the AS− group (86% versus 54%, $P = 0.03$). The AS+ group had significantly higher CTL activity compared with the AS− group. There was no significant difference in DH between the two groups. The cytokine expression pattern in the AS+ group became similar to that of the AS− group in which the grafts were rejected.

Conclusions. These findings indicate that AS impairs ocular immune privilege by mediating CTL activity, but with-

From the Department of Ophthalmology, Jichi Medical School, Tochigi, Japan.

Supported in part by a grant for Scientific Research (A09771465) from the Ministry of Education, Science, and Culture of Japan.

Submitted for publication November 18, 1998; revised February 18, 1999; accepted March 23, 1999.

Proprietary interest category: N.

Presented at the 1998 annual meeting of the Association for Research in Vision and Ophthalmology, Fort Lauderdale, Florida, May 1998.

Corresponding author: Satoru Yamagami, Schepens Eye Research Institute, Harvard Medical School, 20 Staniford Street, Boston, MA 02114. E-mail: yamagami@vision.eri.harvard.edu

out intensifying the DH response. Therefore, AS is a critical risk factor in allograft rejection in a murine model of corneal transplantation. (*Invest Ophthalmol Vis Sci.* 1999; 40:2422–2426)

The ocular anterior segment is considered to have immunologic privilege. The cornea in particular has several advantages: lack of vessels, a deficiency of antigen-presenting cells in the central cornea, immunosuppressive activity by corneal fibroblasts and the endothelium, and Fas ligand expression that suppresses immunoreaction.[1] Because of these unique immunologic properties, the success rate of human corneal transplantation, compared with other types of vascularized organ transplants, is high in a normal corneal bed.[2]

Allograft rejection of corneal transplants, however, is a critical unresolvable problem, particularly in high-risk patients with vascularized corneas, previously failed corneal grafts, or both.[2,3] Anterior synechiae (AS) of the iris to the corneal endothelium is also a complication that often occurs after corneal transplantation. Two decades ago, the presence of AS was reported as a possible risk factor for rejection in human corneal transplantation.[4–7] However, whether or not AS is a real risk factor in corneal allografts and how it modulates the anterior segment immune reaction and cellular immunity, including cytokine expression, have not been fully addressed.

The cytokine network, which regulates the immune reaction, is a critical factor in determining immunologic properties. Cytokines, produced by $CD4^+$ T cells, are divided into T helper (Th)1 (interleukin [IL]-2, interferon-gamma [IFN-γ], and IL-12) and Th2 (IL-4, IL-5, IL-6, and IL-10) groups. These cytokines affect T-cell–mediated immune responses and cross-regulate each other. In corneal allorejection, a predominance of Th1 cytokine expression in cells infiltrating the graft has been reported in murine models.[8,9]

We developed a new AS mice corneal transplantation model and investigated the local and systemic immunologic properties of AS, including cytokine expression. We showed that AS is a risk factor for rejection in corneal transplants and that AS elicits cytotoxic T-lymphocyte (CTL) activity without intensifying delayed hypersensitivity (DH).

Materials and Methods

Animals

Inbred strains of male BALB/c ($H\text{-}2^d$) mice (Clea Japan Co., Tokyo, Japan) were the recipients of the grafts. C57BL/6 ($H\text{-}2^b$) and BALB/c mice were the respective donors of the allografts and isografts. The major and minor histocompatibility antigens differ in the BALB/c and C57BL/6 strains. Male mice 8 to 14 weeks of age were used in all experiments. All animals were treated in accordance with the ARVO Statement for the Use of Animals in Ophthalmic and Vision Research.

Surgical Technique of Orthotopic Corneal Transplantation

Orthotopic penetrating keratoplasty was performed as described previously with some modification.[8] Briefly, corneas of the mydriated recipients were marked with a trephine and excised with microscissors. Donor corneas excised with a 2.0-mm trephine (Inami, Tokyo, Japan) were transplanted to the same size recipient corneas, and 12 interrupted 11-0 nylon sutures (Mani, Tochigi, Japan) were placed without AS (AS− group). To create the AS (AS+ group), the last three sutures were passed through the iris and the cornea in three quadrants. The corneal sutures were removed 8 days after surgery. Grafts with an opacity score of 3+ or greater at suture removal were eliminated from the study because of the development of postoperative complications. When AS was absent in eyes in the AS+ group and vice versa, the eyes were excluded.

Definition of Rejection and Clinical Observation

The corneal grafts were observed weekly for 8 weeks under an operating microscope. Graft opacity was scored from 0 to 5+ based on the following criteria[10]: 0, clear; 1+, some opacity at the graft margin or superficial edema; 2+, iris vessels readily visible; 3+, some iris vessel discernible; 4+, only pupil margin visible; and 5+, anterior chamber not visible. Corneal grafts were considered to be rejected when the opacity scores were greater than 2+.

Histologic Evaluation

Some of the grafted mice were killed for histologic study 3 weeks after surgery. The enucleated eyes were fixed in 4% paraformaldehyde and then stained with hematoxylin and eosin for light microscopy.

Immunohistochemical Study

The biotin-conjugated monoclonal antibodies (mAbs) used for immunostaining were anti-mouse IFN-γ (XMG1.2, 4 μg/ml; PharMingen, San Diego, CA), anti-mouse IL-2 (JES6-5H4, 4 μg/ml; PharMingen), anti-mouse CD4 (H129.19, 4 μl/ml; PharMingen), and anti-mouse CD8a (53-6.7, 4 μg/ml; PharMingen). The immunoperoxidase technique was performed as follows. Frozen specimens (7 μm) were sectioned in a cryostat, then fixed in acetone for 10 minutes, and washed with phosphate-buffered saline (PBS). The mAbs were applied overnight, after which the mAb-labeled sections were exposed for 20 minutes to horseradish peroxidase–labeled streptavidin. The sections were incubated for 1 minute in diaminobenzidine and then stained with Mayer's hematoxylin for 10 seconds. Biotin-conjugated rat IgG1 and IgG2b (PharMingen) were used for the negative control study. Positive cells were scored on a scale of 0 to 4+ per 100× high power field: +, 1 to 10 cells; ++, 11 to 20 cells; +++, 21 to 30 cells; and ++++, ≥ 31 cells. Counting and grading on the stained slides were limited to the central zone of each graft and host area to avoid the host–graft junction area. The gradings were the averages obtained from three separate compilations of the numbers of positive cells performed during immunohistochemical study.

Assay for DH

DH responses to alloantigens were determined by measuring ear swelling. B6 splenocytes were irradiated with 30 Gy, resuspended at a concentration of 1×10^6 cells in 10 μl, and injected into the right pinnae. PBS was injected into the left pinnae. Naive mice and mice immunized by subcutaneous injection of 1×10^7 B6 splenocytes into the back, the negative and positive controls, respectively, were used. After 24 hours, ear thickness was measured with a low-pressure micrometer (Mitsutoyo, Tokyo, Japan). DH-dependent ear swelling was calculated according to the following formula:

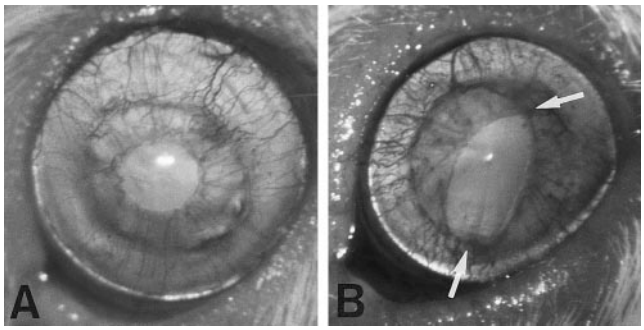

FIGURE 1. Photographs show the absence or presence of anterior synechiae (AS) on day 10 after transplantation. (**A**) A round pupil without AS. (**B**) Two areas of AS (*arrows*). A portion of the AS has been removed.

Specific ear swelling=

(24-*hour measurement of right ear*

−0-hour measurement of right ear)

−(24-hour measurement of left ear

−0-hour measurement of left ear)$\times 10^{-3}$ mm.

CTL Assay

Recipient mice were killed, and their spleens and draining lymph nodes (LNs) were removed. Cervical LNs from the same side as the corneal graft were harvested as draining LNs. Single-cell suspensions from 5×10^6 splenocytes and 4×10^6 LN cells were restimulated for 3 days, respectively, with irradiated (30 Gy) 5×10^6 and 4×10^6 splenocytes from the donor syngeneic mice. Draining LNs were recovered from four to six mice per group and processed together. Naive mice LNs and splenocytes were the negative controls. Allospecific CTLs were assayed with a 4-hour chromium-51 (^{51}Cr) release assay using donor syngeneic EL-4 (H-2^b) tumor target cells. Maximum and spontaneous ^{51}Cr release rates, respectively, were determined by measuring the amount of ^{51}Cr released into the medium by ^{51}Cr-labeled targets incubated with 1% Nonidet P-40 and into the medium without effector cells. The percentage of cytotoxicity was calculated according to the following formula:

% Specific ^{51}Cr release=(experimental release cpm

−spontaneous release cpm)

÷(maximum release cpm

−spontaneous release cpm)$\times$100.

Statistical Analysis

The Mann–Whitney *U* test was used to compare the opacity scores and the DH, and the Student's *t*-test was used to compare the CTLs. Graft rejection rates were compared using Fisher's exact method. $P < 0.05$ was considered significant.

RESULTS

Clinical Course

The isografts with AS ($n = 10$) remained clear during the postoperative observation period (data not shown). All the allografts with or without AS became clear before and after suture removal. Figures 1A and 1B show anterior segment photographs with or without AS on postoperative day 10. Unlike the round pupil in the AS− group, the iris in the AS+ group was connected to the cornea. In the AS+ group, mild vascular invasion of the cornea was observed around the iris synechiae. Figure 2 shows the average postoperative corneal graft opacity scores of both groups. In the AS− group, 50% (14/28) of the corneal grafts had stromal opacity with edema and were considered rejected (AS−Rej group), whereas 50% of the corneal grafts remained transparent 3 weeks after surgery (AS−Acc group). However, 81% (17/21) of the corneas in the AS+ group had graft opacity scores higher than 2+. The mean opacity scores of the AS+ group were consistently higher than those of the AS− group throughout the observation period. At the last observation (8 weeks), the recipient grafts had opacity scores of 3+ or more in 54% (15/28) of the AS− group and 86% (18/21) in the AS+ group ($P = 0.03$).

Histologic Evaluation

Many mononuclear cells infiltrated both the host and the graft, and the corneal grafts were edematous in both the AS+ and AS−Rej groups 3 weeks after transplantation. In the AS+ group in which the grafts were successful, many mononuclear cells were observed at the site of AS. In contrast, some infiltrating cells were present, but graft edema was not evident in the AS−Acc group (data not shown).

Immunohistochemical Study of the Cornea

Table 1 shows the average number of cytokine-positive, $CD4^+$ and $CD8^+$ cells in the host and graft observed by microscopy 3 weeks after surgery. In the AS+Rej and AS−Rej groups, there were numerous $CD4^+$ and $CD8^+$ cells in both the host and the graft of the cornea, with more $CD8^+$ cells in the graft detected in the AS+Rej group. Th1 cytokine–positive cells were present

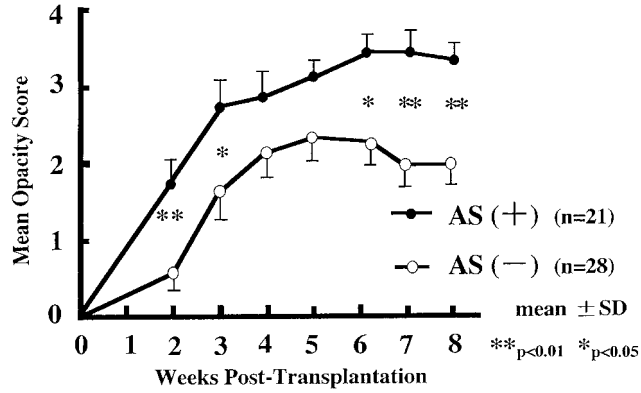

FIGURE 2. Average graft opacity scores of mice with and without anterior synechiae (AS) that underwent engraftment. Scores of the AS+ group are higher than those of the AS− group. Significant statistical differences between the AS+ and AS− groups are shown for opacity scores at 2, 3, 6, 7, and 8 weeks. The presence of AS increased the opacity score of the corneal grafts.

TABLE 1. Immunohistochemical Study of Corneal Grafts 3 Weeks after Surgery

	AS+Rej		AS+Acc		AS−Rej		AS−Acc	
Group	**Host**	**Graft**	**Host**	**Graft**	**Host**	**Graft**	**Host**	**Graft**
CD4+	+++	++++	++	+++	+++	++++	++	++
CD8+	++	+++	++	++	++	++	+	+
IFN-γ	+++	++++	++	++	+++	++++	+	+
IL-2	+++	++++	++	+++	+++	++++	++	++

Gradings of the averaged positive cells are presented for each group ($n = 3$). AS+Acc group was examined in a section with anterior synechiae ($n = 1$).

+, 1–10; ++, 11–20; +++, 21–30; ++++, ≥31 cells.

AS, anterior synechiae; Rej, rejected allograft; Acc, accepted allograft; IL-2, interleukin-2; IFN-γ, interferon-gamma.

in the host and the graft in the AS−Acc group, but there were fewer cells than in the AS+Rej, AS+Acc, and AS−Rej groups.

DH Assay

In the AS− group, DH responses to the donor alloantigens correlated well with the determination of rejection or acceptance of the grafts during the third week after surgery (Fig. 3). There was a significant difference between the AS−Rej and AS−Acc groups ($P < 0.01$). Some mice in the AS+ group in which the corneal grafts were rejected, however, had lower DH responses to donor alloantigens. No significant differences in DH responses to donor alloantigens were found between the AS− (both the rejected and accepted groups) and AS+ groups.

CTL Assay

Allospecific CTL responses during the third week are shown in Figure 4. Splenocytes of the AS+ group had greater CTL responses compared with the AS− group (effector/target ratio; 50, 100, $P < 0.05$) and the normal control groups (all effector/target ratios, $P < 0.05$) (Fig. 4A). There were no significant differences between the AS− Acc and AS+Rej groups (data not shown) or between the AS− and normal control groups in the splenocytes. CTL activity of the draining LNs in the AS+ group was higher than in the AS−Rej and AS−Acc groups. (Fig. 4B). Data are representative of two experiments.

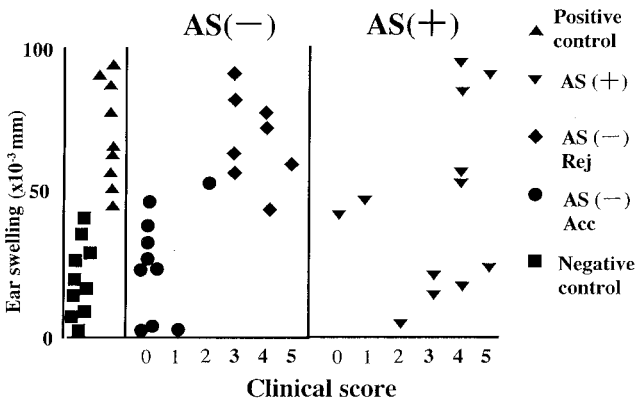

FIGURE 3. Delayed hypersensitivity responses in the anterior synechiae AS+ and AS− groups 3 weeks after surgery. Clinical scores of 3, 4, and 5 indicate rejection of the grafts. All the operations were performed on 2 consecutive days. Mice immunized with donor syngeneic splenocytes and naive mice were the positive and negative controls, respectively. Ear thickness was measured 24 hours after ear challenge with donor-syngeneic, irradiated splenocytes. The correlation between the clinical opacity score and ear swelling shows a significant difference between the AS−Rej and the AS−Acc groups ($P < 0.01$). Some mice in the AS+ group had low DH responses together with clinical scores of 3, 4, and 5 that indicate rejection of the grafts. There is no significant difference between the AS+ and AS− groups.

DISCUSSION

In this strain combination of a murine corneal transplantation model, the disparity in minor histocompatibility, rather

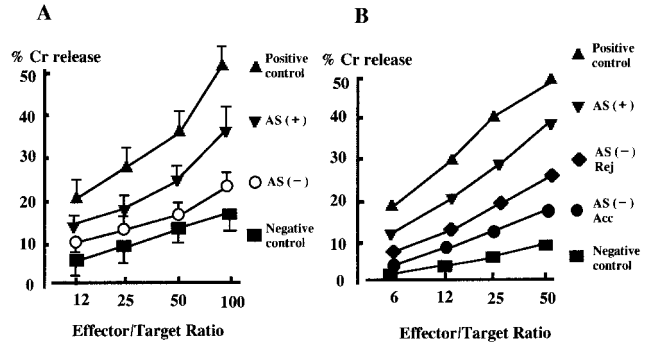

FIGURE 4. Cytotoxic T-lymphocyte (CTL) responses 3 weeks after transplantation. Effector cells derived from BALB/c mice (H-2^d) engrafted with a corneal from C57BL/6 (H-2^b) (B6) mice were stimulated for 3 days with B6-irradiated splenocytes. A 4-hour ^{51}Cr release assay with EL-4 (H-2^b) as the target cells at the indicated effector:target ratios was performed. Mice immunized with a 1×10^7 subcutaneous injection of B6 splenocytes and naive mice were the positive and negative controls, respectively. Results are given as the mean percentage of specific lysis (error bars, ±SEM). Spontaneous release was less than 10% of the maximum release. (**A**) Splenocytes used as the effector cells. The anterior synechiae (AS) group shows significantly greater cytotoxicity against the donor syngeneic alloantigen than do the mice without AS (effector:target ratios: 50, 100, $P < 0.05$) and normal control mice (all effector: target ratios, $P < 0.05$). There is no significant difference between AS−Rej and AS−Acc groups (data not shown). Ten mice constituted the AS− group; four to six mice constituted the other groups. One of two representative data sets is shown. (**B**) Draining lymph nodes (DLNs) used as effector cells with a group of four to six mice. LNs of mice with AS (AS+) and mice without AS in which the grafts were rejected (AS−Rej) have greater CTL activity than mice without AS in which the grafts were successful (AS−Acc). One of two representative data sets is shown.

than the major histocompatibility complex (MHC) alloantigen, is a greater barrier to allograft acceptance.[11] Moreover, DH responses, rather than CTL activities, were closely associated with the incidence of allograft rejection.[12] These unique characteristics, distinct from other vascularized organ transplants, may be correlated with immune privilege and are the reasons why further immunologic mechanisms must be determined.

We analyzed immunologic properties 3 weeks after transplantation, the critical point in determining the fate of a corneal graft[10] and for clarifying dynamic cellular immunity.[12] Our findings clearly show that the presence of AS increased the rejection rate in the murine corneal transplantation model and that enhanced rejection was mediated by CTL activity. Allorejection in corneal transplantation is Th1 cytokine predominant; Th2 cytokines do not have a major role in allograft rejection.[8,9] In the present study, the corneal Th1 cytokine expression pattern in the AS+ group became the same as that of the rejected group without AS, indicating that AS increases the probability of having the same cytokine expression pattern as in the AS−Rej group in the cornea. Although both the DH response and CTL activity are mediated by Th1 cytokines,[13] these cytokines in the AS+ group were associated with upregulation of CTL activity rather than the DH response, as indicated by the low DH response in some of the mice with AS in which the graft was rejected.

It is unclear why AS, which adds another pathway for presenting alloantigens to recipient T cells, enhances CTL activity alone. The cornea forms the anterior border of the ocular anterior chamber, and antigens may be introduced only through the corneal limbus and aqueous humor in normal eyes. Contact with a donor cornea by recipient iris vessels in the AS+ group, however, may have increased the chance of allorecognition by MHC class I–restricted $CD8^+$ lymphocytes and elicited CTL activity by using donor-derived MHC class I antigen expression on the corneal graft. The greater $CD8^+$ T-cell infiltration in the graft supports the enhancement of CTL activity in the AS+ group. Moreover, compared with the clear graft found in most of the AS− group 2 weeks postoperatively, the high opacity score of the grafts in the AS+ group may indicate that the vascular-rich iris induces allorecognition, which leads to shortening of the time from transplantation to rejection.

A similar high-risk model of corneal transplantation, a prevascularization model of the graft bed, has been reported.[14] Interestingly, this model enhanced both CTL in the draining LNs and DH responses 2 weeks after grafting.[14,15] The actual mechanisms by which this prevascularized model and our AS model show different cell-mediated immune responses are not known. In the prevascularized model, allorecognition through preexisting vessels around the corneal limbus may accelerate cell-mediated immunity, both the CTL and DH responses, and easily override ocular immune privilege.

In conclusion, AS is a critical risk factor for allograft rejection in murine corneal transplantation because it intensifies CTL activity, not the DH response. Corneal cytokine expression patterns in the AS+ group became similar to those in the rejected allograft group without AS.

References

1. Streilein JW, Ksander BR, Taylor AW. Immune deviation in relation to ocular immune privilege. *J Immunol.* 1997;158:3557–3560.
2. Price FW, Whitson WE, Marks RG. Graft survival in four common groups of patients undergoing penetrating keratoplasty. *Ophthalmology.* 1991;98:322–328.
3. Williams KA, Roder D, Esterman A, Muehlberg SM, Coster DJ. Factors predictive of corneal graft survival. *Ophthalmology.* 1992; 99:403–414.
4. Bourne WM. Reduction of endothelial cell loss during phakic penetrating keratoplasty. *Am J Ophthalmol.* 1980;89:787–790.
5. Cherry PMH, Pashby RC, Tadros ML, et al. An analysis of corneal transplantation: 1-graft clarity. *Ann Ophthalmol.* 1979;11:461–469.
6. Tragakis MP, Brown SI. The significance of anterior synechiae after corneal transplantation. *Am J Ophthalmol.* 1972;74:532–533.
7. Smolin G, Biswell R. Corneal graft rejection associated with anterior iris adhesion: case report. *Ann Ophthalmol.* 1978;10:1603–1604.
8. Yamagami S, Kawashima H, Endo H, et al. Cytokine profiles of aqueous humor and graft in orthotopic mouse corneal transplantation. *Transplantation.* 1998;66:1504–1510.
9. Sano Y, Osawa H, Sotozono C, Kinoshita S. Cytokine expression during orthotopic corneal allograft rejection in mice. *Invest Ophthalmol Vis Sci.* 1998;39:1953–1957.
10. Yamagami S, Kawashima H, Tsuru T, et al. Role of Fas-Fas ligand interactions in the immunorejection of allogeneic mouse corneal transplantation. *Transplantation.* 1997;27:1107–1111.
11. Sonoda Y, Streilein JY. Orthotopic corneal transplantation in mice: evidence that the immunogenetic rules of rejection do not apply. *Transplantation.* 1992;54:694–703.
12. Joo CK, Pepose JS, Stuart PM. T-cell mediated responses in a murine model of orthotopic corneal transplantation. *Invest Ophthalmol Vis Sci.* 1995;36:1530–1540.
13. Mosmann DA, Coffman RL. Heterogeneity of cytokine secretion patterns and functions of helper T cells. *Adv Immunol.* 1989;46:111–147.
14. Sano Y, Ksander BR, Streilein JW. Fate of orthotopic corneal allografts in eyes that cannot support anterior chamber-associated immune deviation induction. *Invest Ophthalmol Vis Sci.* 1995;36: 2176–2185.
15. Ksander BR, Sano Y, Streilein JW. Role of donor-specific cytotoxic T cells in rejection of corneal allografts in normal and high-risk eyes. *Transplant Immunol.* 1996;4:49–51.

Bioactivity of Peptide Analogs of the Neutrophil Chemoattractant, *N*-Acetyl-Proline-Glycine-Proline

Jeffrey L. Haddox,[1] *Roswell R. Pfister,*[1] *Donald D. Muccio,*[2] *Matteo Villain,*[2] *Charnell I. Sommers,*[1] *Manjula Chaddha,*[2] *G. M. Anantharamaiah,*[2] *Wayne J. Brouillette,*[2] *and Lawrence J. DeLucas*[2]

Purpose. The release of *N*-acetyl-proline-glycine-proline (PGP), a chemoattractant resulting from direct alkaline hydrolysis of corneal proteins, is believed to be the initial trigger for neutrophil invasion into the alkali-injured cornea. The purpose of this study is twofold: (1) to compare the activity of *N*-acetyl-PGP with the bioactivities of other similar synthetic peptides in an effort to uncover information about this chemoattractant molecule, and (2) to test these peptide analogs as potential antagonists of *N*-acetyl-PGP.

Methods. The polarization assay was used to measure the potential chemotactic response of human neutrophils to peptides. Bioactivity was expressed as the peptide concentration required to produce 50% neutrophil polarization (EC_{50}). Antagonist activity was expressed as the peptide concentration required to produce 50% inhibition (ID_{50}) of polarization activated by *N*-acetyl-PGP.

Results. Peptide bioactivities (EC_{50}) were ranked as follows: APGPR (0.34 mM) > *N*-acetyl-PGP (0.5 mM) > *N*-$(PGP)_4$-PGLG (3 mM) = *t*-Boc-PGP (3 mM) > *N*-acetyl-PG (3.4 mM) > *N*-methyl-PGP (15 mM) = PGP (15 mM) > peptides without detectable activity (*t*-Boc-PGP-OMe, *N*-acetyl-P, PG, PGG, GP, GG and gly-pro-hyp). Peptides with no detectable bioactivity were tested as potential antagonists of neutrophil polarization induced by *N*-acetyl-PGP. Gly-Pro-Hyp inhibited *N*-acetyl-PGP activation of polarization at 20 mM (ID_{50}). No other synthetic peptide demonstrated a capacity for inhibition.

Conclusions. The minimum requirement to elicit bioactivity was the presence of PGP alone or derivatives of PG in which the *N*-terminal proline is blocked. Using this approach, active and inactive mimetic peptides of *N*-acetyl-PGP were produced. The most active peptide, APGPR, was equal to or slightly greater than *N*-acetyl-PGP, suggesting that more potent analogs might be designed. Gly-pro-hyp was the only inactive peptide analog to inhibit the chemoattractant. (*Invest Ophthalmol Vis Sci.* 1999;40:2427–2429)

Alkali-injury of the eye provokes a severe inflammatory reaction, largely composed of neutrophils.[1,2] This acute inflammatory response is responsible for corneal ulcerations and perforations, so characteristic of this disease. The release of *N*-acetyl-proline-glycine-proline (PGP), a chemoattractant resulting from direct alkaline hydrolysis of corneal proteins, is believed to be the initial trigger for neutrophil invasion into the alkali-injured cornea.[3,4] This finding created an opportunity to determine the active portions of the *N*-acetyl-PGP molecule. One avenue of approach is to investigate the activity of peptide analogs, which are structurally related to *N*-acetyl-PGP. To develop these structure–activity relationships, we synthesized a series of peptide analogs and evaluated them in a system that measures neutrophil polarization, the earliest stage of chemotaxis.

The major purpose of this study was to compare the activity of these peptides to the chemoattractant in an effort to uncover information about the relative importance of different portions of the *N*-acetyl-PGP molecule to biological activity. Additionally, these peptide analogs were tested as potential antagonists of *N*-acetyl-PGP.

Materials and Methods

Materials

Hanks' balanced salt solution (HBSS) was purchased from Gibco Laboratories (Chagrin Falls, OH). Calcium chloride, magnesium chloride, sodium chloride, glutaraldehyde, and Ficoll (type 400) were purchased from Sigma Chemical Co. (St. Louis, MO). Sodium phosphate monobasic and sodium phosphate dibasic were obtained from Fisher Scientific (Fair Lawn, NJ). Hypaque-76 was acquired from Winthrope Laboratories (New York, NY). Leukotriene B_4 (LTB_4) was purchased from Biomol Research Laboratories (Plymouth Meeting, PA). Solvents and reagents for peptide synthesis were purchased from VWR Scientific Products (West Chester, PA). Resin and suitably derivatized amino acids were purchased from Advanced Chem Tech (Louisville, KY) or PerSeptive Biosystem (Framingham, MA).

Peptide Synthesis and Isolation

Several peptide analogs, *N*-acetyl-P, GG, PGG, gly-pro-hyp, and APGPR, were obtained from Sigma Chemical Co. Other peptides, PG, GP, PGP, *N*-acetyl-PG, *t*-Boc-PGP, and *t*-Boc-PGP-OMe, were synthesized by conventional solution phase peptide chemistry. However, for large-scale synthesis of *N*-acetyl-PGP, an alternative method was used to increase the yield of the product. In this method, the dipeptide *t*-Boc-PG was coupled to Pro-Merrifield resin (Nova Biochem, San Diego, CA) using the dicyclohexylcarbodiimide/1-hydroxybenzotriazole procedure. After the removal of the N-terminal protection and acetylation using acetic anhydride, the peptide was cleaved from the resin, using anhydrous hydrofluoric acid. The product was purified on a silica gel column, using chloroform:methanol (90:10, vol/vol) as the eluent.

The starting compound for the synthesis of *N*-methyl-PGP was *t*-Boc-PGP. The removal of N terminus *t*-Boc and the addition of *N*-methyl group were accomplished by a modified Mannich reaction.[5] Briefly, the reaction mixture consisted of

From [1]The Eye Research Laboratories, Brookwood Medical Center, Birmingham, Alabama; and the [2]University of Alabama at Birmingham.

Supported by National Eye Institute Grant EY04716. Mass spectrometry was performed by Marion Kirk at the UAB Comprehensive Cancer Center Mass Spectrometry Shared Facility, which is supported in part by a National Cancer Institute Core Research Support Grant P30CA13148. The mass spectrometer was purchased by funds from a National Institutes of Health Instrumentation Grant S10RR06487 and from UAB.

Submitted for publication September 28, 1998; accepted November 6, 1998.

Proprietary interest category: N.

Corresponding author: Roswell R. Pfister, Suite 504, 513 Brookwood Boulevard, Birmingham, AL 35209.
E-mail: jhaddox@scott.net

30% formaldehyde, 98% formic acid (50 times molar excess to *t*-Boc-PGP), and freshly prepared palladium black. The reaction mixture was incubated overnight at 50°C, and the reaction was followed for completion by thin-layer chromatography. After the filtration of palladium black, the reaction mixture was diluted with water and lyophilized.

The homogeneity of each peptide was confirmed by reversed-phase high-performance liquid chromatography (RP-HPLC) on a Vydac C18-analytical column equilibrated at a flow rate of 1.2 ml/min and eluted with a linear gradient from 0% to 30% acetonitrile in water (0.1% trifluoroacetic acid) in 30 minutes. Characterization was done using Electrospray Mass Spectrometry (Perkin-Elmer-Sciex API-3, Norwalk, CT). Quantitative amino acid analysis was performed to show the correct ratio of amino acids and to determine the peptide content for calculation of the final concentration.

The PGP polymer, *N*-$(PGP)_4$-PGLG, was synthesized on a PerSeptive Biosystem 9050 Peptide synthesizer, using flow solid-phase peptide synthesis with Fmoc chemistry. This technique used preactivated Opfp amino acids with HOAt and preloaded PEG-PS resin. The polymer was purified by RP-HPLC on a Waters Delta Pack C18 A (300 × 39 mm ID). Purity was determined by RP-HPLC on a Dynamax C18 column (300 × 4.8 mm ID) equilibrated at a flow rate of 1 ml/min and eluted with a linear gradient from 5% to 80% CH_3CN (0.1% TFA) in 40 minutes The identity of the polymer was confirmed by TOF-MALDI MS (PerSeptive Biosystem).

Preparation of Solutions

LTB_4 was dissolved in ethanol and diluted with HBSS (pH 7.3) to a final ethanol concentration of 0.001%. Synthetic peptides were dissolved in HBSS (pH 7.3). When necessary, the osmolality was adjusted between 280 and 320 mOsm by adding a small amount of distilled water.

Neutrophil Isolation

These experiments followed the tenets of the Declaration of Helsinki and were approved by the Human Research Committee at Brookwood Medical Center. All donors signed written consent forms explaining the nature and possible consequences of the study. Blood was collected from only one donor each day. Following the technique of Ferrante and Thong, neutrophils were isolated from fresh heparinized human blood by centrifugation on Hypaque–Ficoll (density = 1.114), as previously described.[6,7] Isolated neutrophils (96%–99% viability) were resuspended in HBSS with 15 mM phosphate buffer at room temperature and gently agitated on a shaker. The purity of this cell suspension was ≥ 85% neutrophils and ≤ 5% mononuclear cells and platelets, with the remaining percentage consisting of red blood cells. Purified neutrophils were used in the polarization assay. All incubation mixtures were maintained between an osmolality of 280 to 320, a pH of 7.2 to 7.6, 15 mM phosphate buffer, and 50 μM Ca^{2+} and 50 μM Mg^{2+}.

Neutrophil Polarization Assay

The polarization assay was performed in a blind fashion. This assay was used to measure the neutrophil response to LTB_4 or synthetic peptides by determining the polarization index, a measure of the frequency and degree of cellular shape change after exposure to a chemoattractant.[8] Briefly, preincubated neutrophils (2×10^5) were mixed with preincubated synthetic peptides in HBSS in a reaction chamber (total volume = 100 μl) at 37°C for 5 minutes. At the end of the incubation period, an aliquot was collected and mixed with an equal volume of 4% glutaraldehyde for microscopic observation. The remaining volume of each cell suspension was centrifuged immediately at 15,000*g* for 5 seconds to remove cells. The resulting supernatant was analyzed for lactic dehydrogenase (LDH) activity.[9] All incubations generated LDH activity, correlating with <5% cell death. Neutrophils in each sample were observed microscopically and assigned scores of 0 (resting = spherical cell with a smooth membrane), 1 (activated = irregular cell with uneven membranes), or 2 (polarized = cell length ≥ width × 2). Scores of 100 neutrophils for each sample were added and corrected by subtracting negative control values (neutrophils in HBSS only), which produced a polarization index. Bioactivity (EC_{50}) was expressed as the peptide concentration required to produce a neutrophil polarization index equal to 50% of the positive control (2×10^{-9} M LTB_4). Inhibition (ID_{50}) was expressed as the peptide concentration required to produce 50% inhibition of the EC_{50} level of polarization.

Table 1. Bioactivity of Synthetic Peptide Analogs

Synthetic Peptides	EC_{50} (mM)
APGPR	0.34 ± 0.05
N-acetyl-PGP	0.5 ± 0.1
t-Boc-PGP	3.0 ± 2.3
[*N*-$(PGP)_4$-PGLG]	3.0 ± 1.3
N-acetyl-PG	3.4 ± 2.2
N-methyl-PGP	15.0 ± 2.1
PGP	15.0 ± 3.6
N-acetyl-P	>40.0
GG	>40.0
PG	>40.0
GP	>40.0
PGG	>40.0
Gly-pro-hyp	>40.0
t-Boc-PGP-OMe	>40.0

Values are means ± SD; n = 4 to 9. EC_{50} was interpolated from dose–response curves of the neutrophil polarization index.

Results

Polarization Activity of Peptide Analogs of *N*-acetyl-PGP

Several peptide analogs of *N*-acetyl-PGP were synthesized and evaluated in the neutrophil polarization assay (Table 1). The importance of the terminal amino acid residues was investigated first. Biological activity decreased in a systematic manner when the terminal amino acid(s) was omitted from the structure. *N*-acetyl-PG was sevenfold less active than *N*-acetyl-PGP, and activity was eliminated for the simple blocked proline derivative, *N*-acetyl-P. Simple dipeptides, GG, PG, or GP, and tripeptides, PGG and gly-pro-hyp, also were inactive. Two tripeptides, *t*-Boc-PGP and *t*-Boc-PGP-OMe, were synthesized to determine whether a free carboxyl terminus is needed for biological activity. Although *t*-Boc-PGP demonstrated sixfold less activity than *N*-acetyl-PGP, it did retain substantial activity. The tripeptide with blocking groups at both ends was inactive, suggesting that a free carboxyl group is needed for activity. These results demonstrated the importance of the terminal residues to induce neutrophil polarization.

TABLE 2. Inhibitory Properties of Synthetic Peptides

Synthetic Peptides	ID_{50} (mM)
Gly-pro-hyp	20.0 ± 5.6
N-acetyl-P	>70.0
t-Boc-PGP-OMe	>70.0
PG	>70.0
PGG	>70.0
GP	>70.0
GG	>70.0

Values are means ± SD; $n = 4$. Neutrophils were activated with 500 μM *N*-acetyl-PGP. ID_{50} was interpolated from dose–response curves of the polarization index.

Next, we examined the importance of the *N*-acetyl group on biological activity. The unblocked tripeptide, PGP, was 30-fold less active than *N*-acetyl-PGP. Interestingly, the activity of the *N*-methyl derivative of PGP was comparable to the unblocked tripeptide. Apparently, this amino blocking group added little to the activity of the tripeptide. However, when a bulkier *t*-Boc group was used instead of the *N*-acetyl group to block the N terminus of the tripeptide, the activity of *t*-Boc-PGP was increased relative to PGP, but it was still sixfold less than the activity of *N*-acetyl-PGP. Taken together, the *N*-acetyl group provides an important structural component to *N*-acetyl-PGP; analogs with no or other N-terminal blocking groups have lower activity.

Finally, we investigated if an extended PGP sequence could induce neutrophil polarization. A PGP polymer [*N*-$(PGP)_4$-PGLG] containing 4 repeats of the PGP sequence was prepared. The activity of this peptide was 10-fold less than the simpler *N*-acetyl-blocked tripeptide, suggesting that these extended sequences are less effective than a shorter blocked PGP sequence. The most interesting discovery reported here deals with a pentapeptide, APGPR, containing the PGP sequence. This pentapeptide displayed activity equal to or slightly greater than *N*-acetyl-PGP.

Inhibitory Properties of Synthetic Analogs

Synthetic analogs showing no detectable bioactivity were tested as potential inhibitors of *N*-acetyl-PGP–activated neutrophils. Gly-pro-hyp (ID_{50} = 20 mM) was the only analog showing measurable inhibition when concentrations up to 70 mM were tested (Table 2).

DISCUSSION

N-acetyl-PGP is generated directly by alkali degradation of corneal proteins.[3] The synthesis of peptide analogs of this chemoattractant identified several similar, new bioactive peptides for neutrophils and a number of inactive peptides. The small size of the *N*-acetyl-PGP molecule and the ability to manipulate the amino acid sequence lended itself to studies that differentiated those components of the chemoattractant responsible for its activity. This was accomplished by selecting specific groups on the *N*-acetyl-PGP molecule to add, substitute, and/or omit during synthesis of the peptide analog.

For substantial bioactivity the analog required the presence of PGP alone or derivatives of PG in which the N-terminal proline is blocked. The presence of an acetyl- or *t*-Boc–blocking group on the N terminus of the tripeptide produces an uncharged amide at physiological pH. In contrast, PGP and *N*-methyl-PGP are very similar peptides in that both contain a positively charged amino N terminus at physiological pH. The favorable activity with a neutral amide elucidates a fuller understanding of the determinants of chemoattraction. This information is anticipated to prove useful in the structure-based design of antagonists.

In this study APGPR, an activation pentapeptide for procolipase, produced equal or slightly greater polarization activity than *N*-acetyl-PGP. The potent activity of this agonist, containing the PGP sequence, gives promise that more agonists could be designed to further enhance biological activity. Pursuit of this line of investigation might be in the direction of other tetrapeptides or pentapeptides containing the PGP sequence but with an amide-protected N terminus, such as *N*-acetyl-APGPR. These findings might further studies of the inflammatory process and receptor recognition.

The current approach generated one antagonist of neutrophil chemotaxis. High concentrations of gly-pro-hyp showed measurable inhibition of the chemoattractant. The potency of the gly-pro-hyp antagonist might be enhanced by further alteration of the molecule. A more feasible and powerful approach to secure a potent inhibitor might be the more time and cost efficient technology of using antisense peptides.[10] This technology has yielded promising results in preliminary studies.

Acknowledgments

Amino acid analysis was performed by Kelly Morrison at the UAB Glycoprotein Analysis Core Facility.

References

1. Kenyon KR, Berman M, Rose J, Gage J. Prevention of stromal ulceration in the alkali-burned rabbit cornea by glued-on contact lens. Evidence for the role of polymorphonuclear leukocytes in collagen degradation. *Invest Ophthalmol Vis Sci.* 1979;18:570–587.
2. Foster CS, Zelt RP, Mai–Phan T, Kenyon KR. Immuno-suppression and selective inflammatory cell depletion. Studies of a guinea pig model of corneal ulceration after ocular alkali burning. *Arch Ophthalmol.* 1982;100:1820–1824.
3. Pfister RR, Haddox JL, Sommers CI, Lam K–W. Identification and synthesis of chemotactic tripeptides from alkali-degraded whole cornea: a study of *N*-acetyl-Proline-Glycine-Proline and *N*-methyl-Proline-Glycine-Proline. *Invest Ophthalmol Vis Sci.* 1995;36:1306–1316.
4. Pfister RR, Haddox JL, Sommers CI. Injection of chemoattractants into normal cornea: a model of inflammation after alkali-injury. *Invest Ophthalmol Vis Sci.* 1998;39:1744–1750.
5. March J. *Advanced Organic Chemistry: Reactions, Mechanisms and Structure.* New York: McGraw-Hill Book Co.; 1977:820–823.
6. Ferrante A, Thong YH. A rapid one-step procedure for purification of mononuclear and polymorphonuclear leukocytes from human blood using a modification of the Hypaque-Ficoll technique. *J Immunol Methods.* 1978;24:389.
7. Pfister RR, Haddox JL, Harkins LE, Dodson RW. The effects of citrate on fMLP induced polymorphonuclear leukocyte stimulation and locomotion. *Cornea.* 1984/1985;3:183–188.
8. Haston WS, Shields JM. Neutrophil leukocyte chemotaxis: a simplified assay for measuring polarizing responses to chemotactic factors. *J Immunol Methods.* 1985;81:229–237.
9. Decker LA, ed. Lactate dehydrogenase. *Worthington Enzyme Manual.* Freehold, NJ: Worthington Biochemical Corp.; 1977:19–22.
10. Blalock JE. Genetic origins of protein shape and interaction rules. *Nat Med.* 1995;1:876–878.

Effect of Metalloproteinase Inhibitor on Corneal Cytokine Expression after Alkali Injury

Chie Sotozono, Jiucheng He, Mamoru Tei, Yoich Honma, and Shigeru Kinoshita

Purpose. Interleukin (IL)-1α and IL-6 levels in the cornea are greatly elevated during the early stages after an alkali burn in mice. The authors investigated the effect of synthetic inhibitor of matrix metalloproteinase (SIMP) on the expression of inflammatory cytokines in alkali-burned murine corneas and evaluated the clinical appearance of the eyes.

Methods. After 0.5N NaOH-alkali burns to 400 corneas of ICR mice, 200 received 400 μg/ml of SIMP topically 4 times a day while 200 corneas were similarly treated with vehicle only. At days 4, 7 and 14 after injury, each cornea was assigned a clinical score for corneal opacity, corneal epithelial defect, hyphema and cataract. Extracts of injured corneas in each group were then assayed for cytokine production using ELISA systems for IL-1α, IL-1β, IL-6 and tumor necrosis factor-α (TNF-α).

Results. The levels of IL-1α, IL-1β and IL-6 were significantly lower in the SIMP-treated group than in the vehicle-treated group 7 days after the burn. However, levels of these cytokines were similar in the SIMP and non-SIMP groups at days 4 and 14. Levels of TNF-α did not differ between both groups at any postinjury time. In the SIMP-treated corneas, there was less opacification and hyphema formation and epithelial regeneration was faster.

Conclusions. Topical application of SIMP in alkali-burned murine corneas reduced the expression of IL-1α, IL-1β, and IL-6 and lessened the severity of the injury. (*Invest Ophthalmol Vis Sci.* 1999;40:2430–2434)

The matrix metalloproteinase (MMP) family of enzymes are found in cornea.[1–5] An increased release of MMPs after an alkali burn is thought to be responsible for the destruction of the alkali-burned cornea,[6–9] a condition that is typically uncontrollable. Previous reports have revealed that matrix metalloproteinase inhibitors (MMPI), such as a thiol peptide,[10] tissue inhibitor of matrix metalloproteinase (TIMP),[11] and synthetic inhibitor of matrix metalloproteinase (SIMP)[12,13] are effective in the treatment of alkali injuries. These reports demonstrated that MMPI-treated eyes have less inflammatory cell infiltration and less destruction of corneal collagen compared to vehicle-treated control eyes. However, the mechanisms of effect of MMPIs have not been fully clarified.

Our recent research has demonstrated clearly that interleukin (IL)-1α and IL-6 are highly expressed in the cornea during the early stages after an alkali burn and may play an essential role in polymorphonuclear leukocyte (PMN) infiltration or associated corneal damage after the burn.[14,15] To more fully understand the mechanisms of MMPI action, we investigated the effect of MMPI on cytokine expression in the alkali-burned murine cornea.[14]

Materials and Methods

Synthetic Inhibitor of Matrix Metalloproteinase

We used SIMP developed by Galardy and associates.[12,16] This is an extremely potent inhibitor of fibroblast collagenase, gelatinase, and stromelysin and is also known as Galardin or GM6001. The compound is a dipeptide analogue with the structure *N*-[2(R)-2-(hydroxamido carbonylmethyl)-4-methylpentanoyl]-L-tryptophane methylamide. For topical application, SIMP was dissolved at a concentration of 400 μg/ml in *N*-2-hydroxyethylpiperazine-*N*′-2-ethane sulfonic acid (HEPES) buffer containing 2% dimethyl sulfoxide (pH 7.4). SIMP was gifted from Sankyo Co., Ltd. (Tokyo, Japan). For use as the control vehicle (pH 7.4), HEPES buffer containing 2% dimethyl sulfoxide was prepared. The solutions were stored at 4°C until use.

Animals

Seven-week-old female ICR mice were used in this experiment. The animals were housed in plastic cages in a room with a 12-h light/12-h dark cycle. They were free from ocular disease. All mice were treated in compliance with the guidelines of the ARVO Resolution on the Use of Animals in Ophthalmic and Vision Research, and the experimental protocol was approved by the Committee for Animal Research, Kyoto Prefectural University of Medicine.

Corneal Alkali Burn

An alkali burn was created as described previously.[14] Briefly, 2 μl of 0.5N NaOH was instilled to 400 corneas of ICR mice, with no subsequent eye-washing; 60 unburned corneas were used to confirm normal cytokine levels.

Treatment of Mouse Alkali Burns with SIMP

After alkali injuries to 400 corneas, 200 were randomly assigned for treatment with vehicle containing 400 μg/ml of SIMP, whereas the other 200 controls were assigned for treatment with vehicle only. Treatment was started 2 hours after the burn, and one drop of either SIMP solution or vehicle was applied topically four times a day, every 3.5 hours from 8 AM to 10 PM. This treatment regimen was continued for 14 days after the alkali burn.

At 4, 7, and 14 days after the burn, animals were sacrificed by severing the spinal cord. After the eyes were extracted, external examinations of each eye were performed by two independent examiners who were unaware of whether the animal had received SIMP or vehicle. Eyes were assessed for the presence of corneal opacity, corneal epithelial defects,

From the Department of Ophthalmology, Kyoto Prefectural University of Medicine, Kyoto, Japan.

Supported in part by a grant in-aid for scientific research (09877336, 08457467, 09771459) from the Japanese Ministry of Education, Culture and Science; a research grant from the Japanese Ministry of Health and Welfare; and the intramural research fund of the Kyoto Prefectural University of Medicine.

Submitted for publication January 7, 1999; revised April 6, 1999; accepted May 5, 1999.

Proprietary interest category: N.

Corresponding author: Chie Sotozono, Department of Ophthalmology, Kyoto Prefectural University of Medicine, Hirokoji, Kawaramachi, Kamigyoku, Kyoto 602-0841, Japan.
E-mail: csotozon@eyeeye.ophth.kpu-m.ac.jp

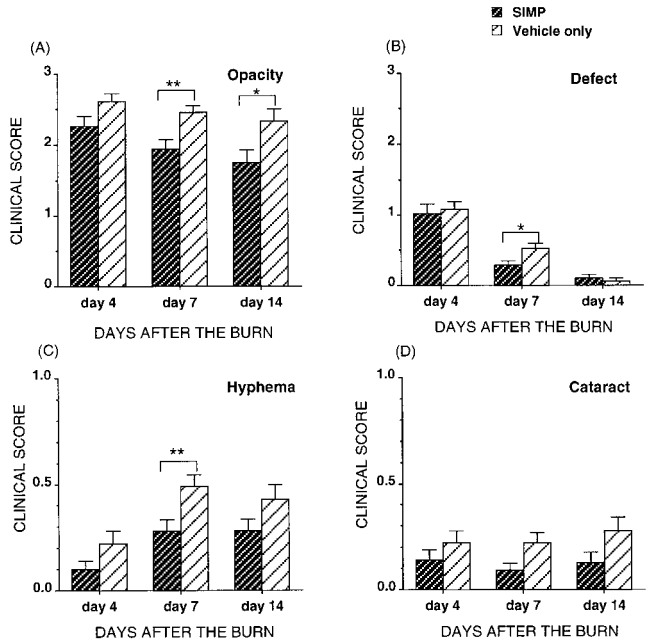

FIGURE 1. Time course for clinical scores after alkali burn. Two hours after 2 μl of 0.5N NaOH was applied to corneas of ICR mice to create an alkali burn, eyes were administered 400 μg/ml SIMP or vehicle only 4 times a day. (**A**) Area of corneal opacity; (**B**) area of corneal epithelial defect; (**C**) hyphema; (**D**) cataract. The details of how these clinical scores were arrived at are described in the Methods section. $^{*}P < 0.05$, $^{**}P < 0.005$ (Mann–Whitney U test).

hyphema, and cataracts. Each cornea was assigned a clinical score according to the area of corneal opacity using the after classification: 0, no opacity; 1, opacity covers less than one third of the corneal surface; 2, opacity covers more than one third and less than two thirds of the corneal surface; and 3, opacity covers more than two thirds of the corneal surface. The corneal epithelial defects were assigned a clinical score as follows: 0, no defects or superficial puctate keratitis; 1, epithelial defects cover less than one third of the corneal surface; 2, epithelial defects cover more than one third and less than two thirds of the corneal surface; 3, epithelial defects cover more than two thirds of the corneal surface. The presence of hyphema or cataract was classified as absent or present: 0, no hyphema; 1, existence of hyphema; 0, no cataract; 1, existence of cataract.

Histologic analyses also were performed for six SIMP-treated and six vehicle-treated eyes 14 days after the burn. These eyes were fixed with 4% paraformaldehyde in 0.1 M phosphate-buffered saline (PBS; pH 7.4) and then dehydrated with 20% sucrose in 0.1 M PBS. Specimens were embedded in O.C.T. compounds (Miles Inc., Elkhart, IN), after which 8-μm cryostat sections were cut, air-dried, and stained with hematoxylin-eosin.

Cytokine Quantitation

To examine changes in cytokine expression with topical application of SIMP, the concentrations of IL-1α, IL-1β, IL-6, and TNF-α were measured in both SIMP- and vehicle-treated corneas 4, 7, and 14 days after the burn, using enzyme-linked immunosorbant assay (ELISA) systems for IL-1α, IL-1β (Genzyme Co., Cambridge, MA), IL-6 (Endogen, Inc., Cambridge, MA), and TNF-α (Genzyme Co.). Uninjured corneas were used to confirm normal cytokine levels. At each time point, the eyes were extracted, and the supernatants of corneal lysates were prepared as described previously.[14,17] Briefly, excised corneas 3 mm in diameter were frozen in liquid nitrogen and then smashed and homogenized in PBS at a ratio of 100 μl per cornea. The supernatants were collected by centrifugation at 1500*g* for 10 minutes and stored at −80°C until use. Each test sample comprised 6 to 7 whole corneas, with 9 to 12 samples (60–80 corneas) used at each time point in both groups.

Statistics

Clinical scores were compared for significance using the Mann–Whitney U test. ELISA values were compared using Student's t-test.

RESULTS

Treatment of Mouse Alkali Burn with SIMP

Corneal opacification was graded as moderate to severe 4 days after an alkali burn in SIMP- and non-SIMP–treated eyes. Thereafter, it gradually receded until 14 days after the burn in both groups. The score for corneal opacification was significantly lower at postinjury days 7 and 14 in the SIMP-treated group than that in controls (Fig. 1A). The score for corneal epithelial defects was significantly lower than controls at day 7 in the SIMP-treated group. At postinjury day 14, the corneal epithelium had almost healed in both groups (Fig. 1B). In the vehicle-only group, hyphema was observed in 22% (average score, 0.22) of eyes 4 days after injury, in

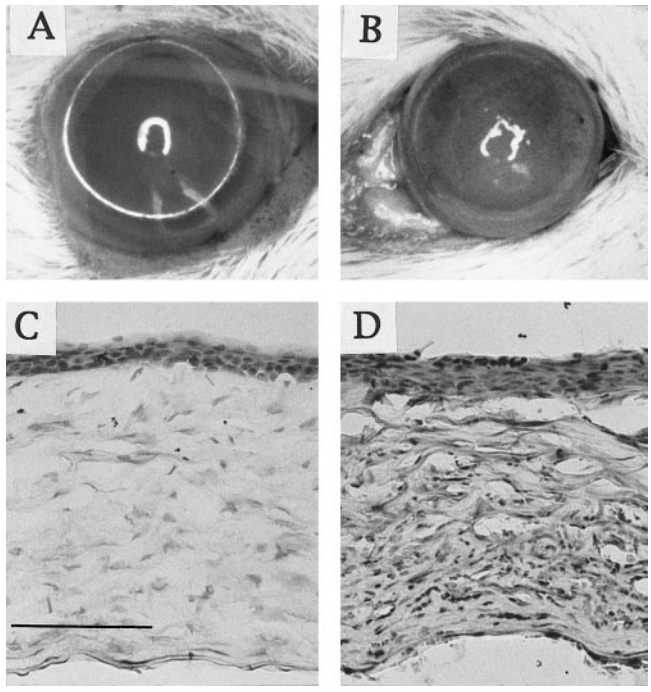

FIGURE 2. Mouse corneas treated for 14 days after an alkali burn with SIMP or vehicle only. Representative appearance of 400 μg/ml SIMP-treated eye (**A**, **C**) and vehicle-treated eye (**B**, **D**) 14 days after a 0.5N NaOH-alkali burn. (**C**, **D**) Histology of the central corneas seen in (**A**) and (**B**). Calibration bar, 100 μm.

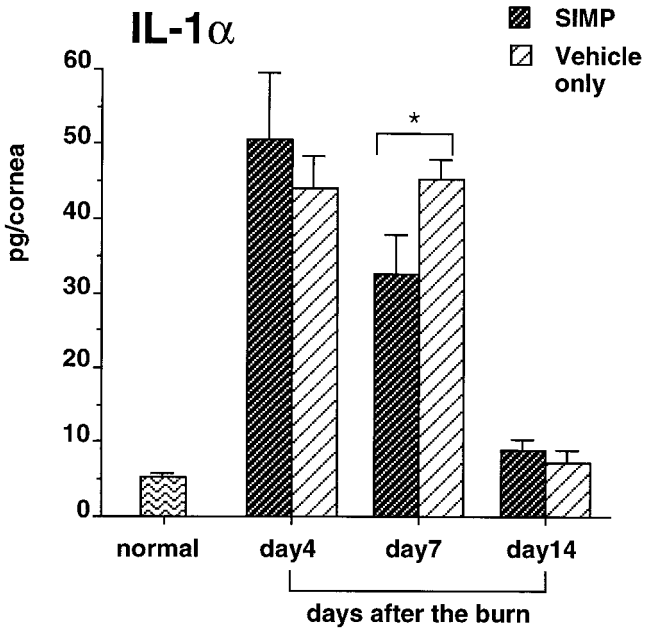

FIGURE 3. IL-1α concentrations in corneas treated with 400 μg/ml SIMP or vehicle only after a 0.5N NaOH-alkali burn. Uninjured corneas were used to confirm normal cytokine levels. The corneas used for the determination of the clinical score (Fig. 1) also were assayed for the presence of IL-1α. Each point represents mean ± SEM of 9 to 12 pooled samples, each sample comprising 6 to 7 corneas. Each column, therefore, represents the mean of 60 to 80 corneas. *$P < 0.025$ (Student's *t*-test).

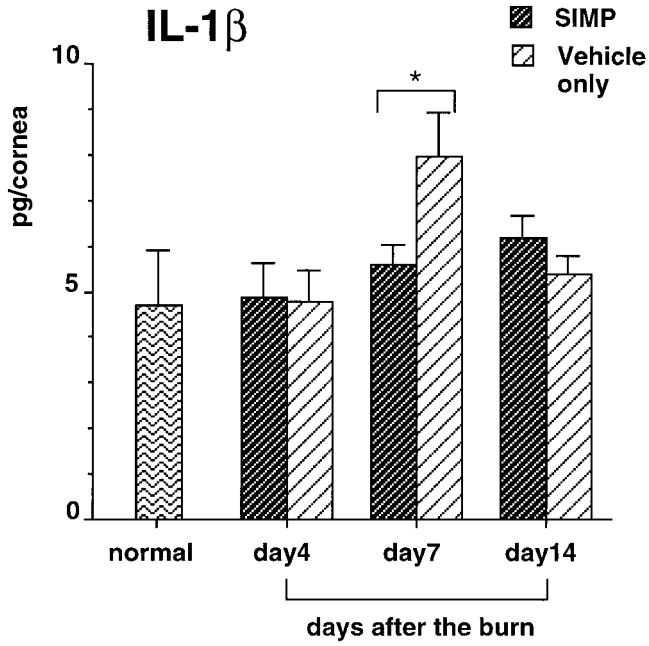

FIGURE 4. IL-1β concentration in corneas treated with 400 μg/ml SIMP or vehicle only after a 0.5N NaOH-alkali burn. The same samples used for the IL-1α measurement (Fig. 3) also were assayed for the presence of IL-1β. *$P < 0.05$ (Student's *t*-test).

49% (average score, 0.49) of eyes 7 days after injury, and in 43% (average score, 0.43) of eyes 14 days after injury. In contrast, in the SIMP-treated group, hyphema was observed in 28% (average score, 0.28) of eyes at day 7. This was significantly lower than in the control group (Fig. 1C). The scores for cataract were lower in the SIMP-treated group than in controls at all time points, but these were not statistically significant (Fig. 1D). Figure 2 shows the typical appearance of corneas 14 days after injury. Although SIMP-treated corneas (Figs. 2A, 2C) contained few inflammatory cells and little tissue destruction, control corneas treated with vehicle only (Figs. 2B, 2D) disclosed massive inflammatory cell infiltration and severe stromal destruction.

Cytokine Quantitation

In vehicle-treated corneas, IL-1α levels were greatly increased 4 and 7 days after the burn (its value was approximately 8.5 times the baseline value). Although the expression of IL-1α 4 days after injury was not different between SIMP- and vehicle-treated corneas, the level of IL-1α in the SIMP-treated group at day 7 was 32.5 ± 5.5 pg/cornea (mean ± SEM), significantly lower than in vehicle-treated corneas (45.2 ± 2.7 pg/cornea) (Fig. 3). At day 14 after the burn, the levels of IL-1α had returned almost to normal levels in both groups. The level of IL-1β at day 7 also was significantly lower in the SIMP-treated group (5.6 ± 0.4 pg/cornea) than in controls (8.0 ± 1.0 pg/cornea) (Fig. 4). At days 4 and 14 after injury, the levels of IL-6 did not differ between the two groups; however, the concentration of IL-6 in the SIMP-treated group at day 7 was 14.1 ± 2.7 pg/cornea, significantly lower than in controls (29.3 ± 6.6 pg/cornea) (Fig. 5). Levels of TNF-α were elevated approximately 1.2 times the baseline value in both the SIMP- and vehicle-treated corneas at day 7; however, the levels did not differ between the two groups (Fig. 6).

DISCUSSION

Alkali injury of the cornea is characterized by the massive infiltration of PMNs into the stroma and the severe destruction of

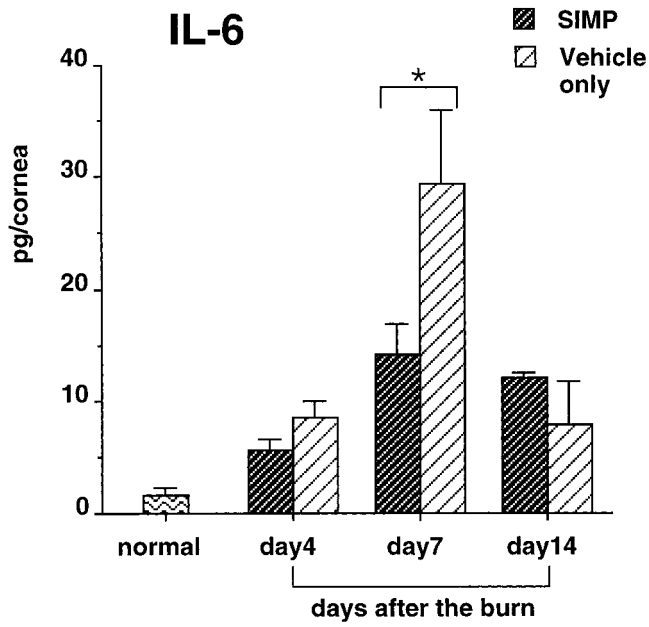

FIGURE 5. IL-6 concentration in corneas treated with 400 μg/ml SIMP or vehicle only after a 0.5N NaOH-alkali burn. The same samples used for the IL-1α measurements (Fig. 3) also were assayed for the presence of IL-6. **$P < 0.025$ (Student's *t*-test).

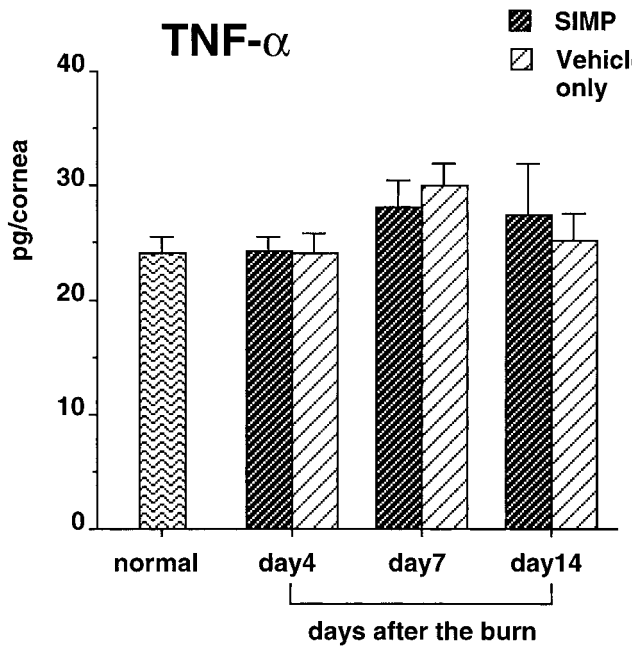

FIGURE 6. TNF-α concentration in corneas treated with 400 μg/ml SIMP or vehicle only after a 0.5N NaOH-alkali burn. The same samples used for the IL-1α measurements (Fig. 3) also were assayed for the presence of TNF-α.

corneal collagens. In our recent experiment, among the 10 cytokines examined, IL-1α and IL-6 were found to be induced strongly in alkali-burned corneas, the peak production of IL-1α being 3 days after injury and the peak production of IL-6 being 7 days after injury.[14,15] IL-1 and IL-6 can lead to infiltration by PMNs, after which these cells release superoxide, prostaglandins, lysosomal enzymes, or MMPs, which may cause corneal stromal melting. IL-1 also induces MMPs in cultured corneal stromal cells[18] and is known to induce corneal epithelial and stromal cells to express IL-6 and IL-8.[19–21] In addition, a recent report has demonstrated clearly that IL-1α induces MMPs and IL-8 in corneal fibroblasts extracted from wounds.[22] In view of this, inflammatory cytokines upregulated after an alkali burn are considered to be responsible for cell infiltration and collagen destruction.

The present study has demonstrated that the topical application of SIMP significantly reduces the expression of IL-1α, IL-1β, and IL-6 in alkali-burned mouse corneas 7 days after the injury. It is noteworthy that at 4 days after injury, the levels of IL-1α, IL-1β, and IL-6 were the same in SIMP- and vehicle-treated corneas, implying that the reduction of these cytokines that are seen 7 days after injury probably is a result of the indirect action of the SIMP. One kind of SIMP (thiol peptide) recently has been shown to have an inhibitory effect on the chemotaxis of PMNs.[23] However, on the basis of our data demonstrating that IL-1α and IL-6 after an alkali burn were mainly expressed in regenerating epithelium as opposed to infiltrating cells,[14] we consider that the reduction of inflammatory cytokines by the SIMP used in these experiments is not the result of the inhibitory effect on the chemotaxis of PMNs. Previous work has shown that the levels of IL-1α and IL-6 after an alkali burn correlate well with the concentration of alkali solution.[14,15] In view of this, it is likely that the expression of inflammatory cytokines in regenerating epithelium[14] correlates with the severity of the destruction of corneal collagens. We speculate that degraded corneal collagens induce regenerating epithelium to express IL-1α, IL-1β, and IL-6 and that the suppression of stromal degradation by SIMP results in less expression of cytokines in alkali-burned cornea. However, we cannot completely exclude the possibility that SIMP may prevent the activation or inhibit the expression of these cytokines by a mechanism(s) independent of stromal collagens.

Previous reports have demonstrated that MMPI prevents the ulceration of rabbit corneas after an alkali burn.[11–13] In this study, using a mouse alkali-burn model, we confirmed the beneficial effect of SIMP on corneal opacification, epithelial regeneration, and hyphema formation after the burn, although the effect is not immediate. Recently, Saika and associates[24] demonstrated that TIMPs enhance the spreading of the corneal epithelium ex vivo and the proliferation of corneal epithelial cells in vitro. Our data indicated that MMPIs also promote epithelial regeneration in vivo. Interestingly, we found that the incidence of hyphema formation was significantly lower in SIMP-treated eyes than it was in non-SIMP treated eyes 7 days after an alkali burn. Because trabecular meshwork cells and ciliary muscle cells express MMPs,[25,26] our results suggest that hyphema formation in alkali-burned eyes may be the result of the destruction of trabecular meshwork, iris, and ciliary body by MMPs. Hyphema complications are clinical features of some cases of alkali-burned eyes, and it is worth considering the possibility that MMPI may be useful in preventing the occurrence of hyphema after alkali injury.

Although IL-1α, IL-1β, and IL-6 are cytokines lacking a transmembrane domain precursor, TNF-α contains a transmembrane domain, and membrane-anchored pro–TNF-α is proteolytically processed to the mature TNF-α.[27] Several MMPs are responsible for the processing of mature TNF-α,[27] a processing that MMPIs can inhibit.[28,29] We found that the protein level of TNF-α after our alkali burn did not differ between the SIMP-treated and control groups. This may be because both precursor and mature TNF-α were contained in the supernatants of each sample, and both were detected by ELISA systems. Alternatively, it could be because the upregulation of TNF-α after the burn is only slight, making it impossible to detect the effect of SIMP on TNF-α expression. We predict that in conditions in which the expression or the processing of TNF-α is excessively upregulated, MMPI may have an inhibitory effect on TNF-α expression. Interestingly, Fas ligand, a major inducer of apoptosis, belongs to the TNF family and is prevented from shedding by MMPI.[30] We predict that further mechanisms may exist in the action of MMPI that need to be established.

The anticollagenase activity of MMPI has been considered to be the main mechanism by which it protects alkali-burned eyes from becoming ulcerated; however, the inhibitory effect of MMPI on the expression of inflammatory cytokines after the burn also may be responsible for the reduced damage seen in MMPI-treated eyes.

Acknowledgments

The authors thank Andrew J. Quantock for helpful comments and critical reading of the manuscript.

References

1. Itoi M, Gnädinger MC, Slansky HH, Freeman MI, Dohlman CH. Collagenase in the cornea. *Exp Eye Res.* 1969;8:369–373.

2. Gordon JM, Bauer EA, Eisen AZ. Collagenase in human cornea: immunologic localization. *Arch Ophthalmol.* 1980;98:341–345.
3. Fini ME, Girard MT. Expression of collagenolytic/gelatinolytic metalloproteinases by normal cornea. *Invest Ophthalmol Vis Sci.* 1990;31:1779–1788.
4. Matsubara M, Girard MT, Kublin CL, Cintron C, Fini ME. Differential roles for two gelatinolytic enzymes of the matrix metalloproteinase family in the remodeling cornea. *Dev Biol.* 1991;147:425–439.
5. Brown D, Chwa M, Escobar M, Kenney MC. Characterization of the major matrix degrading metalloproteinase of human corneal stroma. Evidence for an enzyme/inhibitor complex. *Exp Eye Res.* 1991;52:5–16.
6. Gnädinger MC, Itoi M, Slansky HH, Dohlman CH. The role of collagenase in the alkali-burned cornea. *Am J Ophthalmol.* 1969; 68:478–483.
7. Brown SI, Weller CA, Wassermann HE. Collagenolytic activity of alkali-burned corneas. *Arch Ophthalmol.* 1969;81:370–373.
8. Brown SI, Weller CA, Akiya S. Pathogenesis of ulcers of the alkali-burned cornea. *Arch Ophthalmol.* 1970;83:205–208.
9. Burns FR, Stack MS, Gray RD, Paterson CA. Inhibition of purified collagenase from alkali-burned rabbit corneas. *Invest Ophthalmol Vis Sci.* 1989;30:1569–1575.
10. Burns FR, Gray RD, Paterson CA. Inhibition of alkali-induced corneal ulceration and perforation by a thiol peptide. *Invest Ophthalmol Vis Sci.* 1990;31:107–114.
11. Paterson CA, Wells JG, Koklitis PA, Higgs GA, Docherty AJ. Recombinant tissue inhibitor of metalloproteinases type 1 suppresses alkali-burn-induced corneal ulceration in rabbits. *Invest Ophthalmol Vis Sci.* 1994;35:677–684.
12. Schultz GS, Strelow S, Stern GA, et al. Treatment of alkali-injured rabbit corneas with a synthetic inhibitor of matrix metalloproteinases. *Invest Ophthalmol Vis Sci.* 1992;33:3325–3331.
13. Wentworth JS, Paterson CA, Gray RD. Effect of a metalloproteinase inhibitor on established corneal ulcers after an alkali burn. *Invest Ophthalmol Vis Sci.* 1992;33:2174–2179.
14. Sotozono C, He J, Matsumoto Y, et al. Cytokine expression in the alkali-burned cornea. *Curr Eye Res.* 1997;16:670–676.
15. Sotozono C, Kinoshita S. Growth factors and cytokines in corneal wound healing. In: Nishida T, ed. *Corneal Healing Responses to Injuries and Refractive Surgeries.* The Hague: Kugler Publications; 1998:29–40.
16. Barletta JP, Angella G, Balch KC, et al. Inhibition of pseudomonal ulceration in rabbit corneas by a synthetic matrix metalloproteinase inhibitor. *Invest Ophthalmol Vis Sci.* 1996;37:20–28.
17. Sano Y, Osawa H, Sotozono C, Kinoshita S. Cytokine expression during orthotopic corneal allograft rejection in mice. *Invest Ophthalmol Vis Sci.* 1998;39:1953–1957.
18. Girard MT, Matsubara M, Fini ME. Transforming growth factor-beta and interleukin-1 modulate metalloproteinase expression by corneal stromal cells. *Invest Ophthalmol Vis Sci.* 1991;32:2441–2454.
19. Cubitt CL, Tang Q, Monteiro CA, Lausch RN, Oakes JE. IL-8 gene expression in cultures of human corneal epithelial cells and keratocytes. *Invest Ophthalmol Vis Sci.* 1993;34:3199–3206.
20. Cubitt CL, Lausch RN, Oakes JE. Differences in interleukin-6 gene expression between cultured human corneal epithelial cells and keratocytes. *Invest Ophthalmol Vis Sci.* 1995;36:330–336.
21. Sakamoto S, Inada K, Chiba K, Yoshida M, Tazawa Y. Production of IL-6 and IL-1 α by human corneal epithelial cells. *Nippon Ganka Gakkai Zasshi.* 1991;95:728–732.
22. West–Mays JA, Sadow PM, Tobin TW, et al. Repair phenotype in corneal fibroblasts is controlled by an interleukin-1 α autocrine feedback loop. *Invest Ophthalmol Vis Sci.* 1997;38:1367–1379.
23. Pfister RR, Haddox JL, Sommers CI. Effect of synthetic metalloproteinase inhibitor or citrate on neutrophil chemotaxis and the respiratory burst. *Invest Ophthalmol Vis Sci.* 1997;38:1340–1349.
24. Saika S, Kawashima Y, Okada Y, et al. Recombinant TIMP-1 and -2 enhance the proliferation of rabbit corneal epithelial cells in vitro and the spreading of rabbit corneal epithelium in situ. *Curr Eye Res.* 1998;17:47–52.
25. Weinreb RN, Kashiwagi K, Kashiwagi F, Tsukahara S, Lindsey JD. Prostaglandins increase matrix metalloproteinase release from human ciliary smooth muscle cells. *Invest Ophthalmol Vis Sci.* 1997; 38:2772–2780.
26. Alexander JP, Samples JR, Van BE, Acott TS. Expression of matrix metalloproteinases and inhibitor by human trabecular meshwork. *Invest Ophthalmol Vis Sci.* 1991;32:172–180.
27. Gearing AJ, Beckett P, Christodoulou M, et al. Processing of tumour necrosis factor-α precursor by metalloproteinases. *Nature.* 1994;370:555–557.
28. McGeehan GM, Becherer JD, Bast RJ, et al. Regulation of tumour necrosis factor-α processing by a metalloproteinase inhibitor. *Nature.* 1994;370:558–561.
29. Solorzano CC, Ksontini R, Pruitt JH, et al. A matrix metalloproteinase inhibitor prevents processing of tumor necrosis factor α (TNF α) and abrogates endotoxin-induced lethality. *Shock.* 1997;7:427–431.
30. Tanaka M, Suda T, Haze K, et al. Fas ligand in human serum. *Nat Med.* 1996;2:317–322.

Asymmetric Responses in Cortical Visually Evoked Potentials to Motion Are Not Derived from Eye Movements

James R. Wilson,[1] *William W. Noyd,*[1] *Akhila D. Aiyer,*[1] *Anthony M. Norcia,*[2] *Michael J. Mustari,*[3] *and Ronald G. Boothe*[1]

Purpose. Normal neonates and many adults after abnormal visual development have directional preferences for visual stimulus motions; i.e., they give better responses for optokinetic nystagmus (OKN) and visually evoked potentials (VEPs) in one direction than to those in the opposite direction. The authors tested whether the VEP responses were asymmetrical because of abnormal eye movements.

Methods. VEPs were recorded from the visual cortices of five macaque monkeys: one normal, one neonate, and three reared with alternating monocular occlusion (AMO). They were lightly anesthetized, followed by paralysis to prevent eye movements. They then had "jittered" vertical grating patterns presented in their visual fields. The steady state VEPs were analyzed with discrete Fourier transforms to obtain the amplitudes and phases of the asymmetries.

Results. The normal, control monkey had small, insignificant amplitudes of its asymmetrical Fourier component and random phases that were not 180° out of phase across the left and right eyes. The neonatal monkey and the AMO monkeys all had large, significant asymmetries that were approximately 180° out of phase between the left and right eyes.

Conclusions. The neonate and abnormally reared monkeys continued to have asymmetrical responses even after their eyes were paralyzed. Therefore, eye movements cannot be the source of the asymmetrical amplitudes of the VEPs, and the visual cortex is at least one source responsible for asymmetries observed in neonates and adults reared under abnormal visual inputs. (*Invest Ophthalmol Vis Sci.* 1999; 40:2435–2439)

Infant humans and monkeys have asymmetric responses to moving visual stimuli. For example, the slow phase of the monocular optokinetic nystagmus (OKN) response is stronger for motion in the nasalward than in the temporalward direction.[1] These asymmetrical monocular OKN responses to opposite directions of motion disappear after approximately 5 months or 5 weeks for normal humans and monkeys, respectively.[2] However, if infants are exposed to abnormal visual inputs (such as those created by cataracts or strabismus) that disrupt normal binocular development, the asymmetry, as well as other abnormalities, may remain present even in the adult.[3] Therefore, determining the neural source of these asymmetrical responses has clinical relevance for diagnosis and treatment of human patients and also has relevance to basic research aimed at elucidating the mechanisms underlying the normal and abnormal development of motion processing in the brain.

Initial speculation about the neural source of asymmetric responses to motion focused on the nucleus of the optic tract, which is known to be a primary brain region involved in generating the OKN response.[4] However, there is now accumulating evidence that motion asymmetries are more ubiquitous and also can be revealed in measurements of smooth pursuit eye movements, visually evoked potentials to motion (MVEP), and perception of motion.[1] These latter findings have led some to propose that the visual cortex could be partly or fully responsible for causing the asymmetrical responses and that they are not the result of nystagmus.[3,5]

An alternative explanation for the asymmetric cortical MVEP responses has been proposed that argues asymmetrical movement of the eyes is responsible for motion asymmetry.[6] This eye movement explanation takes two forms. The first and most simple explanation is that the cortical asymmetries are accounted for by eye movements that take place during the measurement of the asymmetry. For example, some of the children with motion asymmetry also have latent nystagmus. The nasal drift that is present during latent nystagmus would be expected to cancel the velocity of motion in the nasal direction and enhance velocity in the temporal direction. Thus, the cortical response would be expected to be asymmetrical in response to stimulus motion of equal velocity in the two directions. The second possible explanation is more complex. An individual with asymmetric eye movements, such as latent nystagmus, is subjecting the brain to prolonged periods of asymmetrical motion input that may lead to motion adaptation effects.[6,7] Thus, even if the eyes are prevented from moving during measurement of a response to motion, the response may be asymmetric due to the lingering effects of motion adaptation that built up earlier during the rearing period.

The purpose of the present study was to test directly both forms of the eye movement explanation of motion asymmetry. We recorded MVEPs from anesthetized, paralyzed monkeys in which all eye movements were eliminated during the recording session. Three animals were reared under conditions of binocular visual deprivation and were known to have asymmetrical cortical MVEPs when tested under nonparalyzed conditions (unpublished data). Our hypothesis was that the asymmetrical MVEPs would still be present under paralyzed conditions. If this could be shown to be correct, then it would allow us to reject the first form of the eye movement explanation.

Second, we recorded from a normal neonatal monkey only 3.5 weeks after birth, also under anesthetized, paralyzed conditions. Our hypothesis was that this neonate would show the expected neonatal asymmetric MVEP response that we have reported previously under nonparalyzed conditions.[2] Normal neonatal monkeys do not have asymmetrical eye movements, such as latent nystagmus. Thus, our rationale was that if our hypothesis could be confirmed, then it would allow us to

From the [1]Yerkes Regional Primate Research Center, Departments of Cell Biology, Psychology, and Ophthalmology, Emory University, Atlanta, Georgia; [2]Smith-Kettlewell Eye Research Institute, San Francisco, California; and [3]Department of Anatomy and Neuroscience, University of Texas, Galveston.

Supported by the National Institutes of Health Grants RR-00165 and EY-05975.

Submitted for publication June 3, 1998; accepted August 11, 1998.

Proprietary interest category: N.

Corresponding author: James R. Wilson, Yerkes Research Center, Emory University, Atlanta, GA 30322.
E-mail: wilson@rmy.emory.edu

TABLE 1. Individual Monkey Backgrounds

Monkey	Treatment	Lens compliance (%)		Length of lens wear (mo)	Age at recording (y)
		OD	OS		
RTl3	AMO	48	50	4	1.75
RCl5	AMO	48	49	6	1.5
RWo5	AMO	48	51	4	1.1
RSd6	Normal	—	—	—	3.5*
RLm3	Normal	—	—	—	4.0

AMO stands for alternating monocular occlusion. Lens compliance is the percentage of total time during rearing that an occluder lens was worn on the eye.

* Age in weeks.

eliminate, at least as a necessary condition, the second form of the eye movement explanation as well.

Finally, as a control, we made similar measurements in a normal juvenile monkey that had been reared under normal conditions. Our hypothesis was that this juvenile would show a symmetric cortical MVEP response under the paralyzed conditions. This was done to rule out the unlikely possibility that all monkeys show an asymmetrical MVEP response when measured under anesthetized, paralyzed conditions. All three of our hypotheses were confirmed. We conclude that asymmetrical cortical MVEP responses do not depend on asymmetric eye movements.

METHODS

Subjects

Five *Macaca mulatta* monkeys were studied in accordance with ARVO and NIH guidelines for use of animals in research. These monkeys were obtained and reared at the Yerkes Regional Primate Research Center. Three were reared with a daily alternating monocular occlusion (AMO), using opaque soft contact lenses. That is, starting on the day of birth, an opaque occluder contact lens was placed on one eye for 24 hours, followed by removal and placement on the fellow eye for the next 24 hours. Using this protocol, each eye was deprived of vision every other day, and no binocular input was allowed. Compliance with the lens wear protocols is shown in Table 1. These animals were recorded at 1 to 2 years of age. The fourth monkey was a normally reared neonate recorded 3.5 weeks after birth. The fifth monkey was a normal juvenile reared under normal binocular visual conditions and recorded at 4 years of age.

All monkeys were given ophthalmic examinations to ensure that no eye pathology was present and that the eyes wearing contact lenses remained in good condition. The three AMO monkeys all exhibited an exotropia, but had acuities within the normal range for each eye.

Recordings

Eye movements were stabilized with a standard preparation used to eliminate eye movements during electrophysiological recordings from the visual system. Briefly, ketamine (15 mg/kg) was used to initially anesthetize each monkey, followed by insertion of an intravenous needle and infusion of sodium pentobarbital (5–10 mg/kg) for further anesthesia, which was titrated to the proper level by closely monitoring blood pressure, heart rate, and electroencephalogram (EEG). A rectal temperature probe monitored and a heating blanket maintained the body temperature at 38°C. After intubating the trachea, gallamine triethiodide was given (10 mg/kg) to block muscle movements, and the monkey was ventilated artificially to maintain the expired CO_2 level at the pre-paralysis level (~5%). A 70%/30% mixture of N_2O/O_2 was given as the inspired respiratory gas.

Contact lenses were placed on the eyes to prevent corneal drying. For the control monkey and two of the AMO monkeys, subdermal needle electrodes were inserted to record VEPs. Two of these electrodes were placed over each occipital lobe near the representation of the foveal region of the striate cortex, i.e., approximately 1 cm lateral to the midline and just above the nuchal ridge. A reference electrode was placed over the parietal cortex at the midline, and a ground electrode was placed over the forehead. The differential signals (sampled at 450 Hz) from the subdermal occipital electrode leads were amplified, filtered (1–100 Hz), and fed into a computer system for monitoring, storage, and analysis. The amplitudes of these signals varies. This system has been thoroughly described previously and carries out a Fourier analysis of the steady state waveforms of the electroencephalograms (see below).[8]

The third AMO monkey first had scalp recordings as before and then received a craniotomy over the left occipital cortex to record the VEPs with bipolar, low-impedance microelectrodes inserted into the cortex. The microelectrodes were held 300 μm vertically apart to restrict the differential recordings to the striate cortex. The electrodes were driven into the striate cortex with a microdrive and recordings were obtained at various depths. Some of the data from this monkey have been reported previously.[5]

Stimuli

Each monkey faced a video monitor (19-inch diagonal) at 30- to 50-cm distance from the eyes. A vertical sinewave grating pattern (0.25–3 cycles/deg) was generated on the screen (80% contrast and average luminance of 110 candela/m^2) and moved horizontally back and forth through a 90° phase shift at a frequency of 6 Hz in a square wave manner. Stimulus frequency was an even division of the video frame rate (60 Hz). This appears as a horizontal "jitter" to a human observer and has been found to generate a large amplitude VEP for both humans and monkeys.[2,8] Each trial consisted of 10 seconds of the stimulus and 5 to 15 trials were vector-averaged.

Analyses

A discrete Fourier transform was carried out on the steady state VEPs to obtain the amplitudes of the EEG components at various temporal frequencies. The two frequencies of interest were 6 Hz (the fundamental or F1 frequency) and 12 Hz (the stimulus doubled or F2 frequency). Frequencies on either side of both of these frequencies were used to estimate the "noise" or non–stimulus-derived levels of the EEG.[8] In addition to the amplitudes of the EEG components measured at various frequencies, the phase of each frequency component was also measured during the stimulus presentation. Phase coherence was used as an indicator that the measured signal was derived from the stimulus and not just part of the normal EEG (using the Circle *t*-test, which is similar to a Student's *t*-test but is used for circular values).[8]

Eye Movement Measurements

We performed a detailed study of oculomotility in one alert monkey raised with AMO (RCl5). We used an electromagnetic method employing scleral search coils to measure accurately movements of both eyes. Our system (CNC Engineering, Seattle, WA) is drift-free and capable of measuring eye movements to 15 minutes of arc resolution. We precisely calibrated the signal obtained from each eye coil by requiring the monkey to monocularly fixate a stationary target at different eccentricities on a tangent screen 57 cm distant. Each eye was calibrated to an accuracy of at least 0.5° for target positions within ±20° (horizontal and vertical) of straight ahead gaze. In addition, the monkey was trained to perform accurate saccadic, smooth pursuit, and vergence eye movements on a small diameter (0.1°) laser spot.

Results

The MVEP was obtained monocularly while the other eye was blocked from viewing the stimulus. Control trials also were obtained to ensure that there was no EEG component at our stimulus frequency when both eyes were blocked from viewing the stimuli. During each cycle of the grating pattern movement (first in one direction and then back in the opposite direction), an MVEP is generated in a normal animal. As a result, there is a large signal obtained at the F2 frequency (12 Hz), which is twice the stimulus frequency (6 Hz). Furthermore, this signal always exhibits phase coherence. This demonstrates that our system is properly recording the EEG evoked by our visual stimulus. For normally reared juvenile or adult monkeys, including our control for this experiment, there is no significant amplitude for the F1 signal (6 Hz) and thus no asymmetry of the MVEP for one direction of the movement (Fig. 1). For the AMO and neonate monkeys, a significant component of the EEG was obtained at the F1 frequency. This demonstrates that there was a stronger MVEP generated in one direction of the stimulus movement than the opposite direction (Fig. 1).[8]

Both the F1 and F2 components of the Fourier analyses are expected to show phase coherence if they are stimulus-driven. Furthermore, when each eye is tested monocularly, the phase of the F2 for each eye is expected to be similar because each eye generates an MVEP at about the same time relative to the stimulus movements in both directions. However, if each eye has a preference for the temporal-to-nasal direction (or the reverse), then the F1 phases are expected to occur at approximately 180° apart for the two eyes. This is because the temporal-to-nasal directions are opposite for the two eyes.

The normal and the AMO monkeys all exhibited similar phases for the F2 signals from the two eyes. The three AMO monkeys also all exhibited approximately a 180° phase shift of the F1 signal between the two eyes (Fig. 1; 156° ±12°; mean ± SD).

The third AMO monkey was recorded with a bipolar set of microelectrodes that were 300 μm vertically apart and were driven through the striate cortex perpendicular to the pial surface to record the MVEPs. Asymmetrical MVEPs were first recorded in layers II/III with amplitudes increasing as the electrodes were driven deeper. At the deepest position of the track, a small lesion was made by current passed through the electrode at the end of the recording session. The lowest position of the electrodes gave the largest F1 signal that we recorded, and the track produced was observed to end in upper layer IV of the striate cortex. It is possible that greater amplitude signals might have been obtained if the electrode had been moved deeper into the infragranular layers. The data from this monkey have been published previously,[5] but are included it here to emphasize that the MVEP asymmetry is derived at least partially from the striate cortex and demonstrate that the cortical asymmetries matches the MVEP asymmetries of our other AMO monkeys.

Eye movement studies were performed for AMO monkey RCl5 when the animal was between 1.5 and 2.5 years of age. These measurements revealed a 12° exotropia of the left eye (57 cm viewing distance). Furthermore, a strong preference for fixation with the right eye was present, despite normal acuity in each eye. Finally, a leftward (slow phase) nystagmus of 5°/s was present, but the direction or velocity of drift did not change, regardless of which eye was viewing. Therefore, this animal had no measurable latent nystagmus.

Discussion

Our results show that asymmetrical cortical MVEP responses do not depend on eye movements. Visually deprived adult monkeys that exhibit an MVEP asymmetry when recorded under unparalyzed conditions continue to have asymmetrical MVEPs when tested under paralyzed conditions. Normal monkeys, including our control monkey, have symmetrical responses when tested under the same conditions. Furthermore, our recordings from a neonate recorded under paralyzed conditions only 3.5 weeks after birth demonstrate that asymmetrical cortical MVEP responses do not require a prior period of motion adaptation, as might occur in an individual that grows up with asymmetrical eye movements.

It should be emphasized that our results do not rule out eye movement explanations for the cortical motion asymmetries that are present in some cases.[6] In other words, our neonatal data demonstrate that eye movements are not a necessary condition for an asymmetry to be present, but do not rule out the possibility that they might be a sufficient condition. At the least, our results demonstrate that eye movements cannot explain all cortical motion asymmetries.

Our eye movement recordings in one AMO monkey revealed no measurable latent nystagmus. However, a conjugate slow phase drift (leftward) was present when tested in the light or dark. The slow phase drift velocity was always low

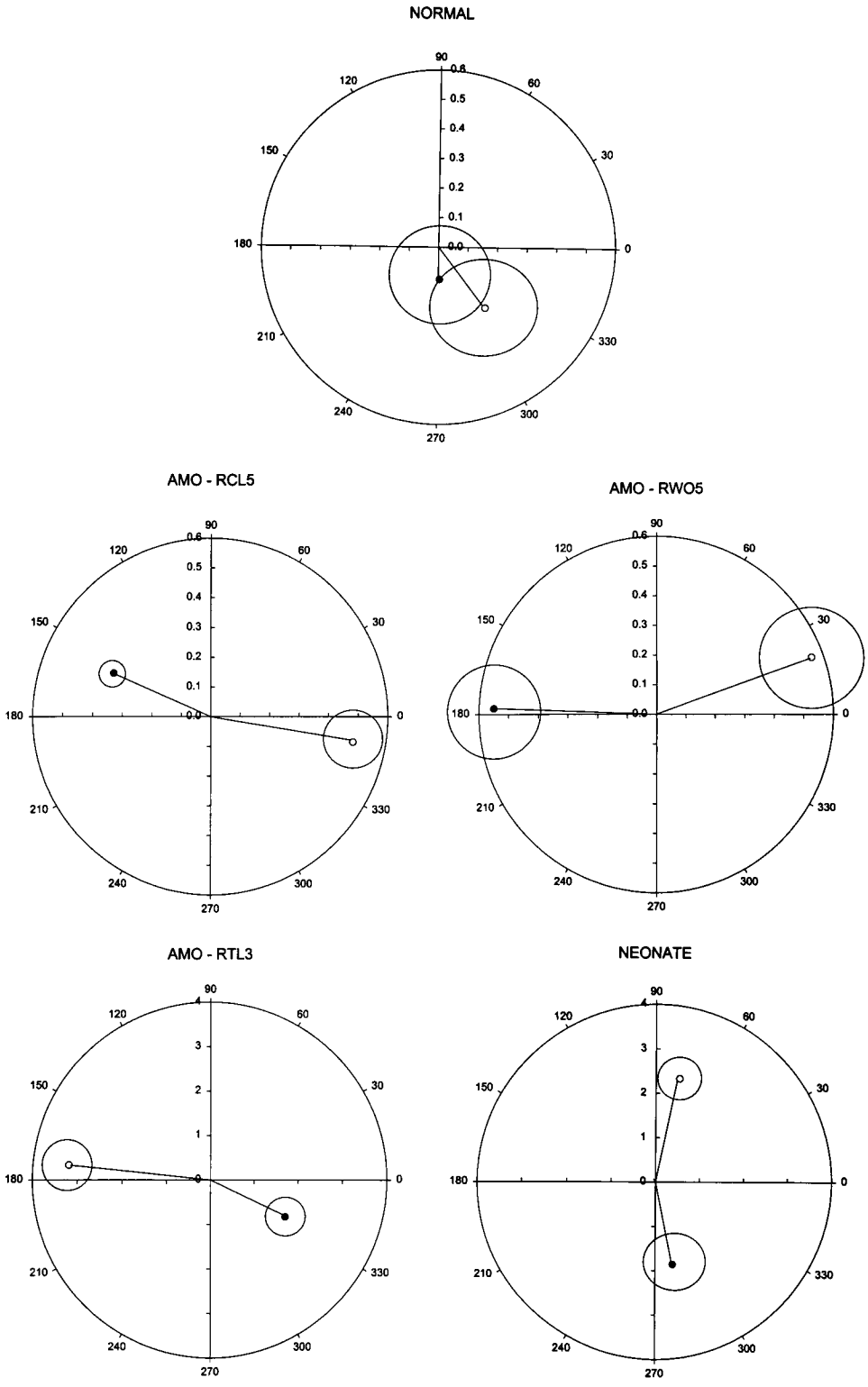

FIGURE 1. Polar plots showing the amplitudes and phases of the asymmetrical component of visually evoked potentials recorded from the visual cortices of five macaque monkeys: one normal adult (RLm3), one normal neonate (RSd6), and 3 monkeys (RTl3, RCl3, RWo5) reared with alternating monocular occlusion (AMO). The right eye's phases and amplitudes are designated by a s*mall solid circle* and the left eye's by a *small open circle*. The *larger circles* around the end points are 1 SE for the vector of the phase and amplitude trial values. Note that the phases of the VEPs of the neonate and AMOs are approximately 180° apart. All eyes for these monkeys had significant phase coherence ($P < 0.05$) for the asymmetrical component. Also note that the amplitudes for the asymmetrical responses are much larger than those of the normal control monkey, which did not have a significant phase coherence for the asymmetries for either eye. All the monkeys had large amplitudes and very significant ($P < 0.01$) phase coherences for the F2 (symmetrical) component for both eyes (not shown because of large values beyond the scales needed to clearly show the asymmetrical values).

(<5°/s) and did not prevent accurate fixation or eye movements. Whether such a unidirectional slow phase drift could contribute to the motion asymmetry measured in this animal is uncertain. However, the unidirectional nature of oculomotor drift for both eyes did not correlate with MVEP data showing a 180° phase difference across the eyes in this animal. Furthermore, the other AMO monkeys generated asymmetrical evoked potentials under paralyzed conditions during which no eye movements were possible.

Important questions concerning motion asymmetries include their localization within the brain and their relationship to binocularity. The latter question arises because disruptions of normal binocular input during development result in a number of abnormalities of the visual system such as amblyo-

pia, strabismus, and latent nystagmus.[9] If normal binocular inputs are major factors for achieving symmetrical MVEPs derived from directional motion, then the striate cortex would be the first stage of visual processing where the neurons have a combination of directional selectivity and binocularity as properties of their receptive fields.

On the other hand, the middle temporal visual cortical area (MT or V5) appears to be particularly important for processing motion information. This area receives direct projections from the striate cortex and also has projections to the NOT in the brain stem.[10] It might be expected, therefore, that in the presence of motion asymmetry, directional sensitivity in MT might be affected. However, in a recent study of the MT cortex of strabismic monkeys, a complete representation of directional preferences was found in the recorded population of single units.[11] This was despite finding a significant asymmetry in smooth pursuit performance favoring nasally directed tracking. Unfortunately, the researchers were unable to identify whether there was any difference in the directional sensitivity for the critical population of lamina V neurons that project to oculomotor brain stem areas involved in eye movements. Thus, their results do not rule out the possibility that it may have been only a subpopulation of neurons within MT that had a directional preference.

Our finding of an asymmetry in V1 suggests another possibility. The NOT is known to be a controlling area for OKN functioning and other horizontal motion effects, and the striate cortex itself has a direct, ipsilateral projection to the NOT.[4] A subpopulation of neurons within V1 might be responsible for producing motion asymmetries that are measured in the VEPs and passed on to the controlling neurons of the NOT.

In summary, we have shown that there is a motion asymmetry neural signal derived from the striate cortex that is not produced by eye movements. This cortical asymmetry could be the basis for many abnormalities that are seen in monkeys and humans that receive abnormal visual inputs during development.

Acknowledgments

The authors thank Jean Torbit for secretarial assistance and the veterinarians and caretakers of the Yerkes Regional Primate Research Center for expert assistance with care of the animals used in this project.

References

1. Brosnahan D, Norcia AM, Schor CM, Taylor D. OKN, perceptual and VEP direction biases in strabismus. *Vision Res.* 1998;38:2833–2840.
2. Brown RJ, Wilson JR, Norcia AM, Boothe RG. Development of directional motion symmetry in the monocular visually evoked potential of infant monkeys. *Vision Res.* 1998;38:1253–1263.
3. Tychsen L. Motion sensitivity and the origins of infantile strabismus. In: Simmons K, ed. *Early Visual Development, Normal and Abnormal*. New York: Oxford; 1993:364–390.
4. Fuchs AF, Mustari MJ. The optokinetic response in primates and its possible neuronal substrate. *Rev Oculomot Res.* 1993;5:343–369.
5. Norcia AM. Abnormal motion processing and binocularity: infantile esotropia as a model system for effects of early interruptions of binocularity. *Eye.* 1996;10:259–265.
6. Kommerell G. The relationship between infantile strabismus and latent nystagmus. *Eye.* 1996;10:274–281.
7. Shallo-Hoffmann J, Falden ME, Acheson JF, Gresty M. Temporally directed deficits for the detection of visual motion in latent nystagmus: evidence for adaptive processing. *Neuro-Ophthalmology.* 1996;16:343–349.
8. Tang Y, Norcia AM. An adaptive filter for steady-state evoked responses. *Electroenceph Clin Neurophysiol.* 1995;96:261–277.
9. Mustari MJ, Fuchs AF, Kaneko CR, Robinson FR. Anatomical connections of the primate pretectal nucleus of the optic tract. *J Comp Neurol.* 1994;349:111–128.
10. Kiorpes L, Walton PJ, O'Keefe LP, Movshon JA, Lisberger SG. Effects of early-onset artificial strabismus on pursuit eye movements and on neuronal responses in area MT of macaque monkeys. *J Neurosci.* 1996;16:6537–6553.
11. Hoffmann K–P, Distler C, Markner C. Optokinetic nystagmus in cats with congenital strabismus. *J Neurophysiol.* 1996;75:1495–1502.

Elevation of Human Intraocular Pressure at Night under Moderate Illumination

John H. K. Liu,[1] *Daniel F. Kripke,*[2] *Rivak E. Hoffman,*[1] *Michael D. Twa,*[1] *Richard T. Loving,*[2] *Katharine M. Rex,*[2] *Brian L. Lee,*[1] *Steven L. Mansberger,*[1] *and Robert N. Weinreb*[1]

Purpose. An endogenous elevation of intraocular pressure (IOP) occurs at night in healthy young adults. The authors studied whether or not this IOP elevation can be detected under moderate illumination.

Methods. Twenty-five healthy volunteers, ages 18 to 25 years, were housed overnight in a sleep laboratory under a strictly controlled light–dark environment. Intraocular pressure was measured in the supine position every 2 hours, using a pneumatonometer. An 8-hour sleep period was assigned to each volunteer according to individual's accustomed sleep cycle. In the early part of this assigned period, sleep was encouraged with room lights off. Researchers performed IOP measurements at two time points with the aid of night vision goggles. In the middle to the late part of the assigned period, lights were turned on twice for a 1-hour interval. The light intensity was the same as before the bedtime. At the ending of each light period, IOP was measured under illumination.

Results. Average IOP was significantly higher in the assigned sleep period versus outside the period. The trough of mean IOP occurred just before the bedtime, and then IOP gradually increased and peaked at the end of the

From the Departments of [1]Ophthalmology and [2]Psychiatry, University of California, San Diego, La Jolla, California.

Supported by National Institutes of Health Grant EY07544.
Submitted for publication February 24, 1999; accepted April 12, 1999.
Proprietary interest category: N.

Corresponding author: John Liu, University of California, San Diego, Department of Ophthalmology, La Jolla, CA 92093-0946.
E-mail: joliu@ucsd.edu

8-hour assigned sleep period. The difference between the trough and peak IOP was 3.5 ± 0.7 mm Hg (mean ± SEM, n = 25). Within the assigned sleep period, the average IOP determined under illumination was significantly higher than the average IOP preceding the illumination.

Conclusions. Elevation of IOP occurred during the assigned sleep period with two 1-hour light exposures of moderate intensity. Environmental light at night had no significant effect on the nocturnal IOP elevation in healthy young adults. (*Invest Ophthalmol Vis Sci.* 1999; 40:2439–2442)

In a strictly controlled laboratory environment, a consistent elevation of intraocular pressure (IOP) occurred at night in healthy young adults.[1] An endogenous circadian (24-hour) oscillator drove part of the nocturnal IOP elevation. It is well known that environmental light is the primary synchronizer for various circadian rhythms.[2] Intermittent light exposures at night blocked the endogenous IOP elevation in laboratory rabbits.[3] Uncontrolled light exposure at night was noticed in many human IOP studies showing inconsistent nocturnal patterns,[4] suggesting that light could be a confounding factor. Is the endogenous elevation of human IOP at night detectable under moderate illumination? We collected overnight IOP data from a group of healthy young adults who received two 1-hour light exposures of moderate intensity at night. Changes in the nocturnal IOP were compared with previous results when no light exposure was applied.[1]

Methods

The study followed the tenets of the Declaration of Helsinki and was approved by the Institutional Review Board. Twenty-five paid volunteers (ages 18–25 years) were recruited mainly from employees and students of our university. Informed consents were obtained after explanation of the nature and possible consequences of the study.

Experimental subjects were nonsmoking, healthy individuals with a mean age of 20.7 ± 2.2 years (mean ± SD). They were selected on the basis of having a regular daily sleep cycle close to 2300 to 0700. Myopes with greater than 4 diopters were excluded. There were 17 men and 8 women, including 17 white, 3 Asian or Pacific Islander, 3 Hispanic, 1 African American, and 1 Native American. Each subject had a complete ophthalmic examination demonstrating absence of any eye disease. None of them had a narrow iridocorneal angle under slit lamp examination. Daytime sitting IOP levels measured by the Goldmann tonometer were in the range of 11 to 18 mm Hg (14.8 ± 2.4 mm Hg, mean ± SD).

Before the laboratory study, subjects were instructed to maintain a daily 8-hour accustomed sleep period (lights off) for 7 days to enhance circadian entrainment. Subjects wore a wrist device (Actillume; Ambulatory Monitoring Inc., Ardsley, NY) to monitor light exposure and physical activity. They were told to abstain from alcohol and caffeine for 3 days and not wear contact lenses for 24 hours. Subjects reported to the laboratory before 1700 and stayed indoors for the entire recording session. Light–dark conditions in each sleep room were strictly controlled. Light intensity (from cool-white fluorescent lights) was held constant at 500 to 1000 lux at eye level when standing. When subjects were in bed lying face-up, light intensity at eye level was at 1000 to 1500 lux in the vertical direction. Onset of darkness in each sleep room was adjusted according to the individual's sleep cycle. The room was absolutely dark when lights were off. Times for IOP measurements were individualized accordingly. For presentation, clock times were normalized as if each subject had an assigned sleep period from 2300 to 0700.

Intraocular pressure was measured every 2 hours in each eye using a pneumatonometer (model 30 Classic; Mentor O&O, Norwell, MA). The subjects were instructed to lie down in bed for 5 minutes before IOP measurement. One or two drops of 0.5% proparacaine were applied to the cornea as local anesthetic. A hard-copy record was produced for each IOP measurement. Before the assigned sleep period, measurements of IOP were taken at 1730, 1930, and 2130. Subjects continued their normal indoor activities. No naps were allowed. Food and water were always available. Meal times were not regulated. Room activities were continuously videotaped using infrared cameras.

Subjects went to bed just before the scheduled lights-off at 2300. Sleep was encouraged. During the 8-hour assigned sleep period, IOP was measured at 2330, 0130, 0330, and 0530. For the first two IOP measurements, subjects were awakened, if necessary, and measurements were taken in near-total darkness.[1] Researchers were equipped with infrared night vision goggles (AN/PVS-7B Dark Invader; Meyers, Redmond, WA) to aid these measurements. Disturbance and subjects' light exposure were kept to a minimum. One hour before the IOP measurements at 0330 and 0530, lights were turned on by the researchers from outside the room. Subjects were not deliberately awakened. Lighting was at the same intensity as before the bedtime. Subject's sleep positions were not controlled. Researcher entered the room according to the scheduled times, and the IOP measurements were performed in a few minutes. Night vision goggles were not needed when lights were on. Lights were turned off after the IOP measurements, and the subjects were encouraged to sleep again. When the assigned sleep period ended at 0700, room lights were turned on and subjects were awakened, if necessary. Measurements of IOP were taken again at 0730, 0930, and 1130. Debriefing interviews were conducted to document how the subjects had slept at night.

Values of IOP from both eyes were averaged, and these averages were used for data analyses. Means of the averages from the 25 subjects at each time point were calculated. Comparisons of IOP were made between different time points and various time blocks. $P < 0.05$ was regarded as statistically significant.

Results

In their debriefing interviews, 15 of 25 subjects indicated that they had slept well, despite the on and off light conditions at night. Eight subjects said that they did not sleep well. The other 2 subjects stated that they slept well when the lights were off, but not with lights on.

The average of all individual IOP data in the 8-hour assigned sleep period was 21.9 ± 0.5 mm Hg (mean ± SEM, n =

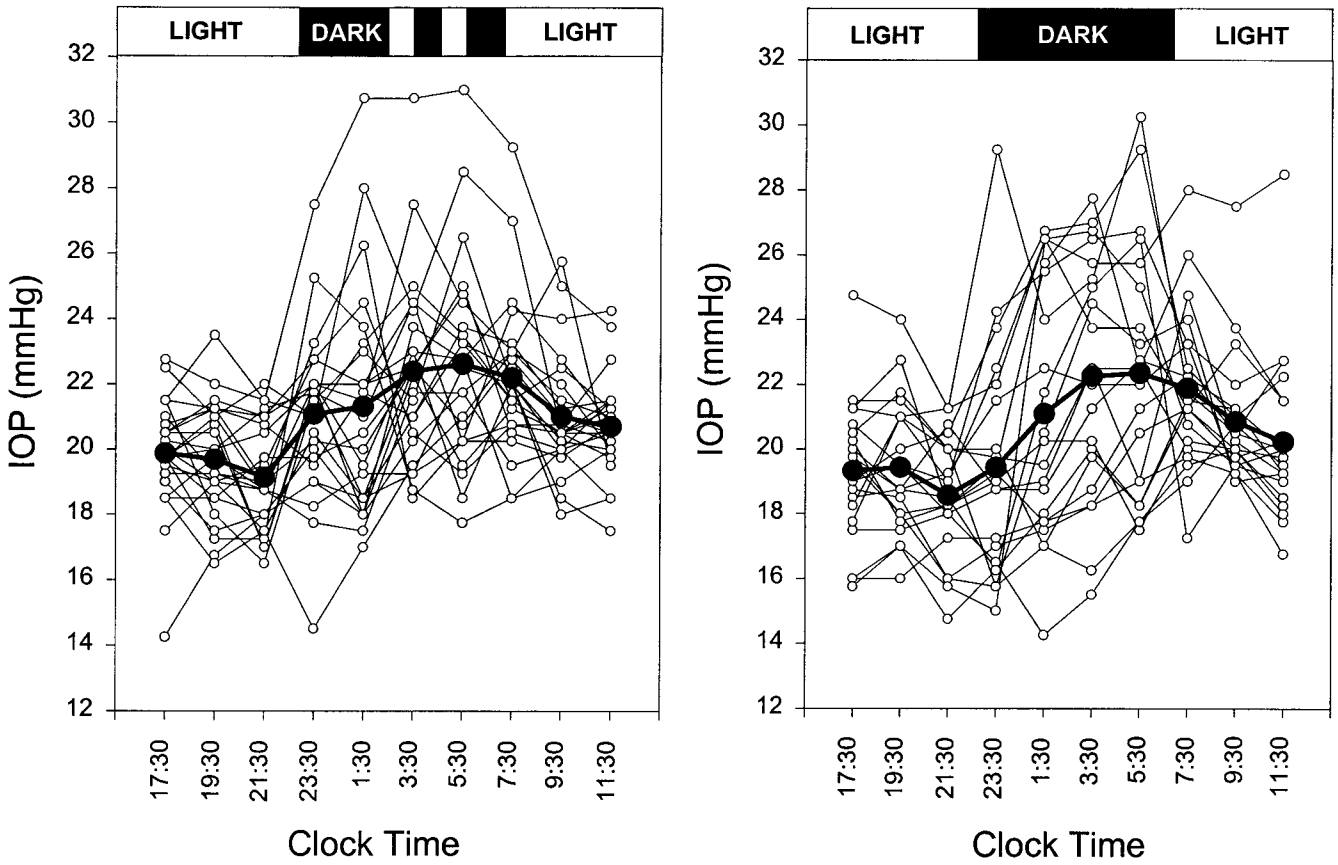

Figure 1. Elevations of intraocular pressure (IOP) in two groups of healthy young adults housed under different light conditions at night. *Left:* the present study of 25 subjects with an 8-hour assigned sleep period (2300–0700), including two 1-hour light exposures. *Black bars* on top of the panel represent the periods of darkness. Intraocular pressure was measured in the supine position using a pneumatonometer. *Open circles* represent individual IOP data; *solid circles* represent the means at various time points. *Right:* a comparable study of 21 subjects received no light exposure at night.[1]

25). It was significantly higher ($P < 0.001$, paired *t*-test) than the average IOP in the light/wake period (20.4 ± 0.3 mm Hg), which contained 6 time points for the IOP measurement. The profile of the IOP change is presented in Figure 1. Mean IOP showed a gradual change throughout the recording period, including the two 1-hour light exposures in the assigned sleep period. The trough of mean IOP appeared at 2130 (19.1 ± 0.3 mm Hg), and the peak of mean IOP appeared at 0530 (22.6 ± 0.6 mm Hg). The difference in IOP between the trough and peak was 3.5 ± 0.7 mm Hg ($P < 0.001$, paired *t*-test, $n = 25$). The mean IOP at 0330 was 22.4 ± 0.6 mm Hg, also significantly higher ($P < 0.001$) than the IOP mean at 2130. During the assigned sleep period with two 1-hour light exposures, IOP continued to increase. The average of IOP determined under illumination at 0330 and 0530 (22.5 ± 0.5 mm Hg) was significantly higher ($P < 0.05$) than the average of IOP determined under darkness at 2330 and 0130 (21.2 ± 0.6 mm Hg). After the 8-hour assigned sleep period, mean IOP decreased in the morning.

The profile of IOP change was very similar to the profile previously seen in a group of young adults[1] who had received no light exposures (Fig. 1, right). Student's *t*-test showed no difference ($P > 0.05$) for the nocturnal IOP elevations (from the IOP at either 1730 or 2130) between these two groups at the 4 time points of IOP measurement in the assigned sleep period. The magnitudes of IOP elevation in the present study for the time periods of 2130 to 0530 and 2130 to 0330 were 8% and 12%, respectively, less than those without light exposures.[1] These small reductions were not statistically significant. Measures of IOP changes by time also showed no difference between the two groups of using the Mann–Whitney rank-sum test.

Discussion

We observed an uninterrupted IOP elevation at night in this group of healthy young adults. In addition, measured under moderate illumination and without the aid of night vision goggles, we detected a significant IOP elevation toward the end of the 8-hour assigned sleep period. The elevation of IOP at night obviously was not related to pupillary dilation in the darkness, inasmuch as the elevation was detectable under illumination. The peak IOP elevation at night, at 6.5 hours into the accustomed sleep period, could not be blocked by two periods of moderate light exposures. The magnitude of IOP elevation was slightly less (not statistically significant) than the magnitude observed in our previous study.[1] This difference may be due to a minor effect of light exposure and/or individual variations in the nocturnal IOP pattern.

It has been suggested[5] that a few minutes after nighttime arousal, the nocturnal IOP elevation may not be detectable. In the present study, the endogenous IOP elevation at night was not short-lived and remained for at least a few minutes under moderate illumination when volunteers were

awakened for tonometry. It seems that a large portion of the endogenous IOP elevation at night was readily detectable if other experimental conditions, including the circadian entrainment, were well controlled.

During the two 1-hour light exposures, some light (up to 14.5% in the red wavelength) would pass through the closed eyelids.[6] Because of subjects' variable sleep positions, however, the amounts of light reaching the retinas were difficult to estimate. Videotape recording showed that many subjects had adjusted their lying down positions, such as turning their heads to the side, which would lessen light exposure. Therefore, the light intensity received by the retina might have been insufficient to affect the body's circadian pacemaker significantly.[7]

A 2-hour light exposure of 2500 lux (measured outside the eyelid) during the early sleep period significantly lowered the nocturnal IOP elevation.[8] However, exposure to the same light intensity during an entire night's sleep did not affect the nocturnal slowdown of aqueous humor flow.[9] The present study suggests that a person, sleeping under lights at night, may adjust the body position to lessen the light exposure, thereby maintaining homeostasis in ocular physiology.

With currently available techniques, it is impossible to measure the steady state IOP in an asleep human while the eyelids are closed. Because of this limitation, we conclude that an awakened young adult at night, while lying in bed, is very likely to have a higher IOP than during daytime hours. This nocturnal IOP elevation can be detected under moderate illumination.

Acknowledgments

The authors thank Richard F. Brubaker for his valuable advice.

References

1. Liu JHK, Kripke DF, Hoffman RE, et al. Nocturnal elevation of intraocular pressure in young adults. *Invest Ophthalmol Vis Sci.* 1998;39:2707–2712.
2. Czeisler CA. The effect of light on the human circadian pacemaker. In: Chadwick DJ, Ackrill K, eds. *Circadian Clocks and Their Adjustment*. Ciba Foundation Symposium 183. New York: John Wiley & Sons; 1995:254–302.
3. Lee TC, Kiuchi Y, Gregory DS. Light exposure decreases IOP in rabbits during the night. *Curr Eye Res.* 1995;14:443–448.
4. Liu JHK. Circadian rhythm of intraocular pressure. *J Glaucoma.* 1998;7:141–147.
5. Brown B. Diurnal variation of IOP [letter]. *Ophthalmology.* 1991; 98:1485–1486.
6. Robinson J, Bayliss SC, Fielder AR. Transmission of light across the adult and neonatal eyelid in vivo. *Vision Res.* 1991;31:1837–1840.
7. McIntyre IM, Norman TR, Burrows GD, Armstrong SM. Human melatonin suppression by light is intensity dependent. *J Pineal Res.* 1989;6:149–156.
8. Wildsoet C, Eyeson-Annan M, Brown B, Swann PG, Fletcher T. Investigation of parameters influencing intraocular pressure increases during sleep. *Ophthal Physiol Opt.* 1993;13:357–365.
9. Koskela T, Brubaker RF. The nocturnal suppression of aqueous humor flow in humans is not blocked by bright light. *Invest Ophthalmol Vis Sci.* 1991;32:2504–2506.

Localization of Cannabinoid CB1 Receptors in the Human Anterior Eye and Retina

Alex J. Straiker,[1] *Greg Maguire,*[2] *Ken Mackie,*[3] *and James Lindsey*[2]

Purpose. To determine the presence and distribution of CB1 cannabinoid receptors within the human eye.

Methods. A subtype-specific affinity-purified polyclonal antibody to the cannabinoid CB1 receptor was used to determine CB1 localization. Postmortem human eyes were fixed in methacarn and embedded in paraffin. Sagittal sections were mounted on slides and immunostained using antibodies to the CB1 receptor. Antibody binding was detected either by using peroxidase conjugated secondary antibodies and developing with diaminobenzidine or by using fluorescent secondary antibodies.

Results. Strong CB1 receptor labeling was detected in the ciliary epithelium, the corneal epithelium, and endothelium of the anterior human eye. Strong-to-moderate levels of CB1 staining were found in the trabecular meshwork and Schlemm's canal. Moderate labeling was detected in the ciliary muscle and in the blood vessels of the ciliary body. Moderate-to-light labeling also was detected in the sphincter papillae of the anterior human eye. Staining for CB1 receptors also was detected in human retina. The two synaptic layers of the retina and the inner and outer plexiform layers, were both moderately stained for CB1. In addition, moderate labeling was detected in the inner nuclear layer, and the ganglion cell layer. Strong labeling was detected in the outer segments of photoreceptors. No staining was observed in the corneal stroma or in the choroid.

Conclusions. The wide distribution of cannabinoid CB1 receptors in both the anterior eye and the retina of humans suggests that cannabinoids influence several different physiological functions in the human eye. (*Invest Ophthalmol Vis Sci.* 1999;40:2442–2448)

From the Departments of [1]Neuroscience and [2]Ophthalmology, University of California School of Medicine, San Diego, California; and [3]Departments of Anesthesiology, and Physiology and Biophysics, University of Washington, Seattle, Washington.

Supported by National Institutes of Health Grants EY09133 (GM), The Glaucoma Foundation (GM), DA05908 (AS), and DA00286 and DA11322 (KM).

Submitted for publication December 7, 1998; revised April 9, 1999; accepted April 21, 1999.

Proprietary interest category: N.

Corresponding author: Greg Maguire, Ophthalmology 0946, UCSD, La Jolla, CA 92093.
E-mail: maguire@eyecenter.ucsd.edu

Ingestion or topical application of cannabinoids present in marijuana and hashish lowers intraocular pressure (IOP), suggesting that they may be useful for treating glaucoma.[1–5] Potential sites of action lie either in the ciliary epithelium, where aqueous humor is formed, or in the aqueous humor

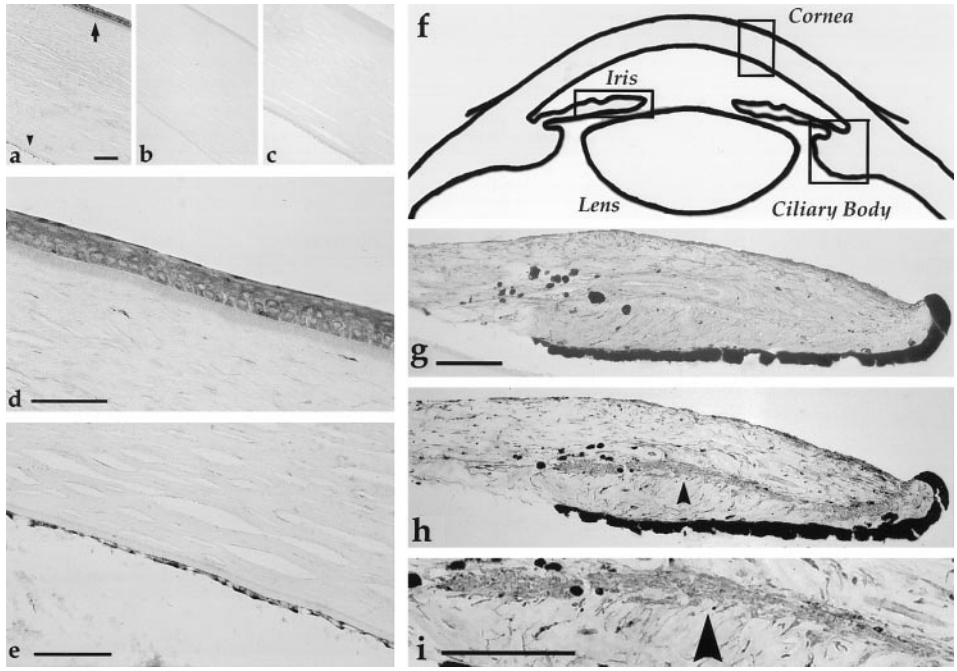

FIGURE 1. CB1 cannabinoid receptor labeling in the cornea and iris. Low magnification photographs of cornea labeled with antibodies to the CB1 receptor (**a**) demonstrate labeling in the corneal epithelium (*arrow*) and corneal endothelium (*arrowhead*). Control sections with CB1 antibody omitted (**b**) and premixed with immunizing protein (**c**). Higher magnification image shows strong labeling of the corneal epithelium (**d**) and corneal endothelium (**e**). The sphincter papillae muscle of the iris is positively labeled (**h,** *arrowhead*), whereas tissue labeled with antibody premixed with immunizing protein is not (**g**). Magnified view of iris (**i**) shows detail of sphincter papillae muscle labeling. Scale bars, (**a**, **b**, **c**) 133 μm; (**d**, **e**, **g**, **h**, **i**) 66 μm. Original magnification, (**a**, **b**, **c**) ×25; (**d**, **e**) ×100; (**g**, **h**, **i**) ×25.

outflow pathways. Cannabinoid consumption also has been linked to corneal opacification, accommodative changes, photophobia, and alterations of vision.[6–8] Though some groups have sought to explain cannabinoid action as non–cannabinoid receptor mediated,[9] little hope existed for settling this question before the cloning of the first cannabinoid receptor.[10] Since then, two cannabinoid, or CB, receptors have been identified. CB1 is enriched in the brain.[11] Another receptor, known as CB2,[12] is thought to be limited to the periphery, with functions relating to the immune system,[13] though some work suggests that CB2 may be present in the CNS, including the retina.[14,15]

Numerous CB1 receptor–mediated effects have been observed, ranging from modulation of nociception and glutamate transmission to inhibition of long-term potentiation.[16–18] In addition, candidate endogenous ligands have been identified: arachidonylethanolamide (anandamide or AEA),[19] 2-arachidonylglycerol (2-AG),[17] and palmitylethanolamide (PEA).[20] Of these, 2-AG and anandamide both lower IOP when applied topically.[9,21,22] PEA, the sole putative ligand for the CB2 receptor,[20] has no effect on IOP.[21] Interestingly, the selective CB1 antagonist SR141716A increases IOP on its own and opposes the effects of a synthetic CB1 ligand CP-55,940 but not that of anandamide.[23] This suggests that anandamide itself may influence IOP by a non–CB1 receptor–mediated pathway. The presence of anandamide amidohydrolase, the enzyme thought to break down anandamide, has been found to be active in the retina.[24] Our own studies detected 2-AG and PEA in the retina but not anandamide (Straiker AJ, Stella N, Piomelli D, Mackie K, Karten HJ, Maguire G, unpublished observations). This does not exclude possible circadian or activity-dependent release of anandamide, nor does it exclude the presence of anandamide elsewhere in the eye.

Recently, RT-PCR has been used to indicate the presence of CB1 mRNA in the retina and anterior eye.[25] Unfortunately, these results give little insight into the actual presence or precise localization of CB1 receptors. The availability of antibodies against the CB1 receptor has made it possible to determine its presence and distribution in the eye. We recently used a CB1 receptor antibody to localize CB1 immunoreactivity in the retinas of monkey, mouse, chick, goldfish, and salamander.[26] Here we report the distribution of CB1 labeling in the anterior segment of the human eye, as well as in human retina.

MATERIALS AND METHODS

Immunohistochemistry

Human tissue consisted of paraffin-embedded sections obtained from eyes received from the San Diego Eyebank. Ten eyes from donors of various ages from 44 to 90 years were fixed in methacarn (60% methanol, 30% chloroform, 10% glacial acetic acid) for 3 hours, then dehydrated, and embedded in paraffin. One of the 10 eyes (eye 80A) was fixed in formalin. Another eye (eye 68) was fixed in paraformaldehyde. For our experiments, anterior eye sections from five donors (49, 80A, 80B, 81, 86) and retina sections from seven donors were used (44, 68, 71, 80A, 81, 87, 90). Sections were heated at 56°C for at least 20 minutes and then deparaffinized in xylenes, followed by rehydration in an ethanol series. After washing in PBS, slides were preincubated with 3% H_2O_2 as a peroxidase suppressor. Tissue was allowed to incubate overnight at 4°C with the affinity-purified rabbit polyclonal CB1 receptor antibodies (1:200 for eyes 80A and 81,1:400 for all others, made in PBS, with 0.3% Triton X-100, 5% normal goat serum, 0.5% BSA). These antibodies have been characterized previously.[27]

Immunoperoxidase labeling was obtained by subsequently treating the tissue with the biotinylated anti-rabbit IgG antibodies and then avidin horseradish peroxidase. The sections then were developed using diaminobenzidine (Biogenix, San Ramon, CA).

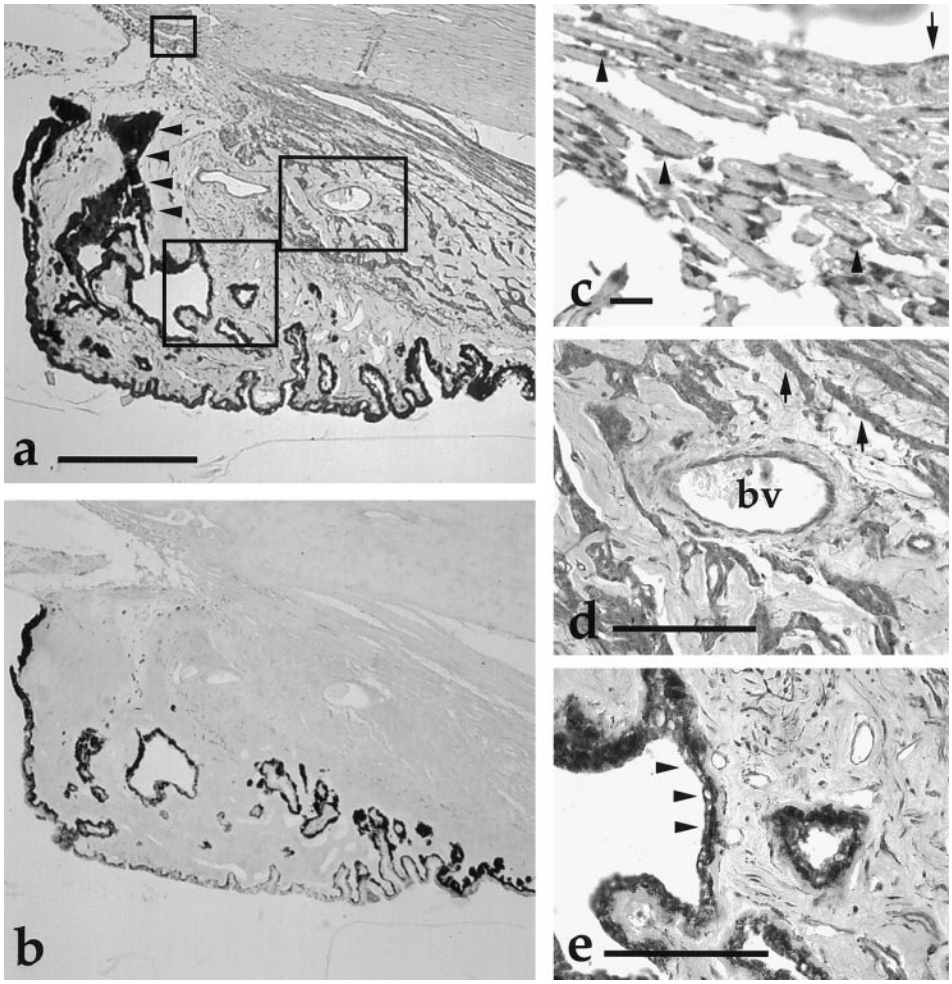

FIGURE 2. CB1 cannabinoid receptor labeling in the ciliary body and angle. Lower magnification image (**a**) shows CB1 labeling in ciliary muscle, nonpigmented ciliary epithelium, trabecular meshwork, and in the blood vessels of the ciliary body. Control section (**b**) shows labeling from antibody premixed with immunizing protein. Section is unlabeled except for partially blocked staining in ciliary epithelium. Note that large patches of black pigment are due to presence of full depth of ciliary process in the sagittal section (**a**, *arrowheads*). Magnified image (**c**) shows greater detail of angle including CB1 labeling on epithelium of the trabecular meshwork (*arrowheads*) as well as on cells lining the Schlemm's canals (*arrow*). Labeling in ciliary muscle is also evident (**d**, *arrows*) with labeled blood vessel (bv) visible. Image from same slice (**e**) shows strong labeling in nonpigmented ciliary epithelium (*arrowheads*). Scale bars, (**a**, **b**) 400 μm; (**c**) 10 μm; (**d**, **e**) 100 μm. Original magnification, (**a**, **b**) $\times$10; (**c**, **d**, **e**) $\times$100.

In one case, an eye was immersed in 4% paraformaldehyde made in 0.1 M sodium phosphate buffer at pH 7.4 overnight. After fixation, the eyecup was kept in a 30% sucrose solution in phosphate buffer for at least 48 hours before being frozen in embedding medium. Sections 10 μm thick were cut on a cryostat and thaw-mounted onto glass slides. Slide-mounted sliced retina was washed in phosphate-buffered saline (PBS), incubated overnight at 4°C with the affinity-purified rabbit polyclonal CB1 receptor antibodies (1:200 dilution made in PBS, with 0.3% Triton, 0.5% BSA). After the overnight incubation, the sections were washed with PBS and then incubated with lissamine rhodamine goat anti-rabbit antibodies (1:100; Jackson Immunoresearch Laboratories, Inc., West Grove, PA) for 90 minutes at room temperature. Finally, the tissue was washed with PBS and coverslipped with glycerine carbonate.

In control experiments, primary antibodies were omitted to determine the level of background labeling, which typically was low. As a second control, the immunizing protein (1–4 μg/ml) was mixed with the CB1 antibodies. In all cases, CB1 labeling was blocked successfully or was diminished substantially by blocking with the immunizing protein. Premixing the CB1 antibodies with a similar quantity of the immunizing protein for CB2 did not diminish labeling, though it did, in some instances, reduce background labeling.

RESULTS

Anterior Eye

CB1 labeling was detected in several locations in the anterior segment of the human eye. In the cornea and angle, strong labeling was detected in the corneal epithelium and endothelium (Fig. 1). Strong labeling also was detected in the trabecular meshwork in a pattern consistent with trabecular epithelium. In one case, moderate labeling also was detected in Schlemm's canal (Fig. 2). Moderate labeling also was detected in the lining of blood vessels in the angle. No labeling was detected in the corneal stroma.

In the uveal tract, the sphincter papillae muscle of the iris was moderately stained for CB1 receptors (Fig. 1). The anterior border layer, stroma, pigment epithelium, and the root of the iris were unstained (not shown). Labeling in the myoepithelium of the iris was difficult to assess because of the heavy pigmentation in these cells. The ciliary smooth muscle fibers were strongly stained for CB1, as was ciliary nonpigmented epithelium (Fig. 2). Labeling in the ciliary pigmented epithelium was difficult to distinguish from inherent pigmentation.

The pattern of CB1 staining generally was consistent in the five eyes examined (Table 1). The notable exception to this was the ciliary nonpigmented epithelium, which in several cases had slight nonspecific staining in the absence of canna-

TABLE 1. Summary of CB1 Receptor Labeling in Human Anterior Segment

CB1 Labeling	80 yo A	81 yo	80 yo B	49 yo	86 yo
Cornea					
Epithelium	+++	+++	+	++	+
Stroma	−	−	−	−	−
Endothelium	+++	na	+	+	+
Iris					
Anterior Border	−	na	−	−	−
Stroma	?	na	−	−	−
Sphincter	++	na	+	?	+
Pigment Epithelium	−	na	−	−	−
Root	?	na	−	−	−
Trabecular Meshwork	+++	+++	na	na	+
Schlemm's Canal	++	?	na	na	+
Ciliary Body:					
Nonpigment epithelium	+++	+++	+	na	+++
Ciliary Muscle Fibers	++	++	+	+	++
Blood Vessels	++	++	?	−	?

(+++) Strong labeling; (++) moderate labeling; (+) light labeling; (−) background labeling

* tissues from donors 80yo A and 81yo were treated with higher (1:200) concentration of antibody than others (1:400).

binoid receptor antibodies. Blocking of the CB1 antibody by premixing with immunizing protein always diminished or eliminated nonspecific staining, except in the ciliary epithelium, where the staining was only diminished, but not eliminated. This suggests that there was some recognition of a ciliary epithelium antigen by the secondary antibody. General differences in intensity of labeling was observed between eyes 80A and 81 and the others, a difference that appeared to be explainable by the fact that eyes from donors 80A and 81 were treated with higher concentrations (1:200) of CB1 antibody than eyes from other donors.

Retina

Antibodies to CB1 distinctly labeled the two synaptic layers of the retina and the outer and inner plexiform layers (Fig. 3). CB1 also heavily stained the photoreceptor outer (and to a lesser extent inner) segments and portions of the ganglion cell layer.

Light CB1 labeling was detected in the inner plexiform layer, with no evidence of stratification. Labeling in the inner nuclear layer was diffuse and difficult to assign to a particular cell type, though the labeling was consistent with the presence

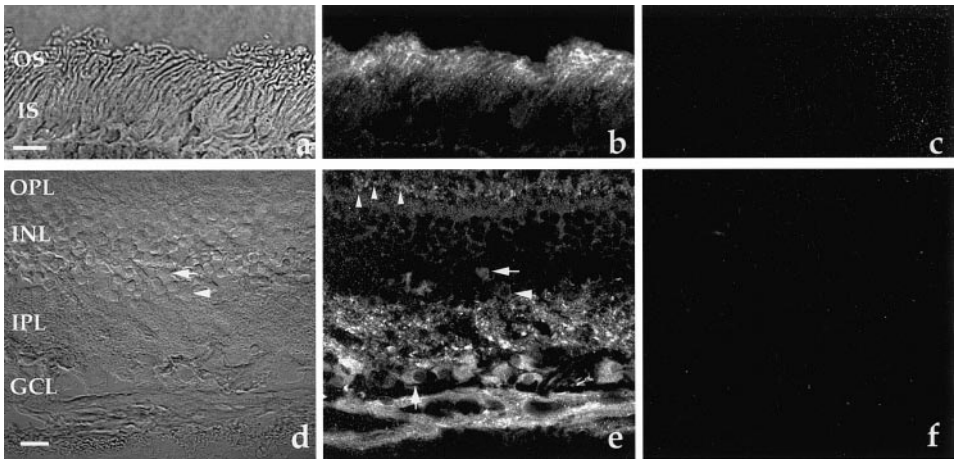

FIGURE 3. CB1 receptors are present in human retina. Photographs of retinal cross sections labeled with CB1 antibodies (**b, e**) and control sections (**c, f**). Reference tissue sections are imaged with DIC optics (**a, d**). Prominent labeling is found in photoreceptor outer segments (**b**), outer plexiform layer, inner plexiform layer and ganglion cell layer (**e**). Labeling is also present in the inner nuclear layer in a pattern consistent with amacrine cell labeling. Outer plexiform layer staining may possess labeled structures corresponding to photoreceptor synaptic terminals (*small arrowheads*), a result that would be consistent with labeling in other species. Amacrine cells appear to possess CB1 receptors (**d**, **e**; *paired left-pointing arrows* and *arrowheads*). Labeling was detected with fluorescent (lissamine rhodamine) secondary antibodies and viewed with a confocal microscope. IS/OS, inner/outer segments of photoreceptors; ONL, outer nuclear layer; OPL, outer plexiform layer; INL, inner nuclear layer; IPL, inner plexiform layer; GCL, ganglion cell layer. Scale bars, (**a**, **b**, **c**) 10 μm; (**d**, **e**) 20 μm. Original magnification, $\times$100.

of CB1 in some amacrine cells (Figs. 3d, 3e, paired left-pointing arrows and arrowheads). CB1 staining was detected in the ganglion cell layer and in the ganglion cell axon layer. In those eyes that had suffered the greatest postmortem retinal degradation (eyes 87, 90, 44, 81), labeling in the IPL was somewhat diminished, whereas labeling in the ganglion cell axon layer was increased (not shown). Additionally, in retinas from these donors, we detected a greater incidence of somatic labeling in a subpopulation of cells in the inner nuclear layer. No labeling was detected in the choroid. Labeling in the retinal pigment epithelium was difficult to assess, given the pigmented nature of the tissue. Negligible staining was observed in the control retina sections. This included controls in which CB1 antibody was incubated with immunizing protein and also in controls in which incubation with the primary antibody was omitted (Figs. 3c, 3f).

Discussion

The presence of cannabinoid receptors in many different parts of the anterior eye is consistent with the many reported physiological effects of cannabinoid consumption. First, labeling in the ciliary pigment epithelium suggests that cannabinoids may have an effect on aqueous humor production. Second, staining in the trabecular meshwork and Schlemm's canal suggests that cannabinoids may influence conventional outflow. Third, the presence of immunolabeling in the ciliary muscle suggests that cannabinoids may influence uveoscleral outflow. These observations suggest that IOP lowering by cannabinoids may reflect direct effects on ocular tissues. However, because CB1 receptors are distributed throughout much of the brain,[11] IOP lowering by cannabinoids may reflect central regulation as well as local control.

The initial discovery in 1971 that cannabinoids decrease IOP generated considerable interest. However, enthusiasm waned when it became clear that the undesired psychoactive properties of cannabinoids made them an imperfect treatment for elevated IOP. Also, the cannabinoid-induced lowering of IOP usually only lasts 4 to 6 hours, necessitating relatively frequent treatment. Tolerance to cannabinoids develops in humans,[28] though the only controlled long-term animal study showed no tolerance in rabbits after 1 year of twice daily application of synthetic cannabinoids.[29] Heavy users who abruptly stop treatment experience a rebound in IOP that temporarily increases it above pretreatment levels.[30] Despite these drawbacks, cannabinoids still hold promise as a therapeutic agent to lower IOP. Thus, the possibility of a CB1-mediated influence on IOP warrants further investigation. Pate et al.[22,23,31,32] have begun to examine endogenous, exogenous, and synthetic cannabinoids as part of a search for more effective means of reducing IOP, with some encouraging results. Establishment of a role for CB1 in the modulation of IOP, along with the ongoing dissection of the pathways activated by cannabinoid receptors, may allow a detailed characterization of the metabolic machinery underlying the maintenance of ocular tension.

The corneal endothelium, located on the posterior surface of the cornea, consists of a thin layer of simple squamous epithelial cells set in a honeycomb array. These cells play a vital role in maintaining corneal hydration, serving effectively to pump aqueous humor out of the cornea to maintain corneal clarity.[33] When corneal hydration rises beyond a certain level, some precipitation occurs, resulting in corneal opacification. Intriguingly, corneal opacification has been seen in primates treated with high doses of tetrahydrocannabinol.[34] It is possible, then, that CB1 receptor activation inhibits corneal endothelial mechanisms for removing aqueous humor from the cornea.

CB1 was also detected in the corneal epithelium, the outermost cellular layer serving primarily as a barrier to protect the eye. Any potential role of cannabinoids in the corneal epithelium remains to be investigated but it is interesting to note that during corneal healing, cell migration occurs in a process mediated by cAMP and accompanied by the development of adhesion complexes.[33] CB1 acts in part by altering levels of cAMP and has been shown to activate focal adhesion kinase, implying a potential role for CB1 in cell migration. These observations suggest CB1 agonists and antagonists may influence corneal wound healing.

Ciliary muscles serve to alter the accommodation of the lens, allowing us to focus on objects at various distances. Because ciliary muscles have an attachment to the trabecular meshwork, contraction of these muscles causes a significant change in the shape of the trabecular meshwork. This facilitates the escape of aqueous humor by conventional outflow via Schlemm's canal, reducing IOP.[35] If cannabinoids were to facilitate the contraction of the ciliary muscles, this might provide another explanation for cannabinoid effects on IOP. However, one would expect ciliary muscle contraction to produce a reduction in the range of accommodation in humans. Such an effect might serve to explain the difficulty reported by some people to read while under the influence of cannabis. Very little work has been done on this in humans, but two authors have observed just such a weakening of accommodation in patients known to smoke marijuana.[8,36] However, to our knowledge no controlled study of the effects of cannabinoids on accommodation has been undertaken. Cannabinoid action on ciliary muscle cells also might influence IOP by altering uveoscleral outflow, which passes through extracellular spaces in ciliary muscle.[34]

The presence of CB1 receptors in the sphincter papillae muscle provides a possible site of action by cannabinoids on pupil dilation/contraction. A number of articles have either reported a constriction of the pupil (miosis) or no effect.[21,37,38] The labeling we observed suggests that a reinvestigation of the phenomenon is in order.

In human retina, the overall pattern of CB1 labeling resembled that found in other vertebrates, particularly that of the primate retina.[26,39] Previous work in our laboratory using fluorescent labeling demonstrated the presence of CB1 receptors in the synaptic terminals of cone and rod photoreceptors, known as pedicles and spherules, respectively.[26] Although CB1 is clearly present in the outer plexiform layer in a pattern similar to that of other vertebrates, including structures suggestive of photoreceptor pedicles and spherules, we were unable to identify with certainty spherule and pedicle structures with either the fluorescence or immunoperoxidase techniques. As in other species, CB1 labeling was detected in the outer and inner segments of the photoreceptors. In contrast to other species in which spherule and pedicle labeling constituted the strongest retinal labeling, we found the outer segments of human photoreceptors to be the most prominent. No labeling was detected

in the somas of rod or cone photoreceptors. A wide range of visual effects have been ascribed to the use of marijuana and hashish, including an alteration of light sensitivity thresholds and glare recovery.[7,40,41] CB1 expression in photoreceptors may explain some of these effects and may thus represent a novel neuromodulatory system at the first level of visual processing. This is particularly so if CB1 is present in the synaptic terminals of human photoreceptors as we found in other vertebrates.[26]

Labeling in the inner nuclear layer was suggestive of the presence of CB1 receptors in amacrine cells. This would be consistent with a recent report of CB1 receptor labeling in some amacrine cells.[39] Activation of CB1 receptors has been shown to reduce cAMP levels by inhibiting adenylyl cyclase, activate inwardly rectifying K channels and I_A currents, and inhibiting P/Q- and N-type calcium channels.[42–48] Some of these channels are known to be present on amacrine, bipolar, and ganglion cells and may be influenced by cannabinoid receptor activation in the IPL. For example, we have shown that cannabinoid receptor agonists inhibit L-type calcium currents in bipolar cells of the tiger salamander (Straiker A, Stella N, Piomelli D, Mackie K, Karten HJ, Maguire G, unpublished observations). Müller cells possess several types of inwardly rectifying K channels in abundance.[49] These channels are thought to play a role in the reuptake of potassium. Any effect of cannabinoids on these channels in Müller cells might serve to influence retinal pathology.[50]

In conclusion, cannabinoid receptors represent part of a novel modulatory system both in the retina and in the anterior eye. Their ubiquity and distribution, combined with their known actions in other parts of the body, are suggestive of a role that extends well beyond the effects generally attributed to cannabinoids as drugs of abuse. Cannabinoids, acting via the CB1 receptor may substantively affect the maintenance of ocular tension, corneal hydration, corneal wound healing, and quite possibly vision itself. As such, further research into the mechanisms underlying these effects may provide a more thorough understanding of a wide range of interesting systems and open new therapeutic avenues in both the anterior eye and the retina.

Acknowledgments

The authors thank Anna M. Cervantes for technical assistance and the San Diego Eye Bank for providing the human eye tissue used in this study.

References

1. Hepler RS, Frank IR. Marihuana smoking and intraocular pressure. *JAMA.* 1971;217:1392.
2. Merritt JC, Perry DD, Russell DN, Jones BF. Topical delta 9-tetrahydrocannabinol and aqueous dynamics in glaucoma. *J Clin Pharmacol.* 1981;21(suppl 8–9):467S–471S.
3. Cooler P, Gregg JM. Effect of delta-9-tetrahydrocannabinol on intraocular pressure in humans. *Southern Med J.* 1977;70:951–954.
4. Purnell WD, Gregg JM. Delta(9)-tetrahydrocannabinol, euphoria and intraocular pressure in man. *Ann Ophthalmol.* 1975;7:921–923.
5. Perez-Reyes M. Clinical study of frequent marijuana use: adrenal cortical reserve metabolism of a contraceptive agent and development of tolerance. *Ann NY Acad Sci.* 1976;282:173–179.
6. Colasanti BK, Powell SR, Craig CR. Intraocular pressure, ocular toxicity and neurotoxicity after administration of delta 9-tetrahydrocannabinol or cannabichromene. *Exp Eye Res.* 1984;38:63–71.
7. Rose S, Dwyer W, Yehle A. Delta 9-Tetrahydrocannabinol: elevation of absolute visual thresholds of rabbits. *Pharmacol Biochem Behav.* 1979;10:851–853.
8. Shapiro D. The ocular manifestations of the cannabinols. *Ophthalmologica.* 1974;168:366–369.
9. Hodges LC, Reggio PH, Green K. Evidence against cannabinoid receptor involvement in intraocular pressure effects of cannabinoids in rabbits. *Ophthalmic Res.* 1997;29:1–5.
10. Matsuda LA, Lolait SJ, Brownstein MJ, Young AC, Bonner TI. Structure of a cannabinoid receptor and functional expression of the cloned cDNA *Nature*. 1990;346:561–564.
11. Herkenham M, Lynn AB, Johnson MR, Melvin LS, de Costa BR, Rice KC. Characterization and localization of cannabinoid receptors in rat brain: a quantitative in vitro autoradiographic study. *J Neurosci.* 1991;11:563–583.
12. Munro S, Thomas KL, Abu-Shaar M. Molecular characterization of a peripheral receptor for cannabinoids. *Nature.* 1993;365:61–65.
13. Schatz AR, Lee M, Condie RB, Pulaski JT, Kaminski NE. Cannabinoid receptors CB1 and CB2: a characterization of expression and adenylate cyclase modulation within the immune system. *Toxicol Appl Pharmacol.* 1997;142:278–287.
14. Skaper SD, Buriani A, Dal Toso R, et al. The ALIAmide palmitoylethanolamide and cannabinoids, but not anandamide, are protective in a delayed postglutamate paradigm of excitotoxic death in cerebellar granule neurons. *Proc Natl Acad Sci USA.* 1996;93:3984–3989.
15. Lu QJ, Straiker AJ, Lu QX, Maguire G. Expression of CB2 cannabinoid receptor mRNA and protein in adult rat retina. [ASCB Abstract]. *Mol Biol Cell.* 1998;9[suppl.]:p354a. Abstract nr 2055.
16. Shen M, Piser TM, Seybold VS, Thayer SA. Cannabinoid receptor agonists inhibit glutamatergic synaptic transmission in rat hippocampal cultures. *J Neurosci.* 1996;16:4322–4334.
17. Stella N, Schweitzer P, Piomelli D. A second endogenous cannabinoid that modulates long-term potentiation. *Nature.* 1997;388:773–778.
18. Calignano A, La Rana G, Giuffrida A, Piomelli D. Control of pain initiation by endogenous cannabinoids. *Nature.* 1998;394:277–281.
19. Devane WA, Hanus L, Breuer A, et al. Isolation and structure of a brain constituent that binds to the cannabinoid receptor. *Science.* 1992;258:1946–1949.
20. Facci L, Dal Toso R, Romanello S, Buriani A, Skaper SD, Leon A. Mast cells express a peripheral cannabinoid receptor with differential sensitivity to anandamide and palmitoylethanolamide. *Proc Natl Acad Sci USA.* 1995;92:3376–3380.
21. Mikawa Y, Matsuda S, Kanagawa T, Tajika T, Ueda N, Mimura Y. Ocular activity of topically administered anandamide in the rabbit. *Jpn J Ophthalmol.* 1997;41:217–220.
22. Pate DW, Järvinen K, Urtti A, et al. Effects of topical anandamides on intraocular pressure in normotensive rabbits. *Life Sci.* 1996;58:1849–1860.
23. Pate DW, Jarvinen K, Urtti A, Mahadevan V, Jarvinen T. Effect of the CB1 receptor antagonist, SR141716A, on cannabinoid-induced ocular hypotension in normotensive rabbits. *Life Sci.* 1998;63:2181–2188.
24. Matsuda S, Kanemitsu N, Nakamura A, et al. Metabolism of anandamide, an endogenous cannabinoid receptor ligand, in porcine ocular tissues. *Exp Eye Res.* 1997;64:707–711.
25. Porcella A, Casellas P, Gessa GL, Pani L. Cannabinoid receptor CB1 mRNA is highly expressed in the rat ciliary body: implications for the antiglaucoma properties of marihuana. *Brain Res Mol Brain Res.* 1998;58:240–245.
26. Straiker A, Karten H, Maguire G. Immunohistochemical localization of cannabinoid CB1 receptors in vertebrate retina. [Neuroscience Abstract]. *Society for Neurosciences Annual Meeting*. 1998;24:p2092. Abstract nr 833.12.
27. Tsou K, Brown S, Sañudo-Peña MC, Mackie K, Walker JM. Immunohistochemical distribution of cannabinoid CB1 receptors in the rat central nervous system. *Neuroscience.* 1998;83:393–411.
28. Flom MC, Adams AJ, Jones RT. Marijuana smoking and reduced pressure in human eyes: drug action or epiphenomenon? *Invest Ophthalmol.* 1975;4:52–55.

29. Green K, Kim K, Wynn H, Shimp RG. Intraocular pressure, organ weights and the chronic use of cannabinoid derivatives in rabbits for one year. *Exp Eye Res.* 1977;25:465–471.
30. Jones RT, Benowitz NL, Herning RI. Clinical relevance of cannabis tolerance and dependence. *J Clin Pharmacol.* 1981;21:143S–152S.
31. Pate DW, Järvinen K, Urtti A, Jarho P, Järvinen T. Ophthalmic arachidonylethanolamide decreases intraocular pressure in normotensive rabbits. *Curr Eye Res.* 1995;14:791–797.
32. Pate DW, Järvinen K, Urtti A, Jarho P, Mahadevan V, Järvinen T. Effects of topical alpha-substituted anandamides on intraocular pressure in normotensive rabbits. *Pharm Res.* 1997;14:1738–1743.
33. Hart W Jr. *Adler's Physiology of the Eye*. 8th ed. St. Louis, Mosby Year Books; 1992:29–71.
34. Colasanti BK. Intraocular pressure, ocular toxicity and neurotoxicity in response to 11-hydroxy-delta 9-tetrahydrocannabinol and 1-nantradol. *J Ocular Pharmacol.* 1985;1:123–135.
35. Lindsey JD, Kashiwagi K, Kashiwagi F, Weinreb RN. Prostaglandin action on ciliary smooth muscle extracellular matrix metabolism: implications for uveoscleral outflow. *Surv Ophthalmol.* 1997;41: S53–S59.
36. Valk LEM. Hemp in connection with Ophthalmology. *Ophthalmologica.* 1974;167:413–421.
37. Brown B, Adams AJ, Haegerstrom-Portnoy G, Jones RT, Flom MC. Pupil size after use of marijuana and alcohol. *Am J Ophthalmol.* 1977;83:350–354.
38. Liu JH, Dacus AC. Central nervous system and peripheral mechanisms in ocular hypotensive effect of cannabinoids. *Arch Ophthalmol.* 1987;105:245–248.
39. Yazulla S, Studholme KM, McIntosh HH, Howlett AC, Deutsch DG. Immunocytochemical localization of cannabinoids in rat retina. [ARVO Abstract]. *Invest Ophthalmol Vis Sci.* 1999;40(4):S978. Abstract nr 5147.
40. Kiplinger GF, Manno JE, Rodda BE, Forney RB. Dose-response analysis of the effects of tetrahydrocannabinol in man. *Clin Pharmacol Ther.* 1971;12:650–657.
41. Moskowitz H, Sharma S, McGlothlin W. Effect of marihuana upon peripheral vision as a function of the information processing demands in central vision. *Percept Motor Skills.* 1972;35: 875–882.
42. Poling JS, Rogawski MA, Salem N Jr, Vicini S. Anandamide, an endogenous cannabinoid, inhibits Shaker-related voltage-gated K+ channels. *Neuropharmacology.* 1996;35:983–991.
43. Mackie K, Lai Y, Westenbroek R, Mitchell R. Cannabinoids activate an inwardly rectifying potassium conductance and inhibit Q-type calcium currents in AtT20 cells transfected with rat brain cannabinoid receptor. *J Neurosci.* 1995;15:6552–6561.
44. Deadwyler SA, Hampson RE, Mu J, Whyte A, Childers S. Cannabinoids modulate voltage-sensitive potassium A current in hippocampal neurons via a cAMP-dependent process. *J Pharmac Exp Ther.* 1995;273:734–743.
45. Deadwyler SA, Heyser CJ, Michaelis RC, Hampson RE. The effects of delta-9-THC on mechanisms of learning and memory. *NIDA Res Monogr.* 1990;97:79–93.
46. Zeltser R, Seltzer Z, Eisen A, Feigenbaum JJ, Mechoulam R. Suppression of neuropathic pain behavior in rats by a non-psychotropic synthetic cannabinoid with NMDA receptor-blocking properties. *Pain.* 1991;47:95–103.
47. Derkinderen P, Toutant M, Burgaya F, et al. Regulation of a neuronal form of focal adhesion kinase by anandamide. *Science.* 1996; 273:1919–1922.
48. Martin WJ, Hohmann AG, Walker JM. Inhibition of noxious stimulus-evoked activity in the ventral posterolateral nucleus of the thalamus by the cannabinoid WIN 55,212–2: correlation of electrophysiological effects with antinociceptive actions. *J Neurosci.* 1996;16:6601–6611.
49. Chao TI, Henke A, Reichelt W, Eberhardt W, Reinhardt-Maelicke S, Reichenbach A. Three distinct types of voltage-dependent K+ channels are expressed by Müller (glial) cells of the rabbit retina. *Pfluegers Arch Eur J Physiol.* 1994;426:51–60.
50. Maguire G, Simko H, Weinreb RN, Ayoub G. Transport-mediated release of endogenous glutamate in the vertebrate retina. *Pfluegers Arch Eur J Physiol.* 1998;436:481–484.

Regional Differences in Retinal Vascular Reactivity

Hak Sung Chung,[1] Alon Harris,[1] Paul J. Halter,[2] Larry Kagemann,[1] Emma J. Roff,[2] Hanna J. Garzozi,[1] Sarah L. Hosking,[2] and Bruce J. Martin[3]

Purpose. Although glaucomatous visual field defects are more common in the superior field than in the inferior field, microaneurysms are more frequent in the superior than in the inferior retina in diabetic retinopathy. The authors hypothesized that differences in vascular hemodynamics in the two areas might contribute to these phenomena.

Methods. The blood flow response to hyperoxia and hypercapnia was evaluated in peripapillary retinal tissue superior and inferior to the optic nerve head using confocal scanning laser Doppler flowmetry. In 14 young, healthy persons, blood flow was measured while breathing room air and during isocapnic hyperoxia (100% O_2 breathing) and isoxic hypercapnia (Pco2 increased 15% above baseline). Histograms were generated from pixel-by-pixel analysis of retinal portions of superior and inferior temporal quadrants of the entire image.

Results. Baseline blood flow in the inferior temporal quadrant was significantly greater than in the superior temporal quadrant ($P < 0.05$). However, the inferior region failed to increase in perfusion during hypercapnia and experienced significant mean blood flow reduction; flow reduction in the pixels at the 25th, 50th, 75th, and 90th percentile of flow; and an increased percentage of pixels without measurable flow, during hyperoxia (each $P < 0.05$). In contrast, in the superior temporal region, hyperoxia failed to reduce blood volume, velocity, or flow, whereas hypercapnia signifi-

From the [1]Department of Ophthalmology, Indiana University School of Medicine, Indianapolis; [2]Division of Vision Sciences, Aston University, Birmingham, United Kingdom; and [3]Medical Sciences Program, Indiana University, Bloomington.

Supported in part by Grant EY10801 (AH) from the National Institutes of Health, Bethesda, Maryland; and by an unrestricted grant from Research to Prevent Blindness, New York, New York. AH is a recipient of the William and Mary Greve Award from Research to Prevent Blindness.

Submitted for publication November 13, 1998; revised April 2, 1999; accepted April 21, 1999.

Proprietary interest category: N.

Corresponding author: Alon Harris, Department of Ophthalmology, Indiana University School of Medicine, 702 Rotary Circle, Indianapolis, IN 46202.
E-mail: alharris@indiana.edu

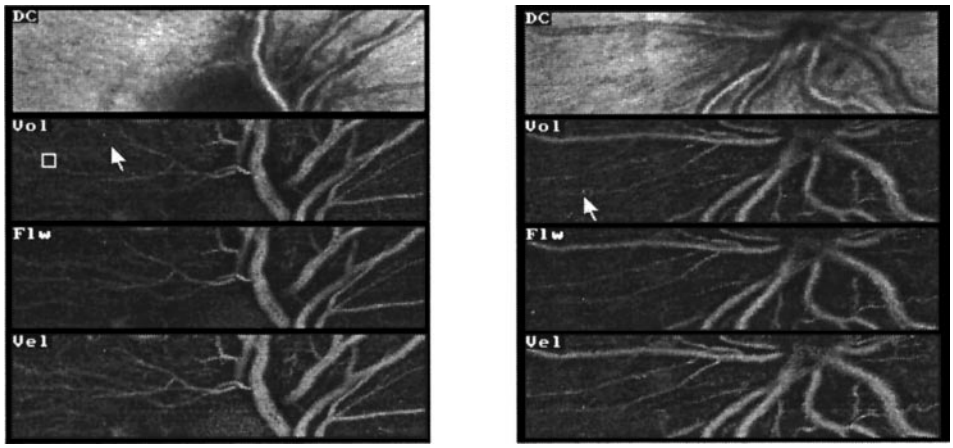

FIGURE 1. Sampling window of the reflectivity image (DC) and volume, flow, and velocity perfusion maps showing the single pixel (*arrow*) analysis of a normal subject in the superior region (*left*) and the inferior region (*right*). The *square* in the *left panel* is the conventional default measurement box (10 × 10 pixels).

cantly increased mean flow; increased flow in the pixels at the 25th, 50th, 75th, and 90th percentile of flow; and reduced the percentage of pixels without measurable flow (each $P < 0.05$).

CONCLUSIONS. The inferior temporal quadrant of the peripapillary retina is, in comparison with the superior temporal region, less responsive to vasodilation and more responsive to vasoconstriction. These differences could contribute to different susceptibility to visual field defect or vascular dysfunction in the superior and inferior retina. (*Invest Ophthalmol Vis Sci.* 1999;40:2448–2453)

Defects in the superior visual field are more common than in the inferior visual field in glaucoma.[1] Further, narrowing of the retinal arteries and veins, a development that occurs in proportion to disease severity, is most pronounced inferiorly.[2] In contrast, in diabetic retinopathy, microaneurysms, and acellular capillaries are more than twice as common in the superior than in the inferior retina.[3] Additionally, enlargement of the retinal veins, a change that correlates with the severity of disease and the magnitude of hyperglycemia, is also most pronounced superiorly.[4] The mechanisms that give rise to these distinct, disease-specific regional differences in vascular and visual field defect have not been defined.

It is possible that differences in vulnerability to ischemic insult or to hyperglycemic damage arise from inherent retinal regional differences in vasoreactivity. To test this hypothesis, we compared the blood flow responses of the inferior and superior retinal regions to vasoconstrictor and vasodilator stimuli. Hyperoxia, which provokes cerebral and whole-retinal vasoconstriction,[5] and hypercapnia, which dilates arteries and arterioles within the brain and the eye,[6] were used as vasoprovocative stimuli. Differing responses of the superior and inferior retina to these stimuli would support the hypothesis that these retinal regions differ in their susceptibility to ischemic or hyperglycemic insult.

MATERIALS AND METHODS

Subjects

Fourteen healthy volunteers (7 men, 7 women; mean age, 27 ± 6 years; age range, 18–40 years) participated in the study. Subjects had normal eye examinations, with corrected visual acuity 20/30 or better, intraocular pressure (IOP) below 22 mm Hg, refractive error between −6.00 and +2.00 diopters, and astigmatism less than 1.50 diopters cylinder. Subjects were free from heart or lung disease, had no family history of glaucoma or diabetes, and were not pregnant or anticipating pregnancy at the time of study. All procedures conformed to the tenets of the Declaration of Helsinki and were reviewed and approved by an institutional review board, with subjects signing informed consent.

Experimental Design

Two experimental sessions, one involving hyperoxia and the other hypercapnia, took place on separate days. The mean interval between experiments was 10 ± 5 days (range, 2–19 days). Ocular blood flow was measured using confocal scanning laser Doppler flowmetry (cSLDF, Heidelberg Retinal Flowmeter; Heidelberg Engineering, Heidelberg, Germany). Heart rate and arterial oxygen saturation were monitored using pulse oximetry. After 5 minutes acclimation, baseline recordings were made with the subject breathing room air. End-tidal CO_2 and O_2 were monitored continuously from a mouthpiece (Pulse Oximeter and End-Tidal Gas Analyzer: POET II model 602-3, Criticare Systems, Milwaukee, WI).

Hyperoxia and Hypercapnia

Hyperoxia was induced by adding 100% O_2 to the inspired gas mixture; CO_2 was added to maintain isocapnia during this procedure. Five minutes after the end-tidal O_2 fraction exceeded 70%, ocular blood flow measurements were made. In experiments involving hypercapnia, end-tidal P_{CO_2} was elevated 15% above baseline levels for 5 minutes before measurement of ocular blood flow. Elevation of P_{CO_2} was accomplished by addition of 4 to 6% CO_2 to the inspiratory gas mixture.

Measurement of Ocular Blood Flow: cSLDF

One eye from each subject was randomly selected for study. With undilated pupils, subjects fixed on a static target 3 feet away. Using a 10° field, two mapped images (superior and inferior) were obtained across the optic nerve head for each experimental condition. Images were focused on the superficial retina, with focus setting and anatomic location constant across all images from a given subject.

One observer reviewed all images (Fig. 1). Unlike conven-

tional analysis that uses a single 10 pixel × 10 pixel sample, each qualifying pixel from the superficial peripapillary retinal field within the 256 × 64 pixel image was included in the analysis (Fig. 1). This methodology significantly increases the reproducibility of measurements of blood velocity, volume, and flow.[7] Excluded were pixels from the cup and rim (which were poorly focused), pixels from major blood vessels, image areas interrupted by movement saccades, and areas without acceptable levels of brightness (any brightness [DC] value <70 or >200). To ensure that the same retinal locations were used for each image, a transparent overlay was used to map the retinal vasculature of each optic nerve head. This template was then overlaid on the image, and the temporal peripapillary area was separated into inferior and superior divisions. To produce a histogram, the total number of pixels for all images was determined, the average was calculated, and a normalized pixel count was calculated that gave equal weight to each subject. Pixels with less than one arbitrary unit of flow were counted as "zero flow" pixels. The number of zero flow pixels and the flow, volume, and velocity in pixels at the 25th, 50th, 75th, and 90th percentile in each category were used for analysis.[7]

Statistical Analysis

Two-tailed paired *t*-tests were used to compare ocular blood volume, velocity, and total flow between baseline and gas perturbation conditions, with $P < 0.05$ regarded as significant. The sample size of 14 was chosen for a power of 80% and $\alpha = 0.05$, while providing the capability for detection of a 12% difference in blood flow.

Results

Hyperoxia and Hypercapnia

Hyperoxia increased end-tidal P_{O_2} from 103 ± 5 (mean ± SD) to 562 ± 80 mm Hg ($P < 0.05$); hypercapnia increased end-tidal P_{CO_2} from 32 ± 2 to 39 ± 4 mm Hg ($P < 0.05$). Hyperoxia reduced heart rate from 84 ± 9 to 78 ± 7 beats/min ($P < 0.05$) at constant arterial blood pressure, while hypercapnia increased systolic blood pressure from 112 ± 8 to 115 ± 8 mm Hg ($P < 0.05$) at constant heart rate and diastolic pressure.

Pixel Counts from HRF images

Group mean pixel counts did not differ between images taken from the superior and inferior peripapillary retina (Tables 1, 2, 3). Pixel counts also did not differ between baseline images and those taken during hyperoxia or hypercapnia (Tables 1, 2, 3). The overall mean pixel count averaged 1156 pixels/image, a quantity 11.5 times larger than the default 10 pixel × 10 pixel box.

Baseline Blood Flow: Superior versus Inferior Temporal Peripapillary Retina

When baseline blood flow before the imposition of hyperoxia was compared between the superior and inferior temporal regions of the retina, mean volume, velocity, and flow were significantly greater in the inferior area (Table 1). A similar, nonsignificant tendency for greater inferior mean volume, velocity, and flow also was present in baseline measurements before the imposition of hypercapnia, and the average baseline volume and flow from the two experiments also was greater inferiorly (Table 1). Inferior and superior portions of the temporal peripapillary retina did not differ in the percentage of zero-flow pixels (Table 1).

Table 1. Baseline Blood Flow in the Superior and Inferior Temporal Peripapillary Retina

	Superior	Inferior
Baseline before hyperoxia		
Mean pixel count	1052	1184
Volume (arbitrary units)	21.7 ± 3.3	23.5 ± 4.1*
Velocity (arbitrary units)	1.21 ± 0.17	1.32 ± 0.25*
Mean flow (arbitrary units)	350 ± 55	386 ± 83*
Baseline before hypercapnia		
Mean pixel count	1151	1233
Volume (arbitrary units)	21.3 ± 3.6	22.8 ± 3.6
Velocity (arbitrary units)	1.17 ± 0.24	1.23 ± 0.26
Mean flow (arbitrary units)	330 ± 69	361 ± 85
Mean of two baselines		
Mean pixel count	1102	1209
Volume (arbitrary units)	21.5 ± 2.9	23.1 ± 3.2*
Velocity (arbitrary units)	1.19 ± 0.18	1.28 ± 0.21
Mean flow (arbitrary units)	340 ± 57	374 ± 69*
Zero-flow pixels (% of total pixels)	10.1 ± 3.2	11.3 ± 4.1

Values are means ± SD; $n = 14$.
* $P < 0.05$ versus superior temporal peripapillary retina.

The two baseline readings, when compared over the same anatomic retinal regions, showed similar volume, velocity, and flow recordings except in regard to superior temporal blood flow at the 90th percentile pixel. This flow value was higher in the prehyperoxia recording (751 ± 34; range, 499–906 arbitrary units) than in the prehypercapnia reading (693 ± 34; range, 499–930 arbitrary units; $P < 0.05$).

Response to Hyperoxia and Hypercapnia: Superior Temporal Peripapillary Retina

In the superior temporal peripapillary retina, hyperoxia failed to change mean blood flow (Table 2). Hyperoxia also failed to change the percentage of zero flow pixels, or the volume, velocity, or flow in either the 25th, 50th, 75th, or 90th percentile pixel (Table 2). In contrast, hypercapnia significantly increased mean blood volume, velocity, and flow; decreased the percentage of zero flow pixels; and increased blood volume, velocity, and flow within pixels at the 25th, 50th, 75, and 90th percentiles of each of these variables (Table 2).

Response to Hyperoxia and Hypercapnia: Inferior Temporal Peripapillary Retina

In contrast to results found in the superior retina, in the inferior temporal peripapillary retina, hyperoxia significantly reduced mean blood flow (Table 3). Although the percentage of zero-flow pixels was unchanged by hyperoxia, mean blood volume and blood volume within pixels at the 25th, 50th, 75th, and 90th percentiles of this variable was reduced (Table 3). In addition, mean velocity was reduced within the 90th percentile pixel (Table 3). Blood flow was reduced during hyperoxia

TABLE 2. Effects of Hyperoxia and Hypercapnia on Blood Volume, Velocity, and Flow in Superior Temporal Peripapillary Retina

Aspect of histogram	Baseline	Hyperoxia	Baseline	Hypercapnia
Mean pixel count	1052	1122	1151	1147
Zero-flow pixels (% of total pixels)	9.9 ± 4.0	10.5 ± 3.1	10.4 ± 4.0	8.9 ± 3.7*
Mean flow (arbitrary units)	350 ± 55	361 ± 132	330 ± 69	400 ± 108*
Flow at specific percentiles (arbitrary units)				
25th	118 ± 32	114 ± 45	106 ± 35	136 ± 54*
50th	266 ± 46	268 ± 86	255 ± 55	294 ± 80*
75th	471 ± 76	477 ± 72	444 ± 88	523 ± 126*
90th	751 ± 158	775 ± 323	693 ± 128	864 ± 242*
Mean volume (arbitrary units)	21.7 ± 3.3	20.5 ± 3.5	21.3 ± 3.6	24.4 ± 5.1*
Volume at specific percentiles (arbitrary units)				
25th	12.1 ± 1.8	11.3 ± 2.2	11.5 ± 2.1	12.9 ± 2.9*
50th	18.5 ± 2.8	16.9 ± 3.4	17.5 ± 3.1	20.0 ± 4.8*
75th	27.9 ± 4.4	26.0 ± 4.6	27.4 ± 4.6	31.2 ± 6.6*
90th	40.0 ± 7.0	37.7 ± 6.8	39.0 ± 6.9	45.4 ± 10.1*
Mean velocity (arbitrary units)	1.21 ± 0.17	1.23 ± 0.39	1.17 ± 0.24	1.35 ± 0.33*
Velocity at specific percentiles (arbitrary units)				
25th	0.44 ± 0.12	0.43 ± 0.16	0.40 ± 0.13	0.50 ± 0.20*
50th	0.93 ± 0.18	0.94 ± 0.32	0.90 ± 0.24	1.03 ± 0.32*
75th	1.67 ± 0.25	1.67 ± 0.53	1.60 ± 0.31	1.83 ± 0.40*
90th	2.56 ± 0.40	2.63 ± 0.98	2.44 ± 0.47	2.87 ± 0.71*

Values are means ± SD; $n = 14$.
* $P < 0.05$ versus baseline.

in the 75th and 90th percentile pixels (Table 3). Hypercapnia, however, failed to change any measured aspect of hemodynamics in the inferior temporal quadrant. During CO_2 elevation, mean volume, velocity, and flow were unaffected, the percentage of zero-flow pixels was unchanged, and at each percentile of the cSLDF histogram, volume, velocity, and flow were unaltered (Table 3).

DISCUSSION

Higher baseline perfusion in the inferior temporal compared with the superior temporal retina may arise from several possibilities. There is evidence that the normal inferior temporal artery and vein are larger than the analogous superior vessels.[2] Past authors have speculated that these vessels are increased in

TABLE 3. Effects of Hyperoxia and Hypercapnia on Blood Volume, Velocity, and Flow in Inferior Temporal Peripapillary Retina

Aspect of histogram	Baseline	Hyperoxia	Baseline	Hypercapnia
Mean pixel count	1184	1174	1233	1186
Zero-flow pixels (% of total pixels)	10.3 ± 4.0	10.8 ± 3.7	12.2 ± 5.9	11.4 ± 5.3
Mean flow (arbitrary units)	386 ± 83	332 ± 40*	361 ± 85	391 ± 109
Flow at specific percentiles (arbitrary units)				
25th	127 ± 49	108 ± 31	105 ± 52	117 ± 57
50th	288 ± 66	254 ± 38	258 ± 63	282 ± 81
75th	509 ± 109	447 ± 53*	474 ± 97	518 ± 132
90th	824 ± 184	702 ± 92*	789 ± 190	880 ± 273
Mean volume (arbitrary units)	23.5 ± 4.1	20.4 ± 2.8*	22.8 ± 3.6	24.5 ± 5.3
Volume at specific percentiles (arbitrary units)				
25th	12.8 ± 2.4	11.2 ± 1.7*	11.9 ± 2.0	12.7 ± 2.5
50th	19.8 ± 3.6	17.4 ± 2.0*	18.8 ± 2.7	20.1 ± 3.9
75th	30.0 ± 5.5	25.9 ± 3.4*	29.1 ± 5.0	31.6 ± 7.1
90th	43.2 ± 9.1	37.1 ± 6.7*	43.1 ± 8.2	46.6 ± 11.8
Mean velocity (arbitrary units)	1.31 ± 0.25	1.18 ± 0.17	1.23 ± 0.26	1.36 ± 0.35
Velocity at specific percentiles (arbitrary units)				
25th	0.47 ± 0.18	0.41 ± 0.13	0.39 ± 0.19	0.44 ± 0.22
50th	1.05 ± 0.23	0.94 ± 0.16	0.94 ± 0.22	1.03 ± 0.29
75th	1.78 ± 0.33	1.62 ± 0.22	1.67 ± 0.31	1.85 ± 0.44
90th	2.78 ± 0.55	2.51 ± 0.40*	2.66 ± 0.55	3.00 ± 0.80

Values are means ± SD; $n = 14$.
* $P < 0.05$ versus baseline.

diameter in the inferior retina in part because the fovea is located slightly inferior to a horizontal midline and in part because the neuroretinal rim is broader inferiorly than superiorly.[2] Our findings suggest in addition that the inferior temporal retina receives a slightly greater capillary perfusion. It is unknown if greater basal perfusion is associated with increased density of ganglion cells, of cells of the intermediate cell layer, or is instead linked to other factors. In other regions of the brain, although differences in metabolic activity are directly tied to differences in oxygen consumption, these differences are only roughly related to differences in blood flow.[8]

A number of previous studies have used hyperoxia and hypercapnia as stimuli for vasoconstriction and vasodilation. Hyperoxia reduces total cerebral blood flow, whereas hypercapnia increases bulk cerebral perfusion, with these effects mediated locally via changes in arteriolar diameter and unrelated (as again seen in this study) to any changes in systemic arterial blood pressure. However, changes in both P_{O_2} and P_{CO_2} give rise to substantial cerebral inter-regional variation in the constrictor or dilator response.[9] This regional variation exists also within the retina, with our results showing the most anatomically localized inter-regional difference yet described in cerebral circulatory responsiveness to vasoactive stimuli.

The mechanisms that underlie regional vasoresponsiveness within the retina remain ill-defined. In the brain as a whole, it is clear that the visual cortex, for example, maintains a relatively high blood flow and high oxygen extraction in comparison to the sensorimotor cortex,[8] but the factors regulating this difference are not known. Cerebral capillary perfusion appears to be controlled at least in part by neuronally derived nitric oxide: inhibition of neuronal nitric oxide synthase blocks the cerebral capillary perfusion increase provoked by hypoxia.[10] However, this generalization does not explain why various tissues (or regions within a relatively homogeneous tissue) may respond differently to vasoactive stimuli. There is evidence, however, that chronically increased or decreased perfusion of regions within a single organ leads to subsequent alterations in vasoreactivity, due to changes in both neuronal and endothelially mediated vascular regulatory processes.[11]

The significance of intraretinal differences in vasodilatory and vasoconstrictor responsiveness also is as yet undefined. There are several possibilities, however, by which these differences might be linked to susceptibility to disease. Reduced vasodilator reserve, as seen in the temporal inferior retina, is associated in other organs with diminished capacity to withstand reductions in perfusion pressure or arterial oxygen content or increases in tissue metabolic demands.[12] For the retina, reduced ocular perfusion pressure, as induced by either elevated IOP or reduced arterial pressure, could create risk for ischemic damage.[13] Although most authors presume that the short posterior ciliary arterial supply of the laminar and prelaminar optic nerve head is of primary importance for the development of ischemia-induced damage in glaucoma, it is indeed in the inferior retina that at least indirect evidence for ischemia is most pronounced in glaucomatous ocular disease.[2]

Although the loss or absence of vasodilator reserve may exacerbate the risk of ischemic damage to tissue, an inability to generate autoregulatory vasoconstrictor responses also may expose cells to potential damage. In diabetes mellitus, a number of primary nonvascular mechanisms, ranging from the induction of angiogenic growth factors to the actions of advanced glycation end products, may underlie development of retinopathy.[14] However, the microvascular complications of chronic hyperglycemia do include impaired vasoconstriction in response to endogenous endothelin-1, neuropeptide Y, and to nonspecific stimuli such as cold exposure.[15] Loss of normal vascular smooth muscle contractile responses could expose tissue to hyperperfusion and subsequent microvascular damage.[15] These cellular level changes may account for the loss of overall retinal vasoconstrictor responsiveness to hyperoxia that proceeds in proportion to progression of diabetes.[16] The relative lack of normal vasoconstrictor responsiveness in the superior temporal retina could explain why that region is more susceptible to development of microaneurysms and acellular capillaries in diabetes[3] and why dilation of the retinal veins, which also occurs in proportion to diabetes severity, is most prominent superiorly.[4]

In summary, variation in vasoreactivity within the healthy retina may help explain differences in regional susceptibility to a number of retinal and optic nerve head diseases. Localized retinal under- or over-perfusion, as induced by a wide range of physiological or pathophysiological perturbations, may occur predictably on the basis of normal tissue autoregulatory capacity.

References

1. Hart WM, Becker B. The onset and evolution of glaucomatous visual field defects. *Ophthalmology.* 1982;89:268–275.
2. Jonas JB, Nguyen XN, Naumann GO. Parapapillary retinal vessel diameter in normal and glaucoma eyes. I. Morphometric data. *Invest Ophthalmol Vis Sci.* 1989;30:1599–1603.
3. Kern TS, Engerman RL. Vascular lesions in diabetes are distributed non-uniformly within the retina. *Exp Eye Res.* 1995;60:545–549.
4. Falck A, Laatikainen L. Retinal vasodilation and hyperglycaemia in diabetic children and adolescents. *Acta Ophthalmol Scand.* 1995; 73:119–124.
5. Langhans M, Michelson G, Groh MJM. Effect of breathing 100% oxygen on retinal and optic nerve head capillary blood flow in smokers and non-smokers. *Br J Ophthalmol.* 1997;81:365–369.
6. Harris A, Anderson DR, Pillunat L, et al. Laser Doppler flowmetry measurement of changes in human optic nerve head blood flow in response to blood gas perturbations. *J Glaucoma.* 1996;5:258–265.
7. Kagemann L, Harris A, Chung HS, Evans DW, Buck S, Martin B. Heidelberg retinal flowmetry: factors affecting blood flow measurement. *Br J Ophthalmol.* 1998;82:131–136.
8. Ishii K, Sasaki M, Kitagaki H, Sakamoto S, Yamaji S, Maeda K. Regional difference in cerebral blood flow and oxidative metabolism in human cortex. *J Nucl Med.* 1996;37:1086–1088.
9. Payen JF, Vath A, Koenigsberg B, Bourlier V, Decorps M. Regional cerebral plasma volume response to carbon dioxide using magnetic resonance imaging. *Anesthesiology.* 1998;88:984–992.
10. Hudetz AG, Shen H, Kampine JP. Nitric oxide from neuronal NOS plays a critical role in cerebral capillary flow response to hypoxia. *Am J Physiol.* 1998;274:H982–H989.
11. Pourageaud F, De Mey JG. Vasomotor responses in chronically hyperperfused and hypoperfused rat mesenteric arteries. *Am J Physiol.* 1998;274:H1301–H1307.
12. Singh TP, Di Carli MF, Sullivan NM, Leonen MF, Morrow WR. Myocardial flow reserve in long-term survivors of repair of anomalous left coronary artery from pulmonary artery. *J Am Coll Cardiol.* 1998;31:437–443.
13. Robinson F, Riva CE, Grunwald JE. Retinal blood flow autoregulation in response to an acute increase in blood pressure. *Invest Ophthalmol Vis Sci.* 1986;27:722–726.
14. Hammes HP, Wellensiek B, Kloting I, Sickel E, Bretzel RG, Brownlee M. The relationship of glycaemic level to advanced glycation end-product (AGE) accumulation and retinal pathology in the spontaneous diabetic hamster. *Diabetologia.* 1998;41:165–170.

15. Nugent AG, McGurk C, Hayes JR, Johnston GD. Impaired vasoconstriction to endothelin 1 in patients with NIDDM. *Diabetes.* 1996; 45:105–107.

16. Grunwald JE, Riva CE, Brucker AJ, Sinclair SH, Petrig BL. Altered retinal vascular response to 100% oxygen breathing in diabetes mellitus. *Ophthalmology.* 1984;91:1447–1452.

Vascular Adhesion Molecules in Vitreous from Eyes with Proliferative Diabetic Retinopathy

G. Astrid Limb,[1] Julian Hickman-Casey,[2] Robert D. Hollifield,[3] and Anthony H. Chignell[3]

Purpose. To investigate whether proliferative vitreoretinopathy (PDR) is associated with a selective increase in vitreous levels of soluble vascular cell adhesion molecules that mediate leukocyte extravasation and interaction with endothelium during processes of inflammation and neovascularization.

Methods. Vitreous from 55 patients undergoing vitrectomy for treatment of PDR complicated by vitreous hemorrhage and/or traction retinal detachment was assayed for the presence of the soluble vascular cell adhesion molecules sICAM-1, sVCAM-1, and sE-selectin using a standard enzyme-linked immunosorbent assays (ELISA). Vitreous from 12 cadaveric eyes matching age and sex of the patients were used as control samples.

Results. Vitreous levels of sICAM-1, sVCAM-1, and sE-selectin were significantly higher in eyes with PDR than in control cadaveric vitreous, and levels of all three molecules did not relate to the type or duration of diabetes mellitus. However, eyes with either traction retinal detachment alone or both traction retinal detachment and vitreous hemorrhage exhibited significantly higher levels of sICAM-1 and sE-selectin than eyes with vitreous hemorrhage alone. Vitreous levels of sVCAM-1 were similar in eyes with either vitreous hemorrhage or traction retinal detachment alone.

Conclusions. The present observations suggest that molecular inflammatory mechanisms may contribute to processes of neovascularization and fibrosis observed in PDR, possibly not as the causative event, but as a result of endothelial, Müller, and retinal pigment epithelial cell activation. The results also indicate that retinal detachment amplifies the existing inflammation within the diabetic retina. Identification of any abnormalities in the production and control of specific adhesion molecules could have important implications in the design of new therapeutic regimens to treat and prevent this sight-threatening complication of diabetes mellitus. (*Invest Ophthalmol Vis Sci.* 1999;40:2453–2457)

From the [1]Department of Pathology, Institute of Ophthalmology and Moorfields Eye Hospital, [2]Kings College Hospital, and [3]St. Thomas' Hospital, London, United Kingdom.

Supported by Gift of Thomas Pocklington Trust and the Guide Dogs for the Blind Association.

Submitted for publication January 21, 1999; revised March 30, 1999; accepted April 20, 1999.

Proprietary interest category: N.

Corresponding author: G. Astrid Limb, Department of Pathology, Institute of Ophthalmology, Bath Street, London EC1V 9EL UK.

Proliferative diabetic retinopathy (PDR) is a common complication of diabetes mellitus, characterized by active neovascularization of the optic disc and the retina, with formation of fibrovascular tissue at the vitreoretinal interface.[1] Neovascularization is thought to be induced by retinal ischemia caused by capillary occlusion, in which platelets and leukocytes may play an important role. Although the idea that inflammation may be involved in the development of insulin-dependent diabetes mellitus (IDDM) is controversial,[2] to our knowledge the concept that inflammation may play a role in the pathogenesis of PDR has not been addressed in the literature. However, all the molecular mechanisms implicated in new vessel formation and fibrosis in PDR[3,4] are those that characterize inflammation in general.[5] Therefore, leukocytes often found within PDR membranes[6] may well have migrated into the retina by the same mechanisms by which they would normally migrate into sites of inflammation.

Inflammation is initiated by activation of endothelial cells by cytokines, which results in their enhanced expression and shedding of vascular cell adhesion molecules.[7] Upregulation of vascular cell adhesion molecules is critical for leukocyte migration through endothelial cell junctions into the abluminal surface of the vessels.[7,8] Rolling and adhesion of leukocytes to vascular endothelium, which are the initial steps for leukocyte extravasation, are mediated by the adhesion molecules P-selectin, E-selectin, and L-selectin,[7,8] whereas more firm leukocyte–endothelial interactions and cell migration are governed by intercellular adhesion molecule (ICAM)-1 and the vascular cell adhesion molecule (VCAM)-1.[7,8]

Extracellular domains of vascular cell adhesion molecules are often found as soluble (s) forms in serum and body fluids, after cleavage by metalloproteinases,[9] and both E-selectin and VCAM-1 are recognized to be angiogenic in vivo and in vitro.[10] It is possible that these molecules play a role in the pathogenesis of PDR. Supranormal serum levels of sICAM-1, sVCAM-1, and sE-selectin may be found in patients with chronic inflammatory[11] and ocular disease[12] and in patients with IDDM, particularly those with retinopathy.[13,14] In addition, high vitreous levels of sICAM-1 are observed in eyes with anterior uveitis[15] and in eyes with proliferative vitreoretinopathy,[16] where they constitute a marker of inflammation severity and a risk factor for development of this complication of retinal detachment.

In view of the above evidence and of the potential angiogenic role of vascular cell adhesion molecules, we investigated whether high vitreous levels of sICAM-1, sVCAM-1, and sE-selectin may be found in vitreous from eyes with PDR and whether they relate to retinal complications of this condition, such as vitreous hemorrhage and traction retinal detachment.

METHODS

Vitreous samples were obtained from 55 patients undergoing vitreoretinal surgery for the treatment of vitreous hemorrhage alone (23 patients), traction retinal detachment alone (21 patients), or both vitreous hemorrhage and traction retinal detachment (11 patients) complicating PDR. Of the patients investigated, 31 had IDDM and 17 had non-IDDM. Forty-one patients had diabetes of more than 20 years' duration (mean, 22 ± 7.3 years), and 16 patients had diabetes of less than 10 years' duration (mean, 6 ± 2.6 years). All patients had undergone laser photocoagulation for treatment of PDR. Cadaveric vitreous samples obtained within 6 to 18 hours after death from donors with no known ocular or systemic inflammatory disease, and matching age and sex of the patients, were used as normal control specimens. Undiluted vitreous samples (approximately 0.75 ml) were centrifuged for 5 minutes at 600g to remove contaminating cells and then transferred to cryotubes for storing at −70°C until use. The study was approved by the ethics committee of St. Thomas' Hospital, and it was performed in accordance with the ethical standards laid down in the 1964 Declaration of Helsinki.

Determination of sICAM-1, sVCAM-1, and sE-Selectin

Levels of vitreous sICAM-1, sVCAM-1, and sE-selectin were determined using commercial enzyme-link immunosorbent assay (ELISA) kits (R&D Systems, Oxon, UK) as follows: Microtiter well plates coated with specific antibodies to individual adhesion molecules were incubated with 100 μl of a 1:10 dilution of vitreous, together with 100 μl of the respective anti-adhesion molecule antibody, after which antibodies and test samples were removed and the plate washed six times with phosphate-buffered saline (PBS) containing 0.05% Tween-20. The amount of conjugated antibodies was detected by addition of 100 μl tetramethylbenzidine (substrate) and incubation for 30 minutes at room temperature. The enzymatic reaction was stopped by addition of 100 μl of 1 M H_2SO_4 and the absorbance read at 450 nm, with a correction wavelength of 620 nm (model MR 5000; Dynatech, Cambridge, MA). Levels of specific adhesion molecules present in vitreous samples were interpolated from specific calibration curves prepared with standard reagents.

Statistical Analysis of the Results

The significance of difference between corresponding groups of observations was evaluated by the nonparametric Mann–Whitney test. Acceptable significance was achieved at $P < 0.05$.

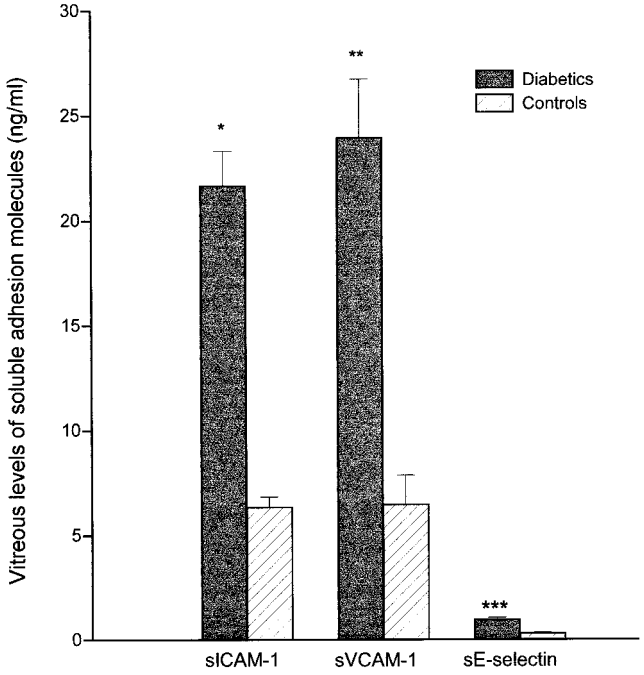

FIGURE 1. Histogram showing the mean levels ± SEM of soluble vascular cell adhesion molecules in vitreous from eyes with proliferative diabetic retinopathy. Comparison with vitreous levels of vascular cell adhesion molecules in normal cadaveric vitreous. Mann–Whitney test: $^{*}P = 0.00008$ (versus control cadaveric vitreous), $^{**}P = 0.00005$ (versus control cadaveric vitreous), $^{***}P = 0.000005$ (versus control cadaveric vitreous).

RESULTS

Vitreous Levels of sICAM-1, sVCAM-1, and sE-Selectin in Eyes with PDR

Figure 1 shows that vitreous from eyes with PDR contained significantly higher levels of sICAM-1 (range, 6.0–65.0 ng/ml) than vitreous from cadaveric control eyes (range, 4.17–9.81 ng/ml; $P = 0.00008$). Vitreous sVCAM-1 levels were also higher in eyes with PDR (range, 5.2–81.6 ng/ml) than in control cadaveric eyes (range, 2.8–14 ng/ml; $P = 0.00001$). In addition, vitreous levels of sE-selectin were significantly higher (range, 0.3–3.93 ng/ml) in eyes with PDR than in cadaveric control eyes (range, 0.1–0.59 ng/ml; $P = 0.000005$). There were no differences in the levels of these molecules between vitreous from patients with IDDM and vitreous from patients with non-IDDM, nor was there any relationship between vitreous levels of these molecules and duration of diabetes mellitus (Table 1).

TABLE 1. Vitreous Levels of Vascular Adhesion Molecules in Relation to Type and Duration of Diabetes Mellitus

	sICAM-1 (ng/ml)	sVCAM-1 (ng/ml)	sE-Selectin (ng/ml)
Type of diabetes mellitus			
IDDM	22.4 (6.0–65.0) [37]	21.4 (5.2–71.3) [30]	0.76 (0.36–4.3) [39]
Non-IDDM	18.0 (8.7–34.2) [11]	19.0 (5.2–93.6) [12]	0.79 (0.2–3.9) [11]
Duration of diabetes			
More than 10 years	20.3 (6.0–64.9) [34]	21.7 (0.22–81.6) [33]	0.72 (0.2–3.9) [38]
Less than 10 years	21.3 (9.7–34.2) [9]	16.4 (5.2–93.6) [10]	0.8 (0.35–4.3) [13]

The figures indicate the median values. Numbers in parentheses indicate the range of values within each group; numbers in brackets indicate the number of samples examined for each adhesion molecule.

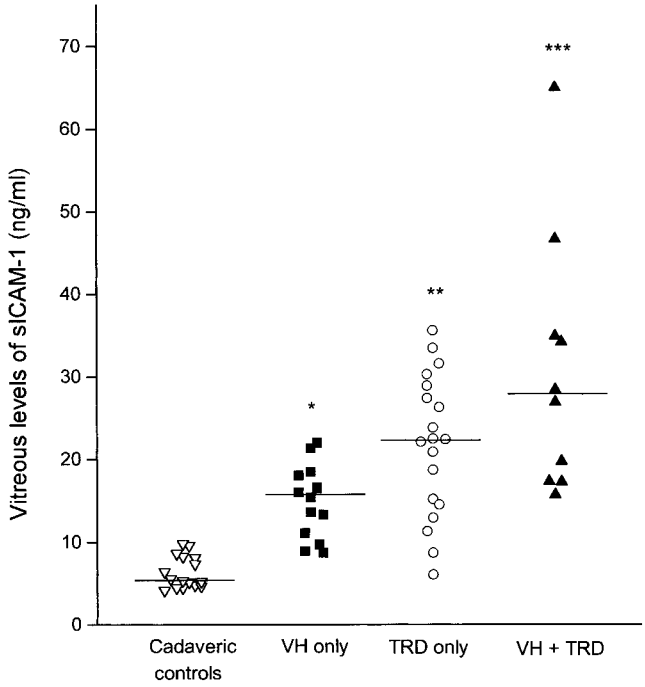

FIGURE 2. Scatter diagram showing the vitreous levels of sICAM-1 in eyes with PDR complicated by vitreous hemorrhage (VH) alone, traction retinal detachment (TRD) alone, or both. Mann–Whitney test: $^{*}P < 0.00001$ (versus control cadaveric vitreous); $^{**}P < 0.00001$ (versus control cadaveric vitreous), $P = 0.017$ (versus VH alone); $^{***}P < 0.00001$ (versus control cadaveric vitreous), $P = 0.0021$ (versus VH alone). The *lines* represent the median values.

Vitreous Levels of sICAM-1 in Relation to Retinal Complications of PDR

As observed in Figure 2, breakdown of the diabetic group into the various retinal complications of PDR showed that all groups contained significantly higher vitreous levels of sICAM-1 ($P < 0.00001$) when compared with cadaveric control samples. In addition, vitreous from eyes with PDR complicated by traction retinal detachment contained significantly higher levels of sICAM-1 (range, 6.04–35.6 ng/ml) than vitreous from eyes with vitreous hemorrhage alone (range, 8.7–22 ng/ml; $P = 0.017$). Likewise, vitreous levels of sICAM-1 in PDR eyes with both vitreous hemorrhage and traction retinal detachment exhibited higher levels of sICAM-1 (range, 15.7–65 ng/ml) than eyes with vitreous hemorrhage alone ($P = 0.0021$). There were no differences between the vitreous levels of this adhesion molecule in eyes with traction retinal detachment alone and eyes with both traction retinal detachment and vitreous hemorrhage ($P = 0.15$).

Vitreous Levels of sVCAM-1 in Relation to Retinal Complications of PDR

Figure 3 shows that vitreous levels of sVCAM-1 in eyes with PDR complicated by vitreous hemorrhage, traction retinal detachment, or both were significantly higher ($P < 0.001$) than in cadaveric eyes. Vitreous levels of sVCAM-1 in eyes with vitreous hemorrhage alone (range, 5.2–32.6 ng/ml) did not differ from those observed in eyes with PDR complicated by traction retinal detachment alone (range, 5.2–38 ng/ml; $P = 0.94$). In contrast, vitreous levels of this molecule were significantly higher in eyes with both vitreous hemorrhage and traction retinal detachment (range, 10.8–71.4 ng/ml) than in eyes with either vitreous hemorrhage ($P = 0.012$) or traction retinal detachment alone ($P = 0.007$).

Vitreous Levels of sE-Selectin in Relation to Retinal Complications of PDR

Figure 4 shows that similar to that seen with sICAM-1 and sVCAM-1, breakdown of the diabetic group into the various retinal complications of PDR showed that all groups contained significantly higher vitreous levels of sE-selectin than cadaveric control samples ($P < 0.0008$). Vitreous levels of sE-selectin in eyes with PDR complicated by traction retinal detachment (range, 0.2–2.9 ng/ml) were significantly higher than in eyes with vitreous hemorrhage alone (range, 0.22–1.19 ng/ml; $P = 0.021$). Similarly, vitreous from eyes with PDR complicated by both traction retinal detachment and vitreous hemorrhage exhibited higher levels of this molecule (range, 0.5–2.71 ng/ml) than eyes with vitreous hemorrhage alone ($P = 0.021$). There were no differences between the vitreous levels of this molecule in eyes with traction retinal detachment alone or traction retinal detachment together with vitreous hemorrhage ($P = 0.7$).

DISCUSSION

In this study, we investigated whether PDR as a complication of IDDM or non-IDDM was associated with raised vitreous levels of soluble vascular cell adhesion molecules that mediate

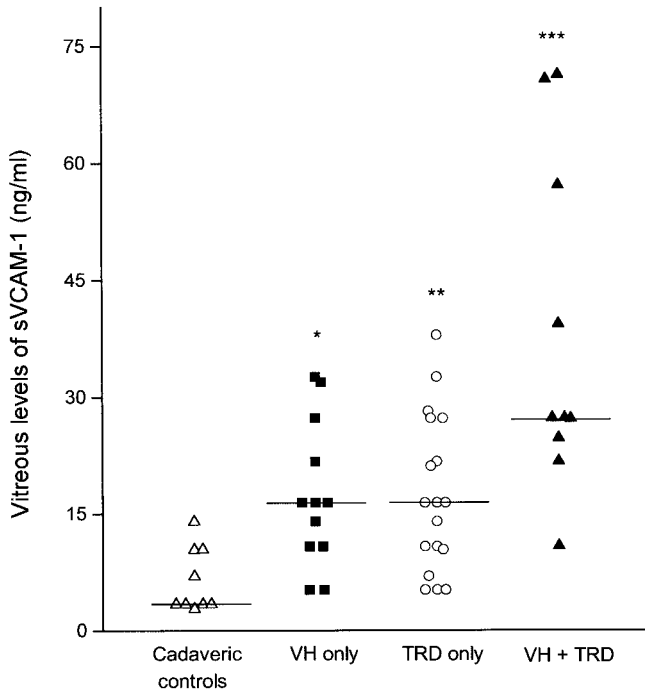

FIGURE 3. Scatter diagram showing the vitreous levels of sVCAM-1 in eyes with PDR complicated by vitreous hemorrhage (VH) alone, traction retinal detachment (TRD) alone, or both. Mann–Whitney test: $^{*}P < 0.001$ (versus control cadaveric vitreous); $^{**}P < 0.001$ (versus control cadaveric vitreous), $P = 0.94$ (versus VH alone); $^{***}P < 0.001$ (versus control cadaveric vitreous), $P = 0.012$ (versus VH alone), $P = 0.007$ (versus TRD alone). The *lines* represent the median values.

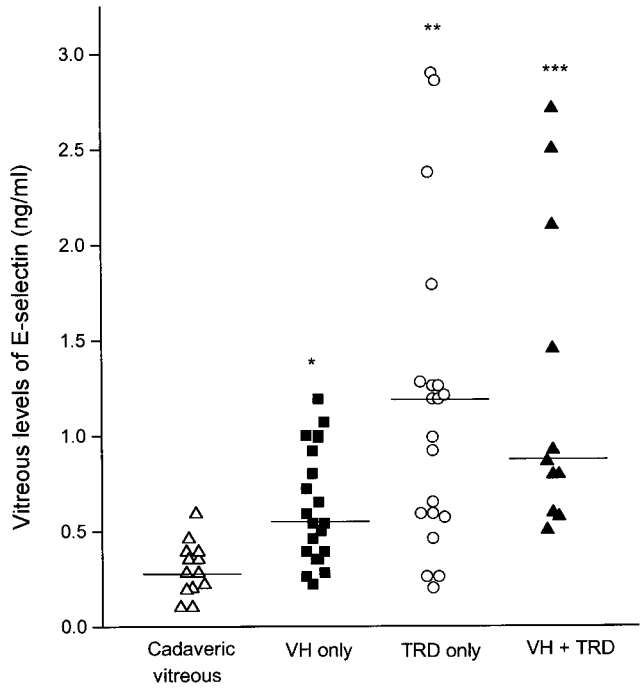

FIGURE 4. Scatter diagram showing the vitreous levels of sE-selectin in eyes with PDR complicated by vitreous hemorrhage (VH) alone, traction retinal detachment (TRD) alone, or both. Mann–Whitney test: $^{*}P < 0.0008$ (versus control cadaveric vitreous); $^{**}P < 0.0008$ (versus control cadaveric vitreous), $P = 0.021$ (versus VH alone); $^{***}P < 0.0008$ (versus control cadaveric vitreous), $P = 0.021$ (versus VH alone), $P = 0.81$ (versus TRD alone). The *lines* represent the median values.

leukocyte extravasation and interaction with endothelium during the inflammatory process. We observed that vitreous levels of sICAM-1, sVCAM-1, and sE-selectin were significantly higher in eyes with PDR than in control cadaveric vitreous, and that levels of these molecules did not relate to the type or duration of diabetes mellitus. Assessment of clinical complications of PDR leading to vitrectomy showed that eyes with either traction retinal detachment alone or with both traction retinal detachment and vitreous hemorrhage exhibited significantly higher levels of sICAM-1 and sE-selectin than those with vitreous hemorrhage alone. These findings suggest that inflammation caused by retinal detachment further amplifies the existing inflammatory process that leads to neovascularization in the diabetic eye. This is supported by previous observations that retinal detachment also amplifies inflammation in eyes with anterior uveitis.[15] The observations that vitreous levels of sICAM-1 and sE-selectin were higher in eyes with traction retinal detachment than in those with vitreous hemorrhage alone and that sVCAM-1 levels in eyes with vitreous hemorrhage were similar to those in eyes with traction retinal detachment suggest that these molecules may be locally produced within the retinal environment and that their levels in the vitreous may not depend on extravasation from the circulation.

Expression of ICAM-1 has been demonstrated in vivo and in vitro in various cells of the retina and choroid and in leukocytes.[8,17,18] Presence of both molecules has been observed in proliferating vascular endothelium of PDR membranes,[19] and ICAM-1, normally expressed by RPE cells,[18] may also be found in the extracellular matrix of these membranes.[19] These observations support the view that sICAM-1 found in vitreous from eyes with PDR may derive from local retinal cells, including retinal vascular endothelium and RPE cells, as well as from leukocytes migrating into the retina. Expression of the vascular adhesion molecules ICAM-1, VCAM-1, and E-selectin on endothelium is crucial for leukocyte recruitment into the inflammatory site,[7,8] and cytokines such as tumor necrosis factor-α, which is found in vitreous[20] and in the extracellular matrix and luminal and abluminal surfaces of vessels in PDR membranes,[19] promote the upregulation and release of these molecules during the inflammatory process.[21] It is therefore possible that release of soluble adhesion molecules into the vitreous from eyes with PDR may be promoted by this cytokine, which is also known to play an important role in the pathogenesis of diabetes mellitus and in the development of proliferative retinopathy complicating this disease.[22,23]

General features that characterize the inflammatory process in general[5] are those that promote neovascularization and fibrosis within the diabetic retina,[3,4] suggesting that cellular and molecular mechanisms of inflammation may operate during the development of PDR. Although there is no evidence to suggest that inflammation may be the main trigger of fibrovascular proliferation in PDR, there is evidence that cell adhesion and angiogenesis are strongly linked.[10] Evidence for the angiogenic properties of VCAM-1 and E-selectin derives from observations that both molecules induce angiogenesis of rat cornea and chemotaxis of human endothelial cells.[10,14] On this basis, it is reasonable to suggest that these molecules may contribute to the angiogenic process observed in PDR, and that the severity of this condition may well be related to levels of production and release of vascular cell adhesion molecules. In turn, adhesion molecule production within the diabetic retina may depend on the profile of cytokine production induced by either retinal hypoxia, as suggested by experimental findings in vitro,[24] or by abnormal glucose metabolites, as indicated by observations that methyl glyoxal–modified proteins, which are highly increased in poorly controlled diabetes,[25] induce expression of mRNA coding for tumor necrosis factor-α.[26]

Further investigation of the mechanisms that promote and control the production and activity of vascular cell adhesion molecules within the eye may aid in a better understanding of the microvascular process leading to PDR and in the development of new therapeutic approaches to treat and prevent this sight-threatening complication of diabetes mellitus.

References

1. Garner A. Histopathology of diabetic retinopathy in man. *Eye.* 1993;7:250–253.
2. Kolb H, Kolb–Bachofen V, Roep BO. Autoimmune versus inflammatory type I diabetes: a controversy? *Immunol Today.* 1995;16: 170–172.
3. Forrester JV, Shafiee A, Schroder S, Knott R, McIntosh L. The role of growth factors in proliferative diabetic retinopathy. *Eye.* 1993; 7:276–287.
4. Hiscott P, Waller HA, Grierson I, Butler MG, Scott DL. The extracellular matrix of reparative tissue in the vitreous: fibronectin production in proliferative diabetic retinopathy membranes. *Eye.* 1993;7:288–292.
5. Spector WG. Healing and repair. In: WE Spector, Ed. *An Introduction to General Pathology.* Churchill Livingstone. 1980;76–92.
6. Jerdan JA, Michels RG, Glaser BM. Diabetic preretinal membranes: an immunohisto-chemical study. *Arch Ophthalmol.* 1986;104: 286–290.

7. Cronstein BN, Weissmann G. The adhesion molecules of inflammation. *Arthritis Rheum.* 1993;36:147–157.
8. Mackay CR, Imhof BA. Cell adhesion in the immune system. *Immunol Today.* 1993;14:99–102.
9. Leca G, Mansur SE, Bensussa A. Expression of VCAM-1 (CD106) by a subset of TCRγδ-bearing lymphocyte clones: involvement of a metalloprotease in the specific hydrolytic release of the soluble isoform. *J Immunol.* 1995;154:1069–1077.
10. Kock AE, Halloran MM, Haskell CJ, Shah MR, Polverini PJ. Angiogenesis mediated by soluble forms of E-selectin and vascular cell adhesion molecule-1. *Nature.* 1995;376:517–519.
11. Gearing AJH, Newman W. Circulating adhesion molecules in disease. *Immunol Today.* 1993;14:506–512.
12. Zaman AG, Edelsten C, Stanford MR, et al. Soluble intercellular adhesion molecule-1 (sICAM-1) as a marker of disease relapse in idiopathic uveoretinitis. *Clin Exp Immunol.* 1994;95:60–65.
13. Fasching P, Veitl M, Rohac M, et al. Elevated concentrations of circulating adhesion molecules and their association with microvascular complications in insulin-dependent diabetes mellitus. *J Clin Endocrinol Metab.* 1996;81:4313–4317.
14. Olson JA, Whitelaw CM, McHardy KC, Pearson DWM, Forrester JV. Soluble leucocyte adhesion molecules in diabetic retinopathy stimulate retinal capillary endothelial cell migration. *Diabetologia.* 1997;40:1166–1171.
15. Webster L, Limb GA, Stanbury RM, Earley O, Chignell AH. Relationship between vitreous levels of sICAM-1 and TNFα in patients with uveitis. *Br J Ophthalmol.* 1998;82:438–443.
16. Limb GA, Chignell AH, Cole CJ, et al. Intercellular adhesion molecule-1 (ICAM-1) in proliferative vitreoretinopathy. *Invest Ophthalmol Vis Sci.* 1997;38:1043- 1048.
17. Tang S, Le-Ruppert KC, Gabel VP. Expression of intercellular adhesion molecule-1 (ICAM-1) and vascular cell adhesion molecule-1 (VCAM-1) on proliferating vascular endothelial cells in diabetic epiretinal membranes. *Br J Ophthalmol.* 1994;78:370–376.
18. Elner SG, Elner VM, Pavilack MA, et al. Modulation and function of intercellular adhesion molecule-1 (CD54) on human retinal pigment epithelial cells. *Lab Invest.* 1992;66:200–211.
19. Limb GA, Chignell AH, Green W, LeRoy F, Dumonde DC. Distribution of TNFα and its reactive vascular adhesion molecules in fibrovascular membranes of proliferative diabetic retinopathy. *Br J Ophthalmol.* 1996;2:168–173.
20. Franks WA, Limb GA, Stanford MR, et al. Cytokines in human intra-ocular inflammation. *Curr Eye Res.* 1992;11:187–191.
21. Camussi G, Albano E, Tetta C, Bussolino F. The molecular action of tumour necrosis factor-α. *Eur J Biochem.* 1991;202:3–14.
22. Pociot F, Briant L, Jongeneel CV, et al. Association of tumor necrosis factor (TNF) and class II major histocompatibility alleles with the secretion of TNF-α and TNF-β by human mononuclear cells: a possible link to insulin-dependent diabetes mellitus. *Eur J Immunol.* 1993;23:224–231.
23. Hawrami K, Hitman GA, Rema M, et al. An association in non-insulin dependent diabetes mellitus subjects between susceptibility to retinopathy and tumor necrosis factor polymorphism. *Hum Immunol.* 1996;46:49–54.
24. Lim Y-C, Gough MJ, Homer–Vanniasinkam S, Parkin SM. Induction of tumour necrosis factor-α release by hypoxia. *Biochem Soc Trans.* 1997;25:231S.
25. McLellan AC, Thornalley PJ, Benn J, Sonksen PH. Glyoxalase system in clinical diabetes mellitus and correlation with diabetic complications. *Clin Sci.* 1994;87:21–29.
26. Webster L, Limb GA, Thornalley PJ. Induction of TNFα and IL-1β mRNA in mononuclear cells by methylglyoxal and age modified human serum albumin. *Biochem Soc Trans.* 1997;25:251S.

Acuity Recovery and Cone Pigment Regeneration after a Bleach in Patients with Retinitis Pigmentosa and Rhodopsin Mutations

Michael A. Sandberg, Basil S. Pawlyk, and Eliot L. Berson

Purpose. To assess visual acuity recovery times and cone photopigment regeneration kinetics after a bleach in the fovea of patients with dominant retinitis pigmentosa due to rhodopsin mutations.

Methods. The authors measured acuity recovery times by computerized photostress testing in 13 patients with dominant retinitis pigmentosa and one of eight rhodopsin mutations. The authors also measured their time constants of cone photopigment regeneration with a video imaging fundus reflectometer to determine whether acuity recovery time depended on pigment regeneration kinetics. These values were compared with those of normal subjects, by the Mann–Whitney *U* test. The relationship between acuity recovery time and the time constant of cone photopigment regeneration among the patients was quantified by the Spearman rank correlation.

Results. The visual acuity recovery times, which averaged 22.0 seconds for the patients with retinitis pigmentosa and 11.2 seconds for the normal subjects, were significantly slower for the patient group ($P < 0.001$). The time constants of cone pigment regeneration, which averaged 172 seconds for the patients with retinitis pigmentosa and 118 seconds for the normal subjects, also were significantly slower for the patient group ($P = 0.043$). The authors also found a significant, positive correlation between the visual acuity recovery time and the time constant of pigment regeneration for the patients with retinitis pigmentosa ($r = 0.65$, $P = 0.017$).

Conclusions. A slowing of foveal visual acuity recovery and cone pigment regeneration, which are related to each other, can occur in patients with retinitis pigmentosa, due to a rod-specific gene defect. (*Invest Ophthalmol Vis Sci.* 1999;40:2457–2461)

From the Berman-Gund Laboratory for the Study of Retinal Degenerations, Harvard Medical School, Massachusetts Eye and Ear Infirmary, Boston, Massachusetts.

Supported by National Eye Institute Grant EY00169; the Foundation Fighting Blindness, Hunt Valley, Maryland; and the Massachusetts Lions Eye Research Foundation, Inc.

Submitted for publication December 29, 1998; revised April 5, 1999; accepted April 28, 1999.

Proprietary interest category: N.

Corresponding author: Michael A. Sandberg, The Berman-Gund Laboratory, The Massachusetts Eye and Ear Infirmary, 243 Charles Street, Boston, MA 02114.
E-mail: masandberg@aol.com

Patients with retinitis pigmentosa commonly report slowed daytime visual recovery after exposure to high levels of illumination. Clinical testing has demonstrated slow visual acu-

Table 1. Patient Demographics and Ocular Findings by Age

Age/ Sex	Rhodopsin mutation	Visual acuity	Dark-adapted threshold*	Acuity recovery time (sec)†	Photopigment double density‡	Photopigment regeneration time constant (sec)§
19/M	Pro347Leu	20/20	4.30	44	0.14	365
24/M	Cys110Tyr	20/20	2.18	21	0.17	178
33/F	Pro23His	20/20	1.18	10	0.21	109
33/M	Pro23His	20/20	2.04	14	0.16	97
36/F	Pro23His	20/20	2.18	16	0.14	144
36/M	Phe45Leu	20/20	1.90	11	0.15	94
39/F	Pro171Leu	20/30	4.48	21	0.05	275
40/F	Pro23His	20/25	1.90	17	0.08	162
46/M	Pro23His	20/20	1.90	22	0.19	156
50/F	Pro23His	20/20	2.00	22	0.20	189
51/F	Gly114Asp	20/30	4.18	37.5	0.06	162
52/M	Gly89Asp	20/30	3.78	28.5	0.24	159
57/M	Thr17Met	20/30	3.78	22	0.10	143

* Central 11° white light, in log microapostilbs (normal < 1.7).
† Foveal; upper range of normal is 20 seconds ($n = 15$).
‡ Central 2°; lower range of normal is 0.13 ($n = 11$).
§ Central 2°; upper range of normal is 194 seconds ($n = 11$).

ity recovery in patients with retinitis pigmentosa of unspecified genetic types.[1] Such delayed recovery may be due to slow foveal cone pigment regeneration, which has been found in a patient with dominant retinitis pigmentosa due to an unknown mutation,[2] and in patients with autosomal recessive retinitis pigmentosa,[3] X-linked retinitis pigmentosa,[3] isolate retinitis pigmentosa,[3] and Usher syndrome (type 1).[4]

An estimated 10% of patients with retinitis pigmentosa in the United States have rhodopsin mutations as the cause of their disease.[5,6] Their decline in rod function is followed by a loss of cone function by a presently unknown mechanism.[7] Because some of these patients report impaired daytime visual recovery after exposure to bright lights, it is possible that slowed cone photopigment regeneration may be implicated in their secondary cone degeneration.

The purposes of the present study were to determine whether patients with retinitis pigmentosa due to a rhodopsin mutation show slow visual acuity recovery after a bleach and whether their recovery times reflect their cone photopigment kinetics.

Methods

Subjects

Thirteen patients (7 men and 6 women; age, 39.7 ± 3.1 years; mean ± SE) with dominantly inherited retinitis pigmentosa due to a rhodopsin mutation were tested. Table 1 indicates that each of these patients had 1 of 8 rhodopsin mutations and that 6 patients had the Pro23His mutation. Their corrected visual acuities ranged from 20/20 to 20/30, and their central dark-adapted rod thresholds to an 11° test light in the Goldmann–Weekers dark adaptometer ranged from borderline to 2.5 log-units above normal. We excluded patients by direct ophthalmoscopy who had cystoid macular edema because of the positive associations between macular edema and delayed visual acuity recovery after a bleach[8] and between macular edema and delayed foveal cone pigment regeneration.[9] Also, we excluded patients with cataracts, to minimize light scatter in our fundus reflectometry measurements. Fifteen normal subjects (9 men and 6 women; age, 39.5 ± 4.1 years; mean ± SE) served as controls for the measurements of visual acuity recovery time. Eleven normal subjects (6 men and 5 women; age, 36.9 ± 1.9 years; mean ± SE) served as controls for the measurements of cone pigment regeneration. The differences in mean age between each of these two normal groups and the patient group were not statistically significant by *t*-test ($P = 0.97$ and 0.48, respectively). Before inclusion in this study, all subjects signed informed consent approved by the Investigational Review Boards of the Massachusetts Eye and Ear Infirmary and Harvard Medical School. The methods described herein also adhered to the principles of the Declaration of Helsinki.

Visual Acuity Recovery Time Measurements

Visual acuity recovery time was measured in the fovea by photostress testing[10] after pupillary dilation. The tested eye was the eye with better visual acuity or, if visual acuities were equal bilaterally, the right eye. Patients first attempted to identify letters of progressively smaller size flashed in random alphabetical order on a computer screen. If a letter was correctly named, the next presentation was a letter that was 0.1 log-unit (21%) smaller; if there were two misses at a given letter size, the previous (larger) size became the minimum angle of resolution. Since any of the 26 letters of the alphabet could be presented, the probability of a correct guess by chance for each trial was less than 4%.

The 9° diameter white light of a Welch Allyn direct ophthalmoscope was then focused onto the fovea for 10 seconds at its standard retinal illuminance of 7.0 log-td to produce a cone pigment bleach of ~99%.[11] Immediately afterward, patients tried to identify letters flashed in random order at twice the minimum angle of resolution. The recovery time was the time between the offset of the bleach and the first correct letter identification.

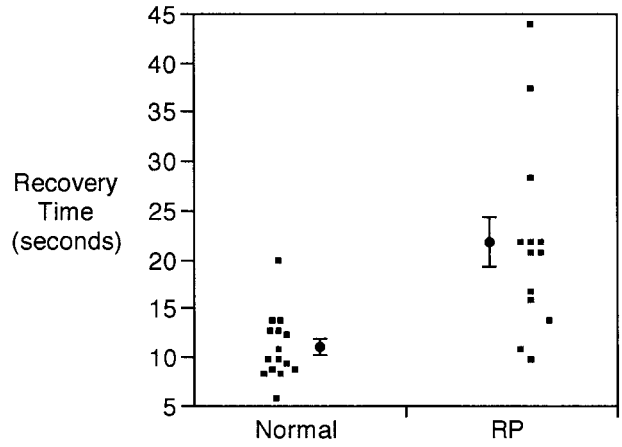

FIGURE 1. Visual acuity recovery times in normal subjects and patients with retinitis pigmentosa. *Filled circles* are means; error bars, ±SE. Points with the same (or similar) value have been shifted horizontally to facilitate their identification.

Cone Pigment Regeneration Measurements

Cone pigment regeneration was recorded with a video imaging fundus reflectometer, based on a modified Kowa fundus camera; the eye evaluated was the same as that tested for visual acuity recovery. Light from an external halogen lamp, attenuated by an infrared blocking filter and conducted by fiberoptic, was the source for a 15° diameter, yellow-green test field (λ_{max} = 560 nm; 10 nm half bandwidth) of maximally 5.1 log-td and an 8° diameter yellow bleaching field (λ50% cut-on = 540 nm) of 6.5 log-td. At its maximal retinal illuminance the test field, exposed for 250 msec, would be expected to bleach only ~1% of the cone visual pigments.[11] The yellow bleaching field, which was presented for 2 minutes, would be expected to bleach ~99% of the middle- and long-wavelength sensitive cone visual pigments and to a lesser extent rhodopsin and the short-wavelength sensitive cone visual pigment and photoproducts. These fields were centered in the dilated pupil as a 6-mm inner diameter, 7-mm outer diameter annulus in Maxwellian-view. The fundus camera also provided a blue light-emitting diode for fixation in Newtonian-view.

After 15 minutes of dark adaptation, the stimulus was presented at retinal illuminances between 4.8 and 5.1 log-td in steps of 0.1 log-unit to obtain a series of baseline images for calibration of fundus reflectance. Immediately after the bleach, the stimulus was presented at 4.8 log-td, at increasing intervals for up to 15 minutes, to monitor cone pigment regeneration. After a 10-minute rest period in darkness to prevent cone pigment bleaching, the sequence of calibration, bleach, and testing was then repeated to increase the likelihood of acquiring reliable data (see below). All patients and normal subjects showed full cone pigment regeneration by the end of each sequence, based on the analytical methods described below.

The fundus was imaged onto the screen of a high-resolution integrating CCD camera (Xybion, Gen-I). The output of this camera was connected to a computer containing a frame-grabber card, frame storage buffer card, and an 8-bit gray scale/color video card. Image frames were analyzed by software (NIH Image 1.49) that converted field brightness to 256 gray levels. Image brightness was evaluated for the central 2° (rod free area) of the fovea to quantify cone pigment regeneration. The differences in pigment double density for each successive postbleach image relative to the initial postbleach image were calculated to obtain the proportion of unbleached pigment as a function of time. An exponential model was used to derive the time constant in seconds (i.e., the time to regenerate ~63% of visual pigment). We also evaluated fundus image brightness as a function of time for a parafoveal area outside the 8° bleach, to determine whether fundus reflectance was affected by systematic changes in eye position during the recovery phase; if there was a significant trend versus time, then the corresponding foveal pigment regeneration series was discarded. If neither the test nor retest parafoveal series showed a significant trend versus time, then we selected the foveal series with the better fit to the exponential model for comparative statistics.

Testing of normal subjects revealed a mean time constant for foveal cone pigment regeneration of 118 seconds (see Results section), within the range of mean normative values reported by others, 98 to 120 seconds.[3, 4, 12,13] On the other hand, our mean normative value for double density was 0.19 log-unit, below the range reported by others, 0.21 to 0.30 log-unit.[3,4,12,14] This presumably occurred because our annular test beam passed through the margin of the pupil, which results in a lower double density.[15] Because some patients with retinitis pigmentosa and good visual acuity have foveal cone photoreceptors with reduced directional sensitivity, as mea-

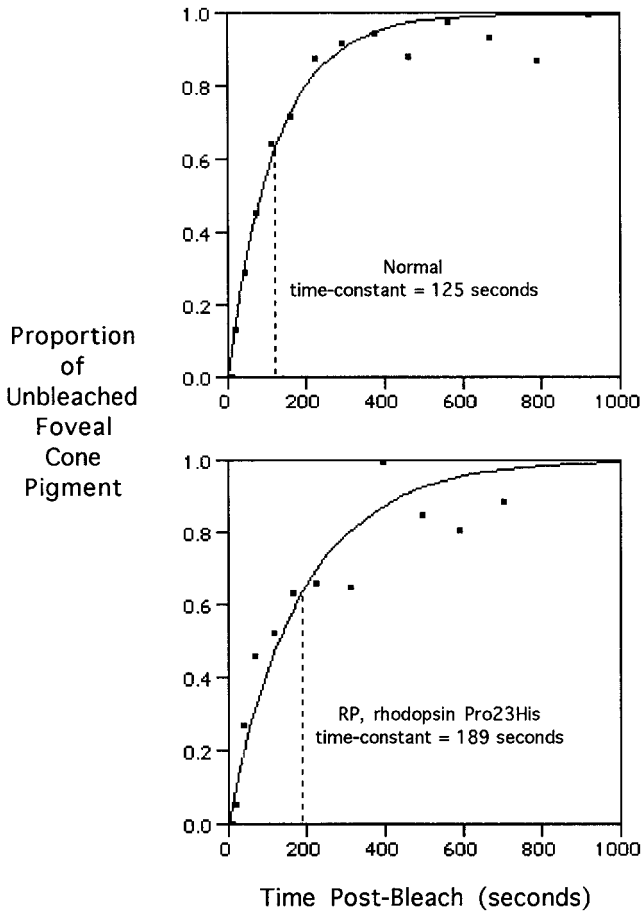

FIGURE 2. Data and fitted exponential curves for representative foveal cone pigment regeneration from a normal subject (*top*) and a retinitis pigmentosa patient with a rhodopsin mutation (*bottom*).

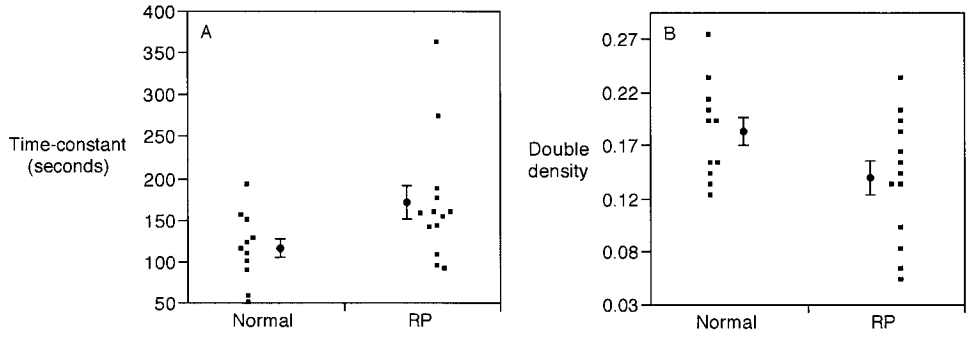

FIGURE 3. Time constants (**A**) and double densities (**B**) from measurements of foveal cone pigment regeneration in normal subjects and patients with retinitis pigmentosa. *Filled circles* are means; error bars, ±SE. Points with the same (or similar) value have been shifted horizontally to facilitate their identification.

sured by the Stiles-Crawford effect,[16] it is possible that the values for our normal subjects, but not those for some of our patients, would have been higher for a fundus reflectometer with a beam entering the center of the pupil.

Statistical Analyses

The visual acuity recovery time, the time constant of foveal cone pigment regeneration, and the foveal cone pigment double density were each compared by diagnosis (retinitis pigmentosa versus normal) using the Mann–Whitney *U* test, a nonparametric test based on ranks that does not require a normal distribution of the data. For the patients with retinitis pigmentosa, we calculated the correlation between their time constant of foveal cone pigment regeneration and their pigment double density to see whether the former was a reflection of their stage of cone degeneration in the fovea. We also calculated the correlation between their visual acuity recovery time and their time constant of foveal cone pigment regeneration to see whether variation in the psychophysical measure could be accounted for by variation in the physiological measure. These two relationships were quantified by the Spearman rank correlation, which does not require the assumption of a bivariate normal distribution. Calculation of pigment regeneration time constants and the above statistical analyses were done with JMP (version 3.2; SAS Institute, Cary, NC) on a Macintosh computer (Apple Computers, Cupertino, CA).

RESULTS

Table 1 lists the visual acuity recovery times for the 13 patients with retinitis pigmentosa. Figure 1 plots these recovery times, which averaged 22.0 seconds, against those for the normal subjects, which averaged 11.2 seconds. The values for the patient group are significantly slower than those for the normal group by the Mann–Whitney *U* test ($P < 0.001$). Eight of the 13 patients (62%), representing 7 different mutations, had recovery times above the normal range.

Figure 2 shows foveal cone pigment regeneration data for a normal subject (top) and for a representative patient with retinitis pigmentosa (bottom). Each graph shows the best-fitting exponential function from which a time constant was derived. For these examples, the time constants are 125 and 189 seconds, respectively.

Table 1 lists the foveal cone pigment regeneration time constants for the patients with retinitis pigmentosa. These time constants, which averaged 172 seconds, and those for the normal subjects, which averaged 118 seconds, are plotted in Figure 3A. The values for the patient group are significantly slower than those for the normal group ($P = 0.043$). Two of the 13 patients (15%), with different mutations, had time constants above the normal range.

Table 1 also lists the cone pigment double-density values for the patients with retinitis pigmentosa. Figure 3B plots these double densities, which averaged 0.15 log-unit, against those for the normal subjects, which averaged 0.19 log-unit. Although these two distributions are not significantly different ($P = 0.098$), the values for the patients tend to be lower than those for the normal subjects. Four of the 13 patients (31%), each with a different mutation, had double densities below the normal range. For the patients with retinitis pigmentosa, the time constant of pigment regeneration and the pigment double density are inversely related by the Spearman rank correlation ($r = -0.26$), but this value is not statistically significant ($P = 0.40$).

Figure 4 plots the visual acuity recovery time versus the time constant of foveal cone pigment regeneration for the patients with retinitis pigmentosa. The correlation (0.65) is statistically significant ($P = 0.017$). If we consider only the data for the 6 patients with the Pro23His mutation, this correlation is 0.84 ($P = 0.036$).

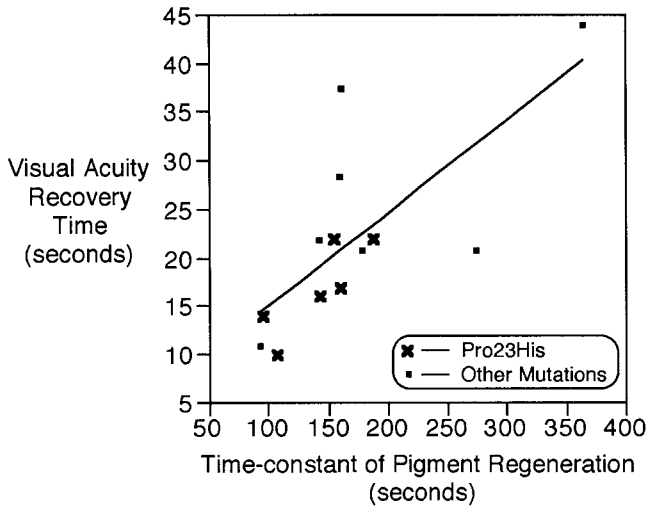

FIGURE 4. Scatter plot of the visual acuity recovery time versus the time-constant of foveal cone pigment regeneration for the patients with retinitis pigmentosa. The *straight line* represents the best least-squares fit to the entire data set.

DISCUSSION

This study shows that patients with dominant retinitis pigmentosa due to rhodopsin mutations, as a group, have visual acuity recovery times and foveal cone pigment regeneration time constants after a bleach that are significantly slower than normal. Although prior studies have reported slow visual acuity recovery or slow foveal cone pigment regeneration in patients with retinitis pigmentosa,[1–4] this is the first demonstration of these abnormalities in patients with retinitis pigmentosa who are known to have rhodopsin gene defects. We also found that the visual acuity recovery times and the time constants of cone pigment regeneration were significantly correlated for our entire group of patients, as well as for the subset of patients with the Pro23His mutation. Just as the rate of foveal cone dark adaptation reflects the rate of foveal cone pigment regeneration among normal subjects of varying age,[12] the visual acuity recovery time similarly reflects the rate of foveal cone pigment regeneration among patients with retinitis pigmentosa and a rhodopsin mutation.

Delayed visual acuity recovery and/or cone pigment regeneration was found in more than half of our patients with disease due to several different dominant rhodopsin mutations. Earlier studies had shown these abnormalities in patients with diverse genetic types of retinitis pigmentosa.[2–4] Therefore, this abnormality is not restricted to patients with a particular rhodopsin mutation or even with dominant disease.

The physiologic basis for impaired cone pigment regeneration in retinitis pigmentosa is not known. Although not statistically significant, our finding of an inverse relationship between the time constant of cone pigment regeneration and the cone pigment optical density could mean that a prolonged time constant is a sign of abnormal cone outer segment morphology. Alternatively, the slowing of cone pigment regeneration could be the direct result of rod photoreceptor degeneration independent of the presence or stage of cone photoreceptor degeneration. It is possible, for example, that loss of rods results in less 11-*cis*-retinal in the retinal pigment epithelium after a bleach. Although cones are about fivefold more efficient than neighboring rods in competing for 11-*cis*-retinal after a bleach,[17] its shortfall in the retinal pigment epithelium might slow cone pigment regeneration, even in otherwise healthy cones. For example, it has been shown that the kinetics of cone dark adaptation are slowed in patients with systemic vitamin A deficiency and are normalized in these patients after vitamin A supplementation.[18,19] It remains to be established whether some critical delay in cone pigment regeneration or some critical slowing of visual acuity recovery time is a predictor of impending cone photoreceptor cell death in patients with retinitis pigmentosa and rhodopsin mutations.

References

1. Gawande AA, Donovan WJ, Ginsburg AP, Marmor MF. Photoaversion in retinitis pigmentosa. *Br J Ophthalmol.* 1989;73:115–120.
2. Ripps H, Brin KP, Weale RA. Rhodopsin and visual threshold in retinitis pigmentosa. *Invest Ophthalmol Vis Sci.* 1978;17:735–745.
3. Van Meel GJ, van Norren D. Foveal densitometry in retinitis pigmentosa. *Invest Ophthalmol Vis Sci.* 1983;24:1123–1130.
4. Fulton AB, Hansen RM. Foveal cone pigments and sensitivity in young patients with Usher's syndrome. *Am J Ophthalmol.* 1987; 103:150–160.
5. Dryja TP, Hahn LB, Cowley GS, McGee TL, Berson EL. Mutation spectrum of the rhodopsin gene among patients with autosomal dominant retinitis pigmentosa. *Proc Natl Acad Sci USA.* 1991;88: 9370–9374.
6. Vaithinathan R, Berson EL, Dryja TP. Further screening of the rhodopsin gene in patients with autosomal dominant retinitis pigmentosa. *Genomics.* 1994;21:461–463.
7. Berson EL, Rosner B, Sandberg MA, Dryja TP. Ocular findings in patients with autosomal dominant retinitis pigmentosa and a rhodopsin gene defect (Pro-23-His). *Arch Ophthalmol.* 1991;109:92–101.
8. Wu G, Weiter JJ, Santos S, Ginsburg L, Villalobos R. The macular photostress test in diabetic retinopathy and age-related macular degeneration. *Arch Ophthalmol.* 1990;108:1556–1558.
9. Van Meel GJ, Smith VC, Pokorny JJ, van Norren D. Foveal densitometry in central serous choroidopathy. *Am J Ophthalmol.* 1984; 98:359–368.
10. Sandberg MA, Gaudio AR. Slow photostress recovery and disease severity in age-related macular degeneration. *Retina.* 1995;15: 407–412.
11. Cornsweet TM. *Visual Perception.* New York: Academic Press; 1970:153.
12. Coile DC, Baker HD. Foveal dark adaptation, photopigment regeneration, and aging. *Vis Neurosci.* 1992;8:27–39.
13. Alpern M, Maaseidvaag F, Ohba N. The kinetics of cone visual pigments in man. *Vision Res.* 1971;11:539–549.
14. Kilbride PE, Fishman M, Fishman GA, Hutman LP. Foveal cone pigment density difference and reflectance in retinitis pigmentosa. *Arch Ophthalmol.* 1986;104:220–224.
15. van Norren D, van der Kraats J. A continuously recording retinal densitometer. *Vision Res.* 1981;21:897–905.
16. Birch DG, Sandberg MA, Berson EL. The Stiles-Crawford effect in retinitis pigmentosa. *Invest Ophthalmol Vis Sci.* 1982;22:157–164.
17. Rushton WA. Rod-cone rivalry in pigment regeneration. *J Physiol.* 1968;198:219–236.
18. Kemp CM, Jacobson SG, Faulkner DJ, Walt RW. Visual function and rhodopsin levels in humans with vitamin A deficiency. *Exp Eye Res.* 1988;46:185–197.
19. Cideciyan AV, Pugh EN Jr, Lamb TD, Huang Y, Jacobson SG. Rod plateaux during dark adaptation in Sorsby's fundus dystrophy and vitamin A deficiency. *Invest Ophthalmol Vis Sci.* 1997;38:1786–1794.